Robot-Assisted Phenotyping of Genome-Reduced *Corynebacterium glutamicum* Strain Libraries to Draft a Chassis Organism

Simon Unthan

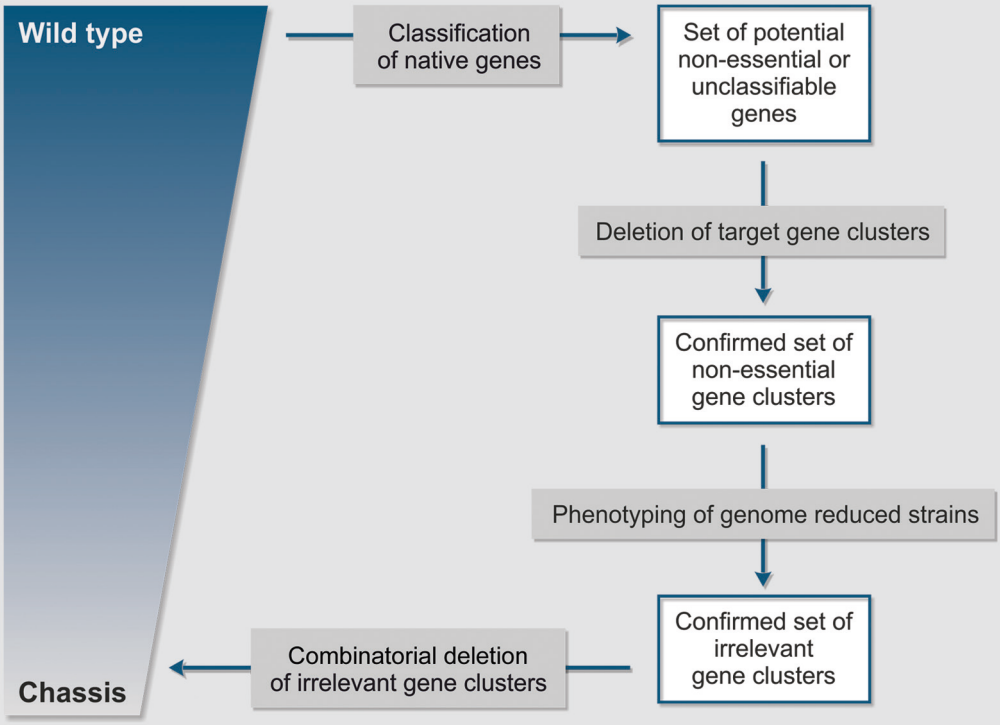

Schlüsseltechnologien / Key Technologies
Band / Volume 132
ISBN 978-3-95806-169-9

JÜLICH FORSCHUNGSZENTRUM

Schriften des Forschungszentrums Jülich
Reihe Schlüsseltechnologien / Key Technologies Band / Volume 132

Forschungszentrum Jülich GmbH
Institute of Bio- and Geosciences
Biotechnology (IBG-1)

Robot-Assisted Phenotyping of Genome-Reduced *Corynebacterium glutamicum* Strain Libraries to Draft a Chassis Organism

Simon Unthan

Schriften des Forschungszentrums Jülich
Reihe Schlüsseltechnologien / Key Technologies Band / Volume 132

ISSN 1866-1807 ISBN 978-3-95806-169-9

Bibliographic information published by the Deutsche Nationalbibliothek.
The Deutsche Nationalbibliothek lists this publication in the Deutsche
Nationalbibliografie; detailed bibliographic data are available in the
Internet at http://dnb.d-nb.de.

Publisher and Distributor:	Forschungszentrum Jülich GmbH Zentralbibliothek 52425 Jülich Tel: +49 2461 61-5368 Fax: +49 2461 61-6103 Email: zb-publikation@fz-juelich.de www.fz-juelich.de/zb
Cover Design:	Grafische Medien, Forschungszentrum Jülich GmbH
Printer:	Grafische Medien, Forschungszentrum Jülich GmbH
Copyright:	Forschungszentrum Jülich 2016

Schriften des Forschungszentrums Jülich
Reihe Schlüsseltechnologien / Key Technologies, Band / Volume 132

D 82 (Diss. RWTH Aachen University, 2015)

ISSN 1866-1807
ISBN 978-3-95806-169-9

The complete volume is freely available on the Internet on the Jülicher Open Access Server (JuSER)
at www.fz-juelich.de/zb/openaccess.

Linus Pauling:

The best way to have a good idea is to have a lot of ideas.

Aristotle:

The one exclusive sign of thorough knowledge is the power of teaching.

Daniel Kehlmann - „Die Vermessung der Welt“:

Humboldt reiste nach Salzburg weiter,
wo er sich das teuerste Arsenal von Messgeräten zulegte,
das je ein Mensch besessen hatte.
[…]
Er blieb ein Jahr und übte.
[…]
Er übte das Zerlegen und Zusammenbauen jedes Instruments,
bis er es blind beherrschte,

auf einem Bein stehend,
bei Regen
oder inmitten einer fliegenumschwärmten Kuhherde.

Die Einheimischen hielten ihn für verrückt.

Declaration on oath

I hereby declare that this thesis is my own scholarly work and no sources otherwise indicated in the text or references have been used. This thesis has not been submitted either in whole or part for a degree at this university or any other institution.

Simon Unthan

Aachen, January 2015

Own publications

Parts of this work have already been published on conferences or in peer-reviewed journals. Graphics used in this work that were already printed in existing own publications are cited in the text. However, any general thought, method, experimental strategy, result or conclusion that was already part of any existing own publications is not explicitly referred to in every sentence, but considered as properly cited by the following list:

Peer-reviewed journal publications

Baumgart M, **Unthan S**, Rückert C, *et al.* (2013) Construction of a prophage-free variant of Corynebacterium glutamicum ATCC 13032 for use as a platform strain for basic research and industrial biotechnology. Appl Environ Microbiol 79:6006–15. doi: 10.1128/AEM.01634-13

Unthan S, Grünberger A, van Ooyen J, *et al.* (2014) Beyond growth rate 0.6: What drives Corynebacterium glutamicum to higher growth rates in defined medium. Biotechnol Bioeng 111:359–71. doi: 10.1002/bit.25103

Unthan S, Baumgart M, Radek A, *et al.* (2014) Chassis organism from Corynebacterium glutamicum - a top-down approach to identify and delete irrelevant gene clusters. Biotechnol J 9–10. doi: 10.1002/biot.201400041

Unthan S, Radek A, Wiechert W, *et al.* (2015). Bioprocess automation on a Mini Pilot Plant enables fast quantitative microbial phenotyping. Microb Cell Fact 14:32. doi: 10.1186/s12934-015-0216-6

Conference talks

Unthan, S., Radek, A., Wiechert, W., Noack S. (2013). Top-down towards a chassis organism. International symposium on synthetic biology, Heidelberg

Unthan, S., Radek, A., Oldiges, M., Wiechert, W., Noack S. (2014). Mini Pilot Plant (MPP) for fast and reliable upstream development. 3rd BioProScale Symposium, Berlin

Conference posters

Unthan, S., Baumgart, M., Frunzke, J., Rückert, C., Kalinowski, J., Noack S. (2013). Emerging synthetic biology of Corynebacterium glutamicum – Genome reduction as a tool of strain development in white biotechnology. ECCE9 / ECAB2 congress, Den Haag

Unthan, S., Rohe, P., Voges, R., Radek, A., Noack S. (2013). Robot-assisted microbial phenotyping. Biotech Day, Jülich

Personal acknowledgements (in german)

Für die Betreuung und Prüfung meiner Promotionsarbeit sowie die Gestaltung einer produktiven und freundlichen Arbeitsatmosphäre am IBG-1 danke ich Herrn Prof. Wolfgang Wiechert auf das Herzlichste. Für kritische Diskussionen und die Prüfung der vorliegenden Arbeit danke ich ebenfalls Herrn Prof. Jochen Büchs sehr herzlich. Für die hervorragende Ausstattung und angenehme Arbeitsatmosphäre in der AG für Bioprozesse und Bioanalytik danke ich weiterhin Herrn Prof. Oldiges.

Mein größter Dank richtet sich an Herrn Dr. Noack, der als Teamleiter für Quantitative Microbial Phenotyping die vorliegende Arbeit hauptmäßig betreut hat. Stephan, ohne die zahlreichen intensiven Diskussionen, dein bedingungsloses Engagement für deine Doktoranden und deine offene Art wäre meine Arbeit in dieser Form nicht möglich gewesen. Ich wünsche dir von Herzen, dass du deinen Weg weiter so enthusiastisch gehst und alles Gute für deine Zukunft.

Weiterhin danke ich allen Technikern, Angestellten und Kollegen des IBG-1 wobei sich besonderer Dank an die Folgenden richtet: Raphael Voges, Peter Rohe, Alexander Grünberger, Jochem Gätgens, Meike Baumgart und Nicole Paczia. Herzlichen Dank richte ich auch an meine Studenten, welche mit viel Engagement und Freude auf diese Arbeit eingewirkt haben: Julian Stopp, Niklas Tenhaef, Andreas Radek, Barbara von Palubicki und Ramona Kloß.

Zum Abschluss meines Studiums möchte ich mich weiterhin bei allen Lehrkörpern und Angestellten der Universität Bielefeld und RWTH Aachen bedanken. Weiterhin danke ich allen Partnern des Verbundprojektes „Genomreduktion“ für die erfolgreiche und freundliche Zusammenarbeit.

Meinen Kollegen vom Brauteam „JuBräu“ danke ich für die jederzeit lustige und erfolgreiche praktische Anwendung der Biotechnologie, welche hoffentlich auch in Zukunft weiter stattfindet (Projekt: Titelverteidigung 2015…). Ebenso danke ich meinen Kommilitonen und Freunden aus Aachen, Bielefeld sowie von der btS e.V. mit denen ich in und außerhalb des universitären Umfelds eine wunderbare Zeit erleben durfte.

Abschließend danke ich meiner Familie, besonders meinen Eltern Katharina und Wolfgang Unthan für die private Unterstützung in den vergangenen Jahren.

Zuletzt möchte ich Dir von Herzen danken, Kristin.
Ohne deine Unterstützung, dein offenes Ohr und deine Liebe wäre ich nicht derjenige der ich heute bin und in Zukunft sein möchte.

Abstract

In this work, concepts were developed and applied to guide the construction of a *Corynebacterium glutamicum* chassis organism for synthetic biology approaches. The aim was to delete irrelevant genes from the wild type strain in order to obtain a chassis growing on defined CGXII medium with D-glucose with unaltered biological fitness, which was defined by the maximum specific growth rate and biomass yield.

Initially, workflows were developed on a robotic Mini Pilot Plant (MPP), for example, to harvest cell-free cultivation supernatants from BioLector cultivations in response to individually defined triggers. Subsequently, assays for amino acids and D-glucose were established in 384-well plate scale in order to quantify these metabolites in cell-free culture supernatants in fully automated workflows [1].

During initial reference experiments, protocatechuic acid was identified as a hidden co-substrate in the well-known defined CGXII medium. The additional TCA feed via acetyl-CoA and succinyl-CoA, which are derived from protocatechuic acid, elevates the growth rate by about 50 % in highly diluted cultures [2].

The first step toward a chassis was the deletion of prophage elements contributing to about 6.7 % of the *C. glutamicum* genome. The respective strain MB001 showed unaltered biological fitness and an increased heterologous protein expression, caused by the removal of a restriction-modification system in prophage CGP3 [3].

As a next step, 36 strains with deletion of non-essential gene clusters were tested thoroughly and 26 clusters were found irrelevant for the biological fitness of *C. glutamicum* and offered the potential to reduce the genome by about 22 % [4]. Some clusters were also deleted in the L-lysine model producer DM1933 and the derived strain GRLP45 showed an 51 % increased L-lysine titer applying the automated MPP methods, what was finally confirmed in lab-scale bioreactors [1].

During the final combinatorial deletion of irrelevant gene clusters, some interdependencies were observed resulting in a decreased of biological fitness of the respective strains. One of those strains was characterized in-depth and revealed the general interplay of ribosome capacity and maximum growth rate of *C. glutamicum*.

In the end, two pre-chassis, namely W127 and W121, were obtained that displayed a total genome reduction of 8.8 % and 12.8 %, respectively. Both strains fulfilled the target criteria of unaltered biological fitness on defined CGXII medium in BioLector cultivations. Finally, the in-depth analysis of both pre-chassis in bioreactors revealed a morphological divergence of W121 which could be narrowed down to a single cluster deletion. However, W127 did not show any drawback compared to the wild type when tested under stress conditions and on different cultivation scales. In fact, this strain even grew faster on some C-sources, making it a good basis for synthetic biology approaches.

Zusammenfassung

Die vorliegende Promotionsarbeit war integraler Bestandteil eines vom BMBF geförderten Verbundprojektes zur Genomreduktion von *Corynebacterium glutamicum*. Ziel war die Entwicklung und Anwendung von Strategien zur Konstruktion eines Chassis-Organismus durch Identifikation und Deletion irrelevanter Gencluster. Zielkriterium der konstruierten Stämme war deren unveränderte biologische Fitness gegenüber der Wildtyp-Form, beurteilt über spezifische Wachstumsgeschwindigkeit und Biomasseausbeute, beim Wachstum auf definiertem CGXII Medium mit D-Glukose.

Unter Verwendung des am IBG-1 verfügbaren Mini Pilot Plant wurden Prozesse zur schnellen Stamm-Phänotypisierung automatisiert und standardisiert. Dazu zählen insbesondere die Schwellwert-abhängige Ernte von zellfreien Überständen aus Mikrotiterplatten-Kultivierungen sowie die parallele Quantifizierung von D-Glukose und Aminosäuren im 384-well Mikrotiterplatten-Maßstab [1].

In ersten Referenzexperimenten wurde Protocatechuat als verborgenes Co-Substrat im CGXII Medium identifiziert. In verdünnten Kulturen erhöht der zusätzliche Kohlenstofffluss aus Protocatechuat über Acetyl-CoA und Succinyl-CoA in den Zitratzyklus die Wachstumsgeschwindigkeit von *C. glutamicum* um etwa 50 % [2].

Zu Beginn der Konstruktion eines Chassis-Organismus wurden drei Prophagen aus dem Wildtyp und damit 6.7 % des Genoms von *C. glutamicum* deletiert. Der resultierende Stamm MB001 zeigte eine unveränderte biologische Fitness sowie eine gesteigerte spezifische Expression heterologer Proteine. Weitere Untersuchungen zeigten, dass diese Steigerung vermutlich durch die Entfernung eines Restriktions- und Modifikationssytems verursacht wurde, welches im Prophagen CGP3 lokalisiert ist [3].

Anschließend wurden 36 nicht-essentielle Gencluster aus dem Stamm MB001 deletiert. Durch Phänotypisierung der Mutanten-Stämme konnten 26 irrelevante Gencluster identifiziert werden, wobei durch deren komplette Deletion das Genom von *C. glutamicum* um insgesamt 22 % reduziert werden könnte [4]. Parallel wurden ausgewählte Gencluster auch aus dem L-Lysin Modellproduzenten DM1933 deletiert. Hierbei zeigte der genomreduzierte Stamm GRLP45 in der Mikrotiterplatte um 51 % erhöhte L-Lysintiter, was im geregelten Bioreaktorsystem bestätigt werden konnte [1].

Bei Untersuchungen von Stämmen mit kombinatorischen Deletionen irrelevanter Gencluster wurden teilweise Abhängigkeiten einzelner Gencluster identifiziert, welche zu einer verringerten biologischen Fitness der betreffenden Mutanten führten. Die detaillierte Charakterisierung der Mutante W65 zeigte einen Zusammenhang zwischen der Anzahl Ribosomen-kodierender Sequenzen und der maximalen Wachstumsrate.

Schließlich konnten die Kombinationsstämme W127 und W121 identifiziert werden, welche eine Genomreduktion von 8.8 % und 12.8 % aufweisen, welche das gesetzte biologische Fitnesskriterium erfüllen. W121 zeigte eine veränderte Morphologie, deren Ursache über die Stammdatenbank des Projektes auf ein einzelnes Gencluster eingegrenzt werden konnte. Stamm W127 zeigte hingegen auch unter Stress-bedingungen unverändertes Wachstum und stellt eine geeignete strukturelle Basis für zukünftige Arbeiten der synthetischen Biologie mit *C. glutamicum* dar.

Table of contents

Abbreviations

Symbols		
μ_{max}	Maximum specific growth rate	[h^{-1}]
BS	Backscatter	[-]
c_{AA}	Amino acid titer	[mol l^{-1}]
CDW	Cell dry weight	[g l^{-1}]
kbp	Kilobase pairs	[-]
k_La	Volumetric oxygen transfer coefficient	[h^{-1}]
ppmv	Parts per million volume parts	[v v^{-1}]
t	Time	[h]
vvm	Normalized aeration rate	[v v^{-1} m^{-1}]
$Y_{X/S}$	Biomass yield	[g g^{-1}] or [backscatter mg^{-1}]

Other	
CGP	*C. glutamicum* prophage
CSV	Comma seperated values
DO	Dissolved oxygen
DWP	Deep-well plate
eYFP	Enhanced yellow fluorescent protein
GC-ToF	Gas chromatography coupled time-of-flight mass spectrometry
GRLP	Genome-reduced L-lysine producer
GRS	Genome-reduced strains
HPLC	High performance liquid chromatography
ISCg	Insertion element of *C. glutamicum*
LC-MS/MS	HPLC coupled tandem mass spectrometry
LOQ	Limit of quantification
MCB	Master cell bank
MPP	Mini Pilot Plant
MTP	Microtiter plate
OD	Optical density
pH	Negative logarithm of the molar H_3O^+ concentration
RPKM	Reads per kilobase gene length and million mapped reads
rpm	Revolutions per minute
TCA	Tricarboxylic acid cycle
WCB	Working cell bank

Substances	
AF204	Antifoam agent 204
DMSO	Dimethylsulfoxid
EtOH	Ethanol
IPTG	Isopropyl-β-D-thiogalactopyranosid
MeOH	Methanol
MOPS	3-(N-morpholino)-propanesulfonic acid
PCA	Protocatechuic acid
RNA	Ribonucleic acid
TRIS	Tris(hydroxymethyl)-aminomethan

Metabolites	
AcCoA	Acetyl coenzyme A
F6P	Fructose-6-phosphate
G6P	Glucose-6-phosphate
NAD(H)	Nicotinamide adenine dinucleotide (reduced)
NADP(H)	Nicotinamide adenine dinucleotide phosphate (reduced)
SucCoA	Succinyl coenzyme A

Enzymes	
G6PDH	Glucose-6-phospate dehydrogenase
HK	Hexokinase
SDH	Shikimate dehydrogenase

1. Theoretical background

1.1 *Corynebacterium glutamicum*

Corynebacterium glutamicum was discovered in 1957 in a soil sample during a screening program for natural amino acid producers. The screening procedure was based on a bioassay in which *Leuconostoc mesenteroids* could only grow, in case an organism in tested samples had excreted the amino acid L-glutamate [5]. Since this isolation for natural L-glutamate excretion capacity, the product spectrum of *C. glutamicum* has been broadened in multiple metabolic engineering approaches to a variety of small molecules including other amino acids, organic acids, bio-plastic precursors as well as ethanol [6, 7]. Nowadays, strains originating from *C. glutamicum* are applied for the industrial production of amino acids at an annual production above 4 million tons, in which L-glutamate, L-lysine and L-methionine are the most prominent ones [8]. These and other amino acids are for example used as flavor enhancer in human nutrition as well as additives for animal feed [9].

One of the key factors for the success of *C. glutamicum* in white biotechnology is its ability to catabolize a variety of carbohydrates, organic acids and alcohols. In contrast to other bacteria, mixtures of such substrates are often metabolized in parallel and monophasic growth is observed without diauxic effects [10]. During growth on substrates entering the energy metabolism directly at the step of AcCoA the glyoxylate shunt is responsible for anaplerotic replenishment [11]. Moreover, during growth and especially during production of TCA cycle derived amino acids such as L-lysine, the oxaloacetate pool needs to be continuously replenished. Here another unique feature of *C. glutamicum* are its two anaplerotic carboxylation reactions using either phosphoenolpyruvate or pyruvate as substrate [12].

Over the decades of strain improvement and systems biology application, first insights into the different omics layers of *C. glutamicum* were gained. One major event in this process was the whole genome sequencing in 2003, which allowed targeted strain modifications in the following [13, 14]. As a consequence, several metabolic engineering approaches were performed to improve production attributes of several strains by targeted gene knockout, gene multiplications and

gradual promoter fine tuning [15–17]. Later, such metabolic modifications were enhanced by the transfer and expression of whole heterologous pathways in *C. glutamicum* in first synthetic biology approaches. With such approaches the product and substrate spectrum of this versatile bacterium can be further extended, i.e. by enabling the efficient catabolism of naturally unusable C-sources like D-xylose or D-methanol [18, 19].

1.2 Synthetic biology

1.2.1 Concept of synthetic biology

Advances in the life sciences in the last decades appeared in major stages which were often driven by methods and technologies available. One of the earliest trends in molecular biotechnology was the analysis and basic alteration of microbes, enabled by molecular tools like Sanger sequencing, cloning and plasmid transfer. Later these investigations were extended to a more overall view in the age of systems biology, which was among others based on genome sequencing, transcriptomics, mass spectrometry and advanced modelling [20].

Based on the resulting knowledge, synthetic biology approaches were started in the early 21th century [5]. Here the focus was shifted from the sole understanding of organisms to a sophisticated construction of artificial biological entities. Therefore, engineering principles were introduced to the field of life sciences which until then lacked such concepts like orthogonality of parts, modular design and standardization. However, once these prerequisites will be completely fulfilled, the design and construction of organism from scratch could revolutionize biotechnology, comparable to the transfer of chemistry from laboratory research to economically relevant chemical engineering around the year 1890 [22].

One exemplary breakthrough in synthetic biology was the establishment of the pathway for artemisinic acid synthesis in baker's yeast, which was transferred from the plant *Artemisia annua* and allows efficient production of precursors for the potential antimalarial drug artemisinin [23]. Noteworthy, over 150 man years were necessary in order to turn the microbe into an efficient producer of artemisinic

acid, what clearly demonstrates that synthetic biology is still far from routine application [24].

Another important step toward the design of artificial cells from scratch was the transfer of a chemically synthesized chromosome to *Mycoplasma capricolum* [25]. However, this event cannot be considered as construction of a synthetic organism, since a natural cell was still necessary as recipient. In contrast, the integration of synthetic pathways in addition to a recipients genome is today routinely applied [26]. In those approaches genetic elements are often referred to as BioBricks, which should operate completely interchangeable like building blocks of electric circuits. Consequently, to stay in the picture of electric circuits, a structural basis comparable to a motherboard is necessary in order to assemble genetic BioBricks and allow their efficient expression in a biological system. In synthetic biology, this structural basis is often referred to as chassis or minimal cell, which should not influence the function of any inserted genetic device (orthogonality principle) and display a minimal biological complexity in order to ensure a fully predictable behavior of the constructed system [27, 28]. However, the vision of this ideal behavior is questionable, as biological systems are extremely context-dependent, tend to counteract and are often not fully understood on molecular level [29].

In summary, the emerging field of synthetic biology aims for the rational construction of artificial pathways and organisms to enable biological functions beyond those occurring in nature. Consequently, engineering principles must be incorporated into life sciences by standardization of methods and devices in order to allow the reproducible construction and robust function of the drafted biological entities [30]. Two prerequisites for those approaches are a library of well-characterized genetic fragments and a robust structural basis. The latter is constructed in this work in form of a chassis organism by heading for the simplification of *C. glutamicum* to its core gene set as defined in the following chapter.

1.2.2 Chassis, minimal cells and relevant genes

Organisms designed as structural basis for synthetic biology are generally described as a cell with a comparable small genome and the minimal properties of any living organism, such as: i) encapsulation ii) storage of information iii) gene expression and iv) cell replication. These rather loose and non-quantitative criteria have resulted in multiple former approaches heading for the construction of such a structural basis, which are not directly comparable among each other [27, 31]. Unfortunately, such inconsistent definitions inherently contradict the engineering principles that are fundamental for synthetic biology. The importance to formulate clear criteria and precisely define the termini used for synthetic biology projects has been emphasized in a recent critical commentary [29].

Consequently, when constructing an organism for synthetic biology it is of outmost importance to formulate clear target criteria, for example, by keeping potential industrial applications in mind. In any case, the identity and quantity of the required gene set is greatly influenced by the criteria the organism should fulfill. One important constraint is the medium in which the organism should be able to grow. In a highly enriched medium (i.e. complex medium) an organism might for example not require the biosynthesis pathways for amino acids, but is strictly depending on the transporters for those molecules.

In this work organisms that are restricted to an essential gene set and, consequently, can grow exclusively in a rich medium are defined as “minimal cells” (Figure 1.1). One example for such an organism is *Mycoplasma genitalium* whose genome consists of only 485 genes from which 100 can be disrupted one at a time [25]. However, the growth of *M. genitalium* is comparably slow and requires a highly enriched medium, since this parasitic bacterium lacks many anabolic pathways, for example, to synthesize fatty and amino acids [32]. Clearly, such minimal cells are unfavorable for industrial biotechnology as reasonable growth rates and strain stability against environmental fluctuations are key factors for any production host.

A more promising type of a genome-reduced organism for industrial applications is a “chassis”, which is in this work defined as an organism that maintains the growth behavior and application range of the respective wild type. Clearly, the genome of such a chassis is larger compared to a minimal cell, since certain gene functions must be added to the essential gene set. Those additional genes are henceforth called “relevant genes” and ensure the biological fitness of the chassis at wild-type level under any predefined condition (for example exponential growth on defined medium). Per definition, the resulting relevant gene set cannot be minimal as it still covers a fully functional anabolism, which is required to establish a reasonable host for a broad range of biotechnological applications.

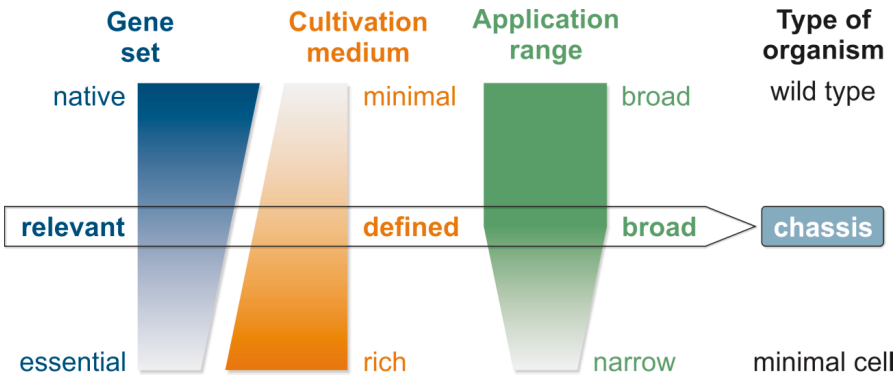

Figure 1.1: Definitions referred to in this work considering types of organisms and the underlying interplay of their gene set, cultivation medium and application range - modified from Unthan *et al.* 2014 [4].

1.2.3 Genome reduction toward a chassis

A chassis construction can either be conducted following a top-down or bottom-up strategy. The latter would include the synthesis and linkage of all essential cell components, starting from an artificial membrane system and ending at a synthetic chromosome. Such a rigorous bottom-up approach is currently not in sight, although the transfer of a large chromosome between two mycoplasma species was reported recently [25]. Hence, at the moment the most promising way to construct a chassis is the top-down strategy, in which an existing cell is trimmed to its relevant gene set following a targeted or untargeted strategy. A prerequisite for the latter approach is a tool that randomly excises parts of the starting genome without deletion hot-spots and allows the subsequent annotation of all deletion sites. An advantage of this untargeted method is that it does not require a detailed knowledge about the starting organism beforehand. However, if such pre-knowledge is available the chassis can be constructed by deletion of specific fragments that are classified as irrelevant in a targeted top-down approach.

In case of *C. glutamicum* a deep insight into the interplay of genome and phenotype was gained during extensive metabolic engineering and systems biology in the last decades. This existing knowledge, together with potential industrial applications, makes *C. glutamicum* a promising candidate for the construction of a chassis. In a previous publication, the targeted deletion of 11 distinct regions with a total size of 250 kilobase pair (kbp) was reported in the strain R [33]. The most successful trial in terms of deletion size was, however, performed via insertion and excision in an untargeted approach, but resulted in multiple growth defects of the constructed strains [34].

In this work, a chassis was constructed from the soil bacterium *C. glutamicum* in a targeted top-down approach (Figure 1.2). The work was performed in a cooperation project with academic partners from Jülich, Bielefeld and Cologne as well as industrial partners from EVONIK industries and Insilico. The project was funded by the Federal Ministry of Education and Research of the Federal Republic of Germany (BMBF, Grant. No. 0316017). Initially, large genome segments without essential genes were identified as target regions for deletion. Those strains were then constructed by the academic project partners and subsequently tested for

biological fitness. This biological fitness was defined as maximum growth rate and biomass yield on defined CGXII medium with D-glucose, as sole carbon and energy source. Both growth parameters represent important criteria in industrial biotechnology. Those clusters that can be deleted from the wild-type background without a drop in both fitness parameters were considered as irrelevant under the tested conditions. Finally, those irrelevant clusters should be deleted in combination to construct a chassis of *C. glutamicum*. After deletion of irrelevant genes, this chassis should show a decreased metabolic burden, what could further improve industrial production processes, for example, when production of amino acids competes with the biomass formation. However, the reduction of lowly transcribed DNA on its own cannot be expected to significantly decrease the energy demand for biomass formation in *C. glutamicum* [35]. Instead, highly expressed but irrelevant genes must be deleted in order to eventually lower the cells metabolic burden, what might result in elevated growth rates, biomass yields or ultimately improved product formation.

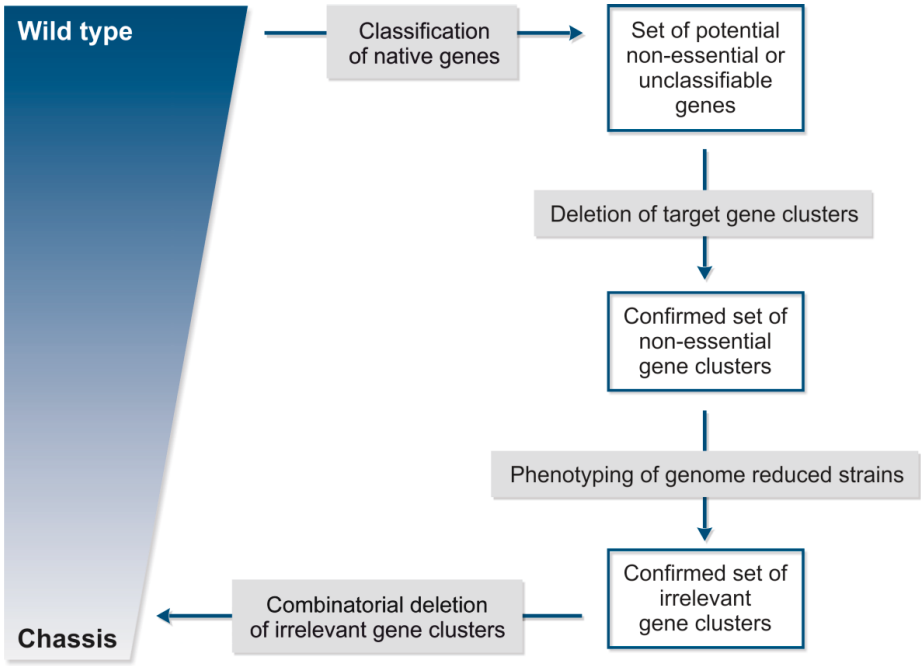

Figure 1.2: Outline of the targeted top-down approach followed in this work to construct a chassis organism based on the *C. glutamicum* wild type ATCC 13032 - modified from Unthan *et al.* 2014 [4].

1.3 Laboratory automation for bioprocess development

1.3.1 Throughput and scale of experiments in biology

Time is one of the limiting factors during the establishment of new bioprocesses, which until now forces process engineers to draw conclusions from few experiments with little process insight. However, miniaturized cultivation devices and liquid handling platforms become more feasible nowadays and will therefore support process engineers to take decisions quicker and based on a deeper process understanding in the near future.

One starting point for this trend was the development of sophisticated parallelized cultivation devices in the last decade. Some of those devices overcame previous limitations in process conditions encountered during low-volume cultivation (i.e. oxygen transfer) and, moreover, allowed process insight by monitoring of biomass, pH, dissolved oxygen, fluorescence or respiratory activity [36–38]. Screening approaches in such sophisticated mini-bioreactors led to better clone selection as compared to incubation in classical microtiter plates [39]. Thus, miniaturized devices have been widely applied to screen mammalian cell lines and microbial producers in the last years [40, 41]. Recently, options for pH regulation and substrate feed were established using microfluidic channels and enzymatic substrate release, respectively [42, 43]. The tremendous success of high throughput cultivation technology in today's bioprocess development was recently summarized by Long et al. [44].

Nevertheless, parallelization of cultivation experiments does on its own not fully remove bottlenecks in bioprocess development, because manual work is still required to start, sample and analyze cultivations. Consequently, cultivation devices should be integrated into liquid handling platforms to allow complete automation of bioprocess development. However, until now only few proof of concept studies exist in this evolving field [45–48].

The general benefits of any liquid handling platform are faster sample processing, automatic generation of log files and higher reproducibility of results, because pipetting actions do not depend on the accuracy of manual operators [49, 50]. Nevertheless, manual operators can proactively optimize their pipetting behavior

(i.e. dispension speed) to a liquids property, while liquid handling platforms strictly follow pre-defined protocols and are therefore less flexible. Consequently, these platforms need to be initially adjusted to different liquid properties and require routine verification in order to obtain reliable results [51].

However, once these routines are established liquid handling platforms can drastically increase the throughput of experiments. Thus, these platforms are already standard in today's red biotechnology industry, for example, during screening of substance libraries for drug target interactions [52, 53]. In contrast, for white biotechnology industry a similar breakthrough of automation technology is desired but still not present. One reason for this delay is most probably that complete bioprocess experiments are much more complex than substance screenings. Nevertheless, the ongoing development of strains by random mutagenesis as well as multifactorial bioprocess optimization make automation strategies a crucial opportunity for white biotechnology industry [54–56].

1.3.2 A Mini Pilot Plant for bioprocess automation

The robotic workstation used in this work was implemented as a tool for screening and optimization of organisms as well as cultivation processes by Rohe et *al.* [57]. It comprises a fully functional toolbox for cultivation, sampling and subsequent sample analysis and is denoted as Mini Pilot Plant (MPP) in the following. An overview of the complete platform is presented in Figure 1.3. Noteworthy, the MPP was specially customized to allow those unit operations that are of special interest during bioprocess development.

The core of the MPP is a Perkin Elmer Janus Workstation equipped with two arms for liquid transfer as well as plate movement. The pipetting arm operates 8 teflon-coated steel tips with individual syringe pumps, using water as hydraulic fluid. The narrow tip diameter allows pipetting in 384-well plates and conductance measurements enable liquid detection during aspiration or dispension steps. Moreover, the hydraulic system as well as the tips can be flushed with 70 % ethanol in order to decontaminate the pipetting system. Noteworthy, the complete MPP is encapsulated in a laminar flow hood to establish a sterile environment.

On the pipetting deck, devices are integrated for sample mixing up to 3000 rpm, cooling down to -10 °C as well as heating up to 95 °C. Next to this deck, a MTP centrifuge and a photometer are placed, which can be reached by the grabber arm due to an elongated movement track. The MPP is completed by a BioLector cultivation device which can be reached by the pipetting arm for dosing and sampling of cultivations.

The BioLector allows the parallel cultivation in 48-well MTPs with a working volume of 1 ml and time-dense online-monitoring of culture properties. This monitoring comprises backscatter as biomass equivalent, fluorescence intensity, pH as well as dissolved oxygen concentration by the use of optodes [37, 58–60]. All these values are measured non-invasively while the plate is shaken, in order to avoid disturbance of the cultures. The baffled geometry of the so called FlowerPlates and optimized shaking diameter allows k_La-values above 600 h^{-1}, which are higher compared to values obtained in standard 96 round well plates (k_La<175 h^{-1}) [61, 62].

Finally, all processes on the MPP are executed using two computer programs. First, the WinPrep software controls the liquid handling platform as well as a centrifuge, photometer and different shakers. Moreover, the WinPrep software allows execution of batch-files, which is useful during handling of CSV-based pipetting lists. The second software is the RoboLector Agent, which controls the interaction of the liquid handling platform with the BioLector. Here, the WinPrep software is advised by the RoboLector to initiate pipetting actions, when pre-defined trigger conditions are reached in any well of the BioLector cultivation.

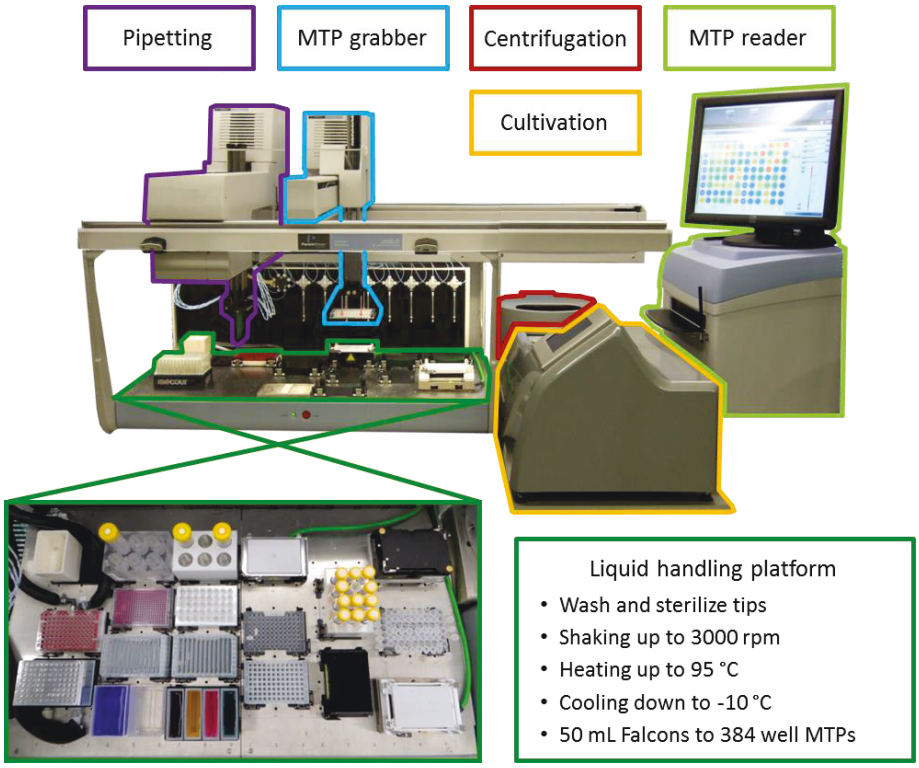

Figure 1.3: Setup of the mini pilot plant (MPP) used in this work. The Janus workstation liquid handling platform was extended by devices for shaking, incubation, microtiter scale cultivation, centrifugation and photometric analysis.

1.4 Aim of this work

The aim of this work is the robot-assisted phenotyping of genome-reduced *Corynebacterium glutamicum* strains in order to guide the way toward a chassis organism for synthetic biology.

To draft a chassis organism the genome of *C. glutamicum* first needs to be analyzed for deletion targets. In the following, these targets are deleted by project partners and the obtained strains need to be characterized. Therefore, workflows are developed and standardized in order to reproducibly handle and characterize a large number of strains. These strains are evaluated for biological fitness, which is defined by maximum growth rate and biomass yield on defined CGXII medium with D-glucose.

Those clusters that can be deleted without a drop in both fitness parameters should considered as irrelevant for the aimed chassis. Finally, a consolidated list of irrelevant gene clusters has to be generated, from which a chassis organism could be constructed by combinatorial deletions. In the end, the question is answered to which degree the genome of *C. glutamicum* can be reduced. Moreover, a chassis organism will allow a deep insight into the organization of the metabolism of *C. glutamicum* based on a simplified genetic arrangement.

During the successive screening of the genome-reduced strain library, some strains are expected to display impaired biological fitness, whenever a non-essential but relevant gene has been deleted. If possible, those strains are quantitatively phenotyped using a variety of omics methods in order to identify a single contributing gene or group of genes and deduce further knowledge about their function. These investigations might ultimately lead to the discovery of so far unknown gene functions that are relevant for the growth of *C. glutamicum* on defined medium.

Some irrelevant gene clusters are also deleted from the model L-Lysine producer DM1933, in order to evaluate if genome reduction serves as a promising tool for industrial strain development. Thus, robotic workflows are designed to screen such producer strain libraries for altered product formation. Here, parallelized cultivations is extended by triggered sampling, supernatant clarification and metabolite quantification.

2. Materials and Methods

2.1 Materials

2.1.1 Chemicals and enzymes

All chemicals used in this work were purchased from SIGMA-ALDRICH or MERCK in research or analytical grade. Enzymes were purchased from SIGMA-ALDRICH or Roche Applied Science. Further details considering the origin or grade of chemicals and enzymes are given in the particular method description if crucial.

2.1.2 Strains

All strains were constructed by the protects partners in Bielefeld (AG Wendisch, AG Kalinowski), Cologne (AG Krämer) and in Jülich (AG Frunzke) by deletion of gene clusters from the *C. glutamicum* genome by double crossover as previously described [3, 4, 63]. Some deletions were carried out in the prophage-free strain MB001 after additional deletion of two insertion elements (ISCg1, ISCg2) and are denoted as genome-reduced strains (GRS). In addition, selected regions were deleted from the prophage-free L-lysine producer DM1933 to obtain genome-reduced L-lysine producers (GRLP). In total, 113 strains were used in this work and listed in the supplement (Table S-1).

2.1.3 Growth media

For growth media all chemicals were purchased from SIGMA Aldrich. Cultivations were performed on the defined CGXII medium [64]. The composition was varied for BioLector or bioreactor cultivation experiments and the medium was enriched for selected experiments (Table 2.1). During medium preparation, some substances were added sterile after autoclaving (D-glucose, PCA, biotin, trace elements, AF204, vitamins) and 4 M NaOH was used to adjust pH 7.0. In selected experiments the concentration of PCA was varied in the range between 0.6 mg l^{-1} and 2.5 g l^{-1}. In experiments with C-source variation 55.5 mM D-glucose was exchanged while keeping carbon moles constant by either of the following: 166.5 mM acetate, 66.6 mM D-arabitol, 55.5 mM citrate, 55.5 mM D-fructose, 55.5 mM D-gluconate,

83.3 mM D-malate, 27.8 mM D-maltose, 111 mM pyruvate, 83.3 mM succinate or 27.8 mM D-sucrose.

Table 2.1: Media used in this work with composition per liter of distilled water.

Substance	CGXII BioLector	CGXII Bioreactor	Enriched CGXII BioLector
$(NH_4)_2SO_4$	20 g	20 g	10 g
K_2HPO_4	1 g	1 g	1 g
KH_2PO_4	1 g	1 g	1 g
$CaCl_2*2H_2O$	13.25 mg	13.25 mg	13.25 mg
$MgSO_4*7H_2O$	0.25 g	0.25 g	0.25 g
$FeSO_4*7H_2O$	10 mg	10 mg	10 mg
Biotin	0.2 mg	0.2 mg	0.25 mg
Protocatechuic acid	30 mg	30 mg	30 mg
$MnSO_4 * H_2O$	10 mg	10 mg	10 mg
$ZnSO_4 * 7 H_2O$	1 mg	1 mg	1 mg
$CuSO_4 * 5 H_2O$	0.313 mg	0.313 mg	0.313 mg
$NiCl_2 * 6 H_2O$	0.02 mg	0.02 mg	0.02 mg
D-glucose	10-40 g	10 g	40 g
Urea	5 g	-	5 g
MOPS	42 g	-	42 g
AF204	-	300 ppmv	-
Yeast extract	-	-	6 g
L-threonine	-	-	238 mg
Thiamine-HCl	-	-	0.5 mg
Cyanocobalamin	-	-	0.1
Pyridoxine-HCl	-	-	2.5 mg

2.1.4 Robotic platform

Robotic workflows were performed on a platform established by Rohe *et al.* 2012 that is denoted as mini pilot plant (MPP) in the following [57]. The MPP consisted of a JANUS Workstation (PerkinElmer, Waltham MA, USA) equipped with a pipetting arm (Varispan) with 8 steel needles and a gripper arm. The movement track of both arms was extended by 40 cm in order to reach positions outside of the pipetting deck. In this open area three devices were placed, namely a BioLector (m2p-labs, Aachen, Germany), a MTP centrifuge IXION (Sias, Hombrechtikon, Switzerland) and a MTP photometer EnSpire (PerkinElmer, Waltham MA, USA). Cooling of samples on the MPP down to -10 °C was performed on a DWP cooling rack (MeCour, Groveland MA, USA) connected to the cryostat Unichiller (Huber, Offenburg, Germany).

2.2 Methods

2.2.1 Strain libraries

All strains were received from project partners on agar plates and colonies were suspended in 0.9 % (w v^{-1}) NaCl with 20 % (v v^{-1}) glycerol and stored at -80 °C as a master cell bank (MCB). From each MCB vial 10 µl were added to two wells of a Flowerplate (m2p-labs, Baesweiler, Germany) of which one well was filled with 990 µl defined CGXII medium and the second well with an equal amount of enriched CGXII medium. This plate was then incubated for 48 h in a shaking device at 1000 rpm, 75 % humidity and 30 °C. In this step, working cell banks (WCBs) of all strains were generated from cultures that had been adapted to both media variants. After incubation, the optical density in each well was measured and adjusted to OD = 20 using a 0.9 % (w v^{-1}) NaCl solution. Finally, glycerol was added to 20 % (v v^{-1}) and the derived WCBs were stored in aliquots in sterile microtiter plates at -80 °C.

2.2.2 Cultivation in microfluidic chips

Cultivation in microfluidic chips were performed in cooperation with the Microscale Engineering group (Jülich, Germany) on the in-house developed polydimethylsiloxane system that enables the spatio-temporal analysis of growing microcolonies with single cell resolution. Each chip device contains of about 400 microfluidic cultivation chambers of 1 µm x 60 µm x 60 µm in size, which are connected to media supply channels. Through these channels, media is continuously perfused to maintain constant environmental conditions and mass transport inside the cultivation chambers is based solely on diffusion. Further details about chip fabrication, cultivation and data analysis are described in detail in publications by Grünberger *et al.* [65, 66]. In some experiments supernatant samples of cultures were taken from lab-scale bioreactor cultivations, filtered (0.22 µm), stored at -20 °C and later used as medium for chip cultivations.

2.2.3 Cultivation in microtiter plates

Microtiter plate cultivations were carried out in 48-well FlowerPlates (m2p-labs GmbH, Baesweiler) with DO and pH optodes in a BioLector (m2p-labs GmbH,

Baesweiler) at 1000 rpm, 95% humidity and 30 °C. After inoculation the Flowerplates were covered with a gas permeable sterile foil (m2p-labs GmbH, Baesweiler). Measurements for backscatter as well as eYFP fluorescence were applied at gain 20. Cultures were started at an OD ≈ 0.2 by inoculating 990 µl medium with 10 µl of a WCB, which had already been grown on the same medium (defined or enriched CGXII) beforehand. For inoculation each WCB-MTP was used only once and discarded after use. Reference strains (wild type or DM1933) were cultivated on every plate as a control.

2.2.4 Maximum growth rates from microtiter cultivations

To derive growth rates from the BioLector cultivation, each backscatter curve was blanked by the mean backscatter values measured during the first 0.5 to 2 hours of the particular well. Then, all blanked values below the limit of quantification (backscatter=10) were deleted from the data set and the end of exponential growth was determined from the time point when the dissolved oxygen stopped dropping in each cultivation. Finally, exponential functions were fitted to the remaining dataset and the estimated growth rates were analyzed for significant changes compared to the reference organisms (wild type or DM1933). Here, the f-test ($p<0.01$) was used to detect significantly altered variances in the growth rate distribution of the particular strain and the reference. Subsequently, the two-sided t-test ($p<0.01$) was performed either as homoscedastic or heteroscedastic test, depending on the outcome of the previous f-test.

2.2.5 Cultivation in lab-scale bioreactors

Lab-scale bioreactor cultivations were carried out in batch mode with 1 l medium in four parallel bioreactors (Eppendorf AG, Jülich, Germany), which were equipped with a stirrer (two rushton turbines), sample port, off gas condenser and probes as denoted in the following. All cultivations were inoculated directly from cryo culture aliquots, which had been prepared from exponentially growing cultures on CGXII medium. During cryo preparation, the cells were harvested at OD = 10 washed with 0.9 % (w v^{-1}) NaCl and stored at -80 °C in NaCl solution containing 20 % (v v^{-1}) glycerol. For later inoculation, one of these aliquots (0.5 ml) was washed and added to the bioreactor. Sampling as well as monitoring of growth was started when

cultures had reached an OD>0.5 on the next day, except for selected experiments that were monitored directly using the sensitive Coulter Counter Multisizer 3 (Beckmann Coulter, Inc.). Aerobic process conditions were maintained by regulation of dissolved oxygen concentration (DO) to 30 % under constant air flow (1 vvm) by adjustment of the stirrer speed (200-1200 rpm, p = 0.1, T_i = 300 s). The pH of the cultures was regulated by addition of 4 M HCl and 4 M NaOH to pH 7.0 (p = 10, T_i =2400 s, no auto-reset, deadband = 0.02 pH). Online measurements were taken for pH (405-DPAS-SC-K80/225, Mettler Toledo), DO (Visiferm DO 225, Hamilton) and exhaust gas composition (GA4, Eppendorf AG, Jülich, Germany).

2.2.6 Biomass quantification from bioreactors

Growth of batch cultures at low initial biomass concentrations (OD<0.5) was tracked with the sensitive Coulter Counter Multisizer 3 (Beckmann Coulter, Inc.), equipped with a 30 µM capillary. Here, samples were diluted with CasyTon (Roche Diagnostics GmbH) to an approximate OD≈0.1 and measured for cell number as well as biovolume of each detected cell. When cultures had grown higher, the measurement of optical density and cell dry weight (CDW) were performed additionally to the Coulter Counter measurements. OD was measured after dilution of samples with 0.9 % NaCl in a photometer (UV PharmaSpec 1700, Shimadzu). For CDW 2 ml samples were centrifuged 10 min at 13,000 rpm (Biofuge pico, Heraeus instruments) in pre-weighted reaction tubes. The pellet was washed once with 1 ml 0.9 % NaCl solution and finally dried for 48 hours at 80 °C (Kelvitron T, Heraeus Instruments) before the dry weight was determined.

2.2.7 GC-ToF-MS measurements

GC-ToF-MS measurements were performed using an Agilent 6890N gas chromatograph coupled to a Waters Micromass GCT Premier high resolution time of flight mass spectrometer for untargeted intracellular and extracellular metabolomics. For the latter, 130 µl of 0.22 µm filtrated culture supernatants were frozen in liquid nitrogen and stored at -20 °C until derivatization. For intracellular fingerprints, culture samples including a total cell dry weight of 33 mg were transferred from bioreactors to pre-cooled tubes and centrifuged for 3 min at 4 °C and 5000 rpm (Labofuge 400R, Heraeus instruments). Then, the supernatant was

discarded and pellets were washed with 4 ml 2.7 % NaCl at 4 °C. After a second centrifugation step the supernatant was discarded and drops remaining in the tubes were wiped off, before the pellets were frozen in liquid nitrogen and stored at -80 °C. Subsequently, all frozen cell pellets were solved in 1 ml pure methanol and metabolites were extracted in a sonicator for 30 min at 65 °C. After a final centrifugation step 130 µl supernatant were transferred to fresh reaction tubes, frozen in liquid nitrogen and stored at -20 °C until derivatization. The subsequent derivatization, MS operation, data acquisition and peak identification was performed as described recently by Paczia *et al.* 2012 [67]. The obtained peak areas were finally normalized by the total biovolume of the extracted sample. The used method cannot be used for absolute quantification and consequently only metabolites which exhibited a higher than twofold difference compared to the wild type were considered for further evaluation. Moreover, not all detected metabolites could be evaluated, for example, in case of co-elution with other substances. Additionally, some metabolites were only detected either in the wild type or in the mutant strain, and thus, in these cases a ratio could not be calculated.

2.2.8 LC-MS/MS Analytics

Metabolite concentrations (PCA or amino acids) were measured on a HPLC (X-LC 3000 Series, JASCO GmbH, Gross-Umstadt, Germany) coupled to a mass spectrometer (API 4000, ABSciex, Foster City, CA) with spray ionization. For the analysis cell-free supernatants were first pre-diluted with distilled water to the linear range of the metabolites of interest as defined by the particular LC-MS/MS protocol. The last dilution step was performed with pure methanol to result in a 50 % methanol fraction in order to eliminate artefacts from the running buffer or internal standard. Finally, isotope dilution mass spectrometry (IDMS) was applied as described elsewhere [68]. Further details regarding LC-MS/MS operation and data analytics were described in detail by Paczia *et al.* [67, 69].

2.2.9 Differential transcriptome analysis

Differential transcriptome analysis of cells grown in bioreactors, were performed in cooperation with the working group Regulatory Switches and Synthetic Biology (Jülich, Germany). In short, cells were cultivated on defined CGXII medium in four

bioreactors of which two were harvested at OD = 0.2 and the remaining at OD = 2. Culture samples were cooled quickly by mixing with crushed ice and cell pellets were obtained by centrifugation at 4 °C, which were finally stored at -20 °C after freezing in liquid nitrogen. Subsequently RNA and fluorescently labeled cDNA were prepared from the cells as described elsewhere [70]. Further processing of samples, microarray preparation, data acquisition and analyses are described in detail in Unthan *et al.* 2013 [2].

2.2.10 Robotic workflow for automated harvest

Robotic workflows were developed on the MPP introduced in chapter 2.1.4. and are in detail described in Unthan *et al.* 2015 [1]. BioLector cultivations that were intended for automated sampling were measured in 22 minute measurement cycles and the derived backscatter values were monitored by the RoboLector agent software (m2p-labs, Aachen, Germany). Harvest actions on the MPP were initialized 3 hours after backscatter thresholds were reached in any of the 48 cultivation wells. In the next step, the RoboLector software paused the BioLector and created a CSV-based handshake file, which was used by the liquid handling platform to transfer 500 µl sample from the BioLector to a DWP. Batch files were executed by the WinPrep software (Version 4.6, PerkinElmer), to first copy and then delete the original file, what triggered the restart of the BioLector cultivation. When the cultivation was running again, the copied handshake file was used to automatically fill a tare DWP and centrifuge both DWPs at 4500 rpm for 5 minutes (IXION, Sias AG, Switzerland). Cell-free supernatants were subsequently aspirated at fixed height of 4 mm above well bottom and frozen in a third DWP at -4 °C (Unichiller, MeCour, Groveland MA, USA) before the tare plate was emptied at the same height. The described cycle took 12 to 17.5 minutes and was in some cases extended by measurements of optical density in 96 well microtiter plates. The developed workflow runs repetitively and completely autonomous with variable number of samples and without manual replacement of consumables.

2.2.11 Automated metabolite quantification

Quantification of D-glucose and amino acids was established on the MPP by adapting established protocols to microtiter scale [1]. First, a two-step enzymatic

assay was used to quantify D-glucose in cell-free supernatants on the MPP. Here, a mastermix was prepared freshly by mixing 47.4 ml TRIS-maleat buffer (100 mM, pH 6.8), 2.2 ml $MgSO_4$ solution (100 mM), 1 ml NAD^+ stock (50 mg ml^{-1}), 1 ml ATP stock (34 mg ml^{-1}) and 236 µl Hexokinase / Glucose-6-phospate dehydrogenase mix (Roche Diagnostics, Mannheim, Germany). In the MPP workflow the first step was the preparation of three independent dilution series of D-glucose standards (0.4 and 0.01 g l^{-1}) from a 1 g l^{-1} stock solution. Of each of those standards, 20 µl were pipetted in triplicates in a 384-well plate to result in 9 replicates for each standard concentration. Then up to 48 cell-free supernatants were automatically diluted to 1:10 as well as 1:40 by successive aspiration of sample and water and combined dispense in a DWP. Of those 96 diluted samples, 20 µl were transferred to the above mentioned 384-well plate in triplicates. Finally, 100 µl glucose assay mastermix were added to each well and the plate was automatically read at λ = 340 nm in the MPP photometer (EnSpire, Perkin Elmer) after incubation at room temperature for 45 min. During data analysis, raw absorbance values were first normalized by wells with water as sample, before the D-glucose concentrations were calculated according to the standard calibration curve.

To quantify amino acids on the MPP a Ninhydrin mastermix was prepared freshly for each experiment by solving 2 g Ninhydrin in 75 ml DMSO and 25 ml 4 M sodium acetate buffer (pH 6.0 adjusted with 25 % acetic acid). As L-Lysine was the amino acid of interest, a 100 mM solution of L-lysine-HCl was prepared in CGXII medium for preparation of a standard calibration curve. From this stock, three dilution series were pipetted on the MPP with CGXII medium as diluent to obtain standards between 100 and 1.56 mM. Of those three standard series, 30 µl were pipetted to a 384-well plate in triplicates, resulting in 9 replicates of each standard concentration. Then, 45 µl from 48 cell-free supernatants were pipetted in triplicates in the 384-well-plate. In the next step, 15 µl of each of those wells were transferred to another well on the 384-well-plate in which the samples were mixed with 15 µl CGXII medium to obtain 1:2 dilutions of all samples in triplicates. Finally, the reaction was started by addition of 30 µl Ninhydrin solution to the complete 384-well plate, which was then incubated at room temperature, before the reaction was stopped exactly after 4 min by addition of 40 µl distilled water. The 384-well plate was then immediately transferred to the photometer of the MPP in which the

formed Ruhemanns purple was measured at λ = 570 nm. For data analysis, all absorbance values were first blanked by wells with sole medium as samples, before L-Lysine concentrations were calculated according to the standard calibration curve.

3. Results and Discussion

3.1 Genetic organization and essential genes in *C. glutamicum*

In order to identify targets for genome reduction existing knowledge was collected and interpreted in cooperation with all project partners of the project "genome reduction". Details regarding bioinformatics, data collection and interpretation are found in Unthan *et al.* 2014 [4]. In the following the outcome of this initial theoretical approach is presented.

In the first step to identify essential genes in *C. glutamicum*, the conservation of genes in organisms in close phylogenetic distance was condensed in a conservation code. Moreover, the expression of every gene under standard conditions had recently been analyzed by RNAseq of fragmented RNA and this data set was normalized to reads per kilobase gene length and million mapped reads (*RPKM*) in order to obtain a comparable value of relative gene expression levels [71]. Both conservation code and RPKM, were shown to correlate with gene essentiality, as observed by analysis of 435 genes which were proved in literature to be either non-essential or strictly essential (Figure 3.1 A). Based on the existing knowledge, 906 essential genes were predicted in remaining uncharacterized parts of the *C. glutamicum* genome, based on low gene conservation (011, 010 or 001) and RPKM score over 20 [4]. Additional data from published as well as unpublished gene knock-out data were taken into account, to finalize the genetic blueprint of gene essentiality (Figure 3.1 B). It was estimated that 1061 genes are essential while 786 genes are unclassifiable, for example when reports in literature were in contrast to each other. Moreover, the genetic organization of the wild type ATCC 13032 is also influenced by three *C. glutamicum* prophages (CGP) [13]. CGP1 and CGP2 are rather small (13.5 kbp and 3.9 kbp respectively) and highly degenerated, whereas CGP3 (187.3 kbp) is one of the largest known prophages constituting about 6 % of the entire genome. The latter still remains its ability to excise from the genome and exist as a circular, double-stranded phage DNA molecule [72]. The information about gene essentiality status and prophage elements was plotted to a genome-wide map to identify target regions for deletion (Figure 3.1 C).

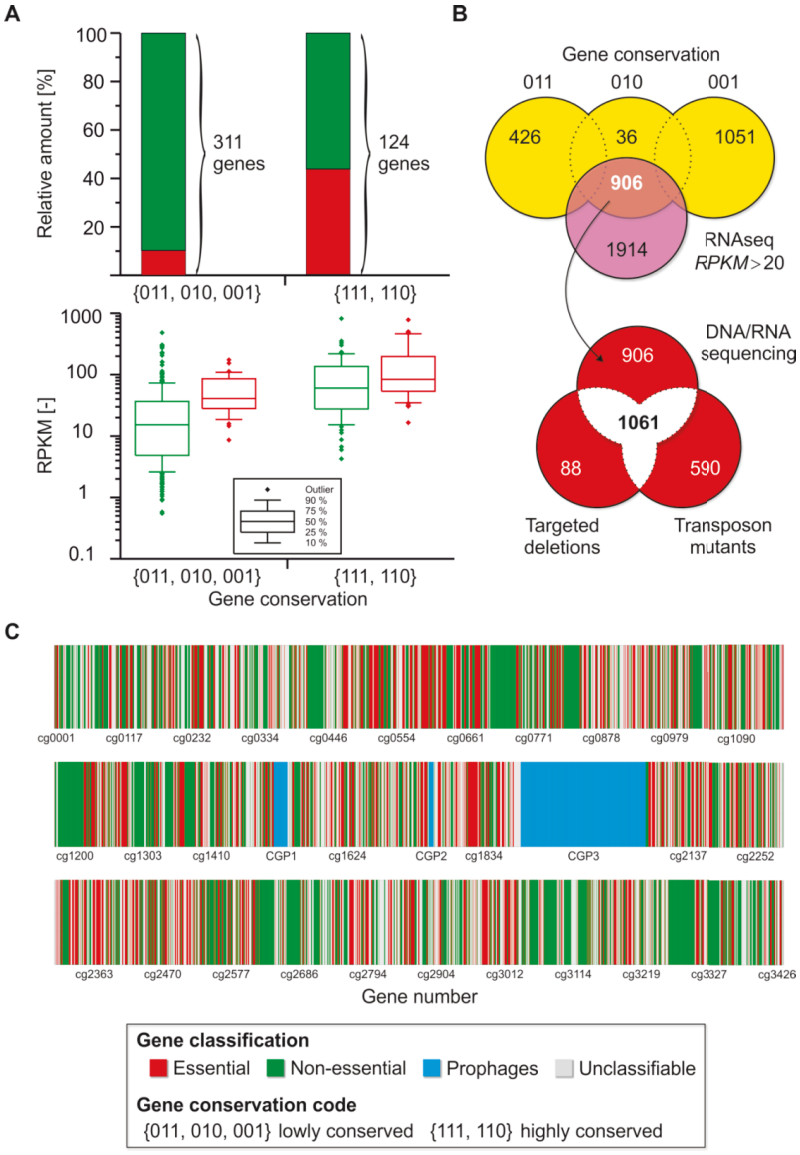

Figure 3.1: Genetic organization and classification of gene essentiality of *C. glutamicum* strain ATCC 13032 - modified from Unthan *et al.* 2014 [4]. (A) A priori analysis based on a set of 435 genes to deduce correlations between gene expression and conservation for a genome-wide gene classification. (B) Estimation of essential genes by combination of RNA and genome sequencing together with knowledge from targeted and untargeted knockout studies. (C) Mapping of genes and their status of the *C. glutamicum* genome to identify deletion targets and draft a chassis organism.

3.2 Validation of wild type growth characteristics on defined medium

3.2.1 Biphasic growth on CGXII medium

Recently it had been reported that *C. glutamicum* wild type grows at specific rates above $\mu = 0.6\ h^{-1}$ on CGXII medium in microfluidic chips, while $\mu \approx 0.4 - 0.45\ h^{-1}$ is typically found in literature [73]. So far, this observation was restricted to this particular cultivation system and had neither been fully understood nor reproduced in any well-established cultivation device. As it was planned to characterize *C. glutamicum* strains after genome-reduction on CGXII medium, the phenomenon was tackled in the beginning of the project to establish a valid standard for the later screening of genome reduced strains.

As a first experiment, the batch growth of *C. glutamicum* wild type was studied in a 1 l bioreactor on CGXII medium in ten biological replicates, each started at comparable low cell densities. The cultivations were inoculated at $N_{t=0} = 1.3 \cdot 10^6 \pm 2.1 \cdot 10^5$ cells ml^{-1} what corresponds to an optical density (OD) of OD≈0.005 or a cell dry weight (CDW) of CDW≈0.002 g l^{-1}. Noteworthy, growth in these highly diluted cultures was tracked by a sensitive Coulter Counter device as the limit of quantification is typically much higher for OD and CDW measurements. The results of the 10 bioreactor cultivations were highly reproducible and indicated that batch growth follows two growth phases with a distinct kink at t≈10 h and a corresponding OD≈0.5 (Figure 3.2 A). This observation was rather surprising, since a biphasic growth pattern is normally not expected during cultivation of *C. glutamicum* on a defined medium with only a single carbon source (here D-glucose). Both phases were analyzed for exponential growth rates separately and are referred to as first and second growth phase in the following.

For the first phase the exponential growth rate was estimated based on cell number measurements as μ_{max} =0.61 ± 0.02 h^{-1} which is in the same range as found for *C. glutamicum* in microfluidic chips [73]. In contrast, during the second phase the growth rate dropped to μ_{max} =0.46 ± 0.02 h^{-1} which is in the range typically reported for growth of *C. glutamicum* on CGXII medium. To exclude any misinterpretation in the separation between the first and second growth phase, the differential growth rates from the data set were determined along the cultivation (Figure 3.2 B). Again, a clear drop in growth rates was observed at 10 h cultivation time, supporting the observation of a biphasic growth pattern on defined glucose medium. Next, potential misinterpretations of the rather unusual biomass signal (cell number) were excluded, by additionally analyzing the total biovolume and the mean single cell volume for all cultivations (supplement, Figure S-1). As a result, the biphasic growth pattern was also observed when relying on total biovolume as biomass parameter. Moreover, the course of the mean single cell volume along the cultivation showed that the cells first grew in size after inoculation, reached a maximum cell size and subsequently became smaller with decreasing substrate availability. These observations are consistent with previous results, in which *C. glutamicum* showed a decreasing mean cell size during carbon limitation after a long-term batch process [67].

In further experiments, the reason for biphasic growth on CGXII medium was investigated. Here it was assumed that a metabolic switch occurred in response to either an accumulation of inhibiting by-products or the limitation of specific media components. To discriminate between these effects, it was necessary to assess the instantaneous growth phenotype in response to dynamically changing media composition at particular time points of the batch cultivation while excluding all side-effects from the cultivation history. Here, cultivation in microfluidic chips was a promising technique, since it can be used to determine division rates and cell morphology, which exclusively result from the predefined medium composition in the inflow. The continuous inflow of fresh medium provides constant substrate availability and prevents the accumulation of potentially growth impairing by-products in the chamber throughout the cultivation [65]. In the following, supernatant samples from the above described bioreactor cultivations were filtrated and subsequently used as growth medium in microfluidic chip

experiments (Figure 3.2 C). As a result, the early bioreactor supernatants that nearly equal the original CGXII medium, led to fast growth of *C. glutamicum* in microcolonies with μ_{max} = 0.65 ± 0.02 h^{-1}, essentially reproducing the results of the first bioreactor phase. Bioreactor samples from later time points led to decreased growth rates of the microcolonies until a local minimum of μ_{max} = 0.46 ± 0.02 h^{-1} was reached, confirming the growth rate of the second bioreactor phase. Interestingly, bioreactor supernatants from late exponential growth phase resulted in a re-switch to fast growth in the microfluidic chip, which might be due to an enrichment of the culture broth with intracellular metabolites during growth on glucose excess [67]. Although only very low concentrations are present (micromolar range) some of these metabolites might serve as additional carbon sources or directly fed into protein synthesis when continuously supplied during microfluidic chip cultivations.

In conclusion, the transfer of supernatants from bioreactor batch cultivations to the continuously flushed microfluidic chip confirmed both bioreactor growth phases and, moreover, excluded artefacts from cell aging or pre-culture as reason for the biphasic growth. Moreover, the key factor for the biphasic growth must have been captured in the culture supernatant as the growth rates from the dynamic batch culture could be transferred to the continuously fed microfluidic chip. Hence, the overall data strongly points to either an accumulation of growth-impairing by-products or limitation of specific media components as reason for decreasing growth rates. Consequently, the composition of the culture supernatant was analyzed over the course of bioreactor cultivation in the following.

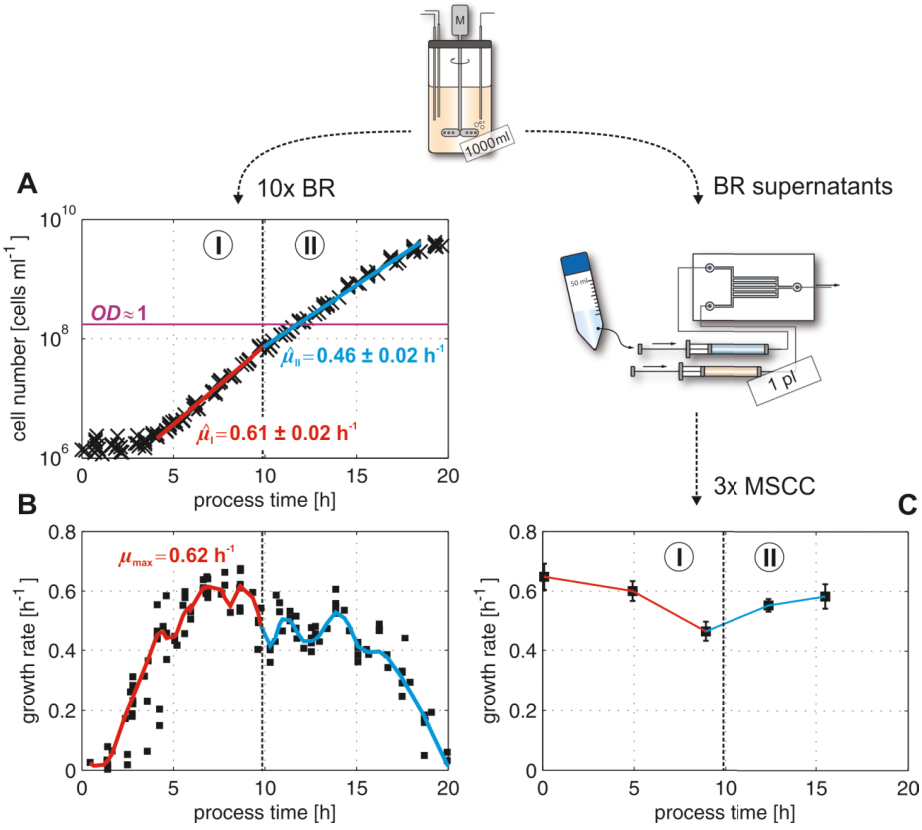

Figure 3.2: Batch cultivation of *C. glutamicum* wild type in 1 L bioreactors in highly diluted cultures reveals a biphasic growth behavior on defined CGXII glucose medium - modified from Unthan *et al.* 2014 [2]. (A) Two distinct growth phases were identified reproducibly (n=10) in which a growth rate of $\mu = 0.61 \pm 0.02$ h^{-1} was encountered during the first phase. (B) Differential growth rates from the cell number measurements were determined along the cultivation to determine the switch from first to second growth phase. (C) Comparable alterations in growth rates were observed, when filtrated culture supernatants of distinct time-points from the bioreactor were used as growth medium in the microfluidic chip.

3.2.2 Identification of a hidden co-substrate in CGXII medium

Metabolite investigations were started with untargeted GC-ToF-MS analysis of supernatant samples from the above shown bioreactor cultivations. It was observed that the potential iron-chelator protocatechuic acid (PCA) vanished from the medium during early cultivation stage (supplement, Figure S-2). Interestingly, it has already been reported that PCA or a comparable iron chelator like, e.g. catechol or citrate, is necessary to initiate cell division in *C. glutamicum* [74, 75]. In the following, PCA was quantified in the bioreactor supernatant samples using targeted LC-MS/MS analytics (Figure 3.3 A). Here, it was observed that PCA was completely consumed within 10 h of cultivation and the time point of total PCA depletion coincided with the minimum in growth rates and the subsequent start of the second growth phase. Most interestingly, recent reports also demonstrated the ability of *C. glutamicum* to consume PCA as carbon source besides its iron chelating function [76–78].

With this target compound at hand a differential transcriptome analysis was carried out to evaluate the gene expression changes accompanied by the turn to the second growth phase. Samples were taken from the bioreactor cultivation 2 hours before and 1.5 hours after the drop in the growth rates and compared to each other with respect of mean mRNA expression (Figure 3.3 B). A complete list of significantly up or down-regulated genes can be found in Table S-2 in the supplement. Nearly all genes of the ß-ketoadipate pathway were significantly up-regulated during the first growth phase (Figure 3.3 C and D). Among other substances, PCA is catabolized in this pathway after the uptake by the putative 4-hydroxybenzoate transporter (encoded as pcaK) via six enzymatic steps to the tricarboxylic acid (TCA) cycle intermediates acetyl-coenzyme-A (AcCoA) and succinyl-CoA (SuCoA) [78, 79]. Interestingly, an up-regulation during first growth phase was also observed for analogous degradation reactions for inositol, gluconate, benzoate and catechol (iolB, iolC, gntP, pobA and catA1). Since *C. glutamicum* originates from soil, this finding might reflect a global transcriptomic response of this organism to substrates occurring in its natural habitat.

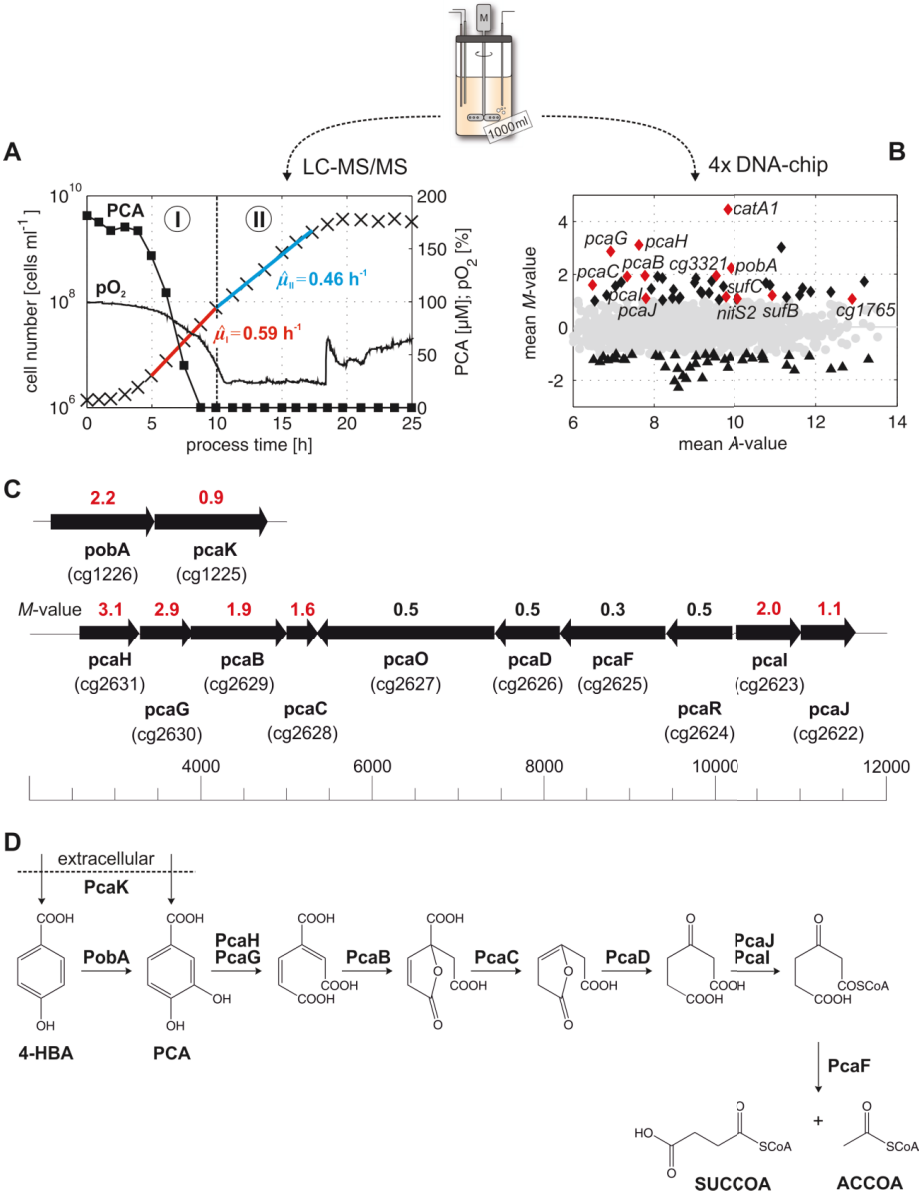

Figure 3.3: In-depth analysis on the biphasic growth of *C. glutamicum* wild type on defined CGXII medium - modified from Unthan *et al.* 2014 [2]. (A) A rapid decrease of extracellular PCA concentration during the first growth phase was revealed via LC-MS/MS measurement. (B+C) Differential transcriptomics revealed an up-regulation of multiple genes encoding for the ß-ketoadipate pathway in cells taken from the first growth phase. (D) PCA catabolism via the ß-ketoadipate pathway of *C. glutamicum*, resulting in TCA intermediates succinyl-CoA and acetyl-CoA.

3.2.3 Medium formulation for strain characterization in microtiter plates

The results from metabolome and transcriptome analysis strongly indicated that PCA causes the biphasic growth of *C. glutamicum* wild type in CGXII batch cultures. However, the effect had never been observed in a bioreactor before because classical biomass indicators (i.e. OD or CDW) cannot resolve culture growth in such highly diluted cultures. However, it was planned to evaluate genome-reduced *C. glutamicum* strains according to their growth rate on CGXII and the newly discovered biphasic growth behavior might affect the later data analysis. Therefore, the applicability of CGXII as medium for strain screening was evaluated in more detail in the following.

In a first attempt it was tested whether PCA can be simply omitted from the growth medium to eliminate the first growth phase. However, in those experiments it was observed that the duration of lag-phases from identically inoculated cultures was prolonged by hours and showed poor reproducibility. Moreover, cultures inoculated at low cell densities often did not establish growth over several days of cultivation (data not shown). These observations with PCA-free medium are in agreement with the first report about the interplay of *C. glutamicum* and PCA, in which it was found that low concentrations of PCA (0.1 mM) are necessary to reproducibly initiate the exponential growth on glucose medium [74]. These early findings had led to the theory that PCA enables the iron import during the complete course of cultivation. The data obtained now, however, indicates that growth at rates typically found for *C. glutamicum* takes place after depletion of PCA (cf. Figure 3.3 A). In conclusion, the biological role of PCA is still not fully understood and may not be restricted to its iron chelating function but should be extended to even the growth of lowly inoculated *C. glutamicum* cultures. As a consequence, PCA was not omitted from the medium formulation during the following cultivations in order to establish an efficient and reproducible screening of genome-reduced strains.

In the following, cultivations were carried out on CGXII medium with different PCA concentrations to test whether the biphasic growth appears in the backscatter signal of the BioLector. Growth media with standard as well as elevated PCA concentrations were used and, as a result, the biphasic growth was visible when

PCA concentration ranged between 4.1 to 16.3 mM, which is 21 to 83-fold above the standard PCA concentration (Figure 3.4 A). Interestingly, the switch in growth rates observed in the PCA rich cultures was accompanied by a step-increase in the DO-signal, which clearly indicated a metabolic switch to a PCA-free phase. Furthermore, the final backscatter value was analyzed with respect to total carbon availability from all cultures (Figure 3.4 B). In short, the increase of PCA at fixed amount of D-glucose led to a proportional increase of the final backscatter values. This observation together with the DO response to PCA-depletion finally proved that PCA is a second carbon source alongside with D-glucose in defined CGXII medium.

Considering the consequences for the strain screening, however, cultures growing on medium with standard PCA concentration of 195 µM undergo the switch of growth phases beneath the LOQ of the backscatter signal. The specific growth rates obtained from backscatter measurements in the second phase were comparable to those found in the bioreactor experiments (cf. Figure 3.2). In conclusion, any BioLector cultivation of *C. glutamicum* on standard CGXII medium exclusively displays the second growth phase after PCA depletion. As this phase is regularly referred to in terms of growth rates, the backscatter measurements from BioLector cultivations can directly be used to evaluate growth phenotypes during screening of genome-reduced *C. glutamicum* strains.

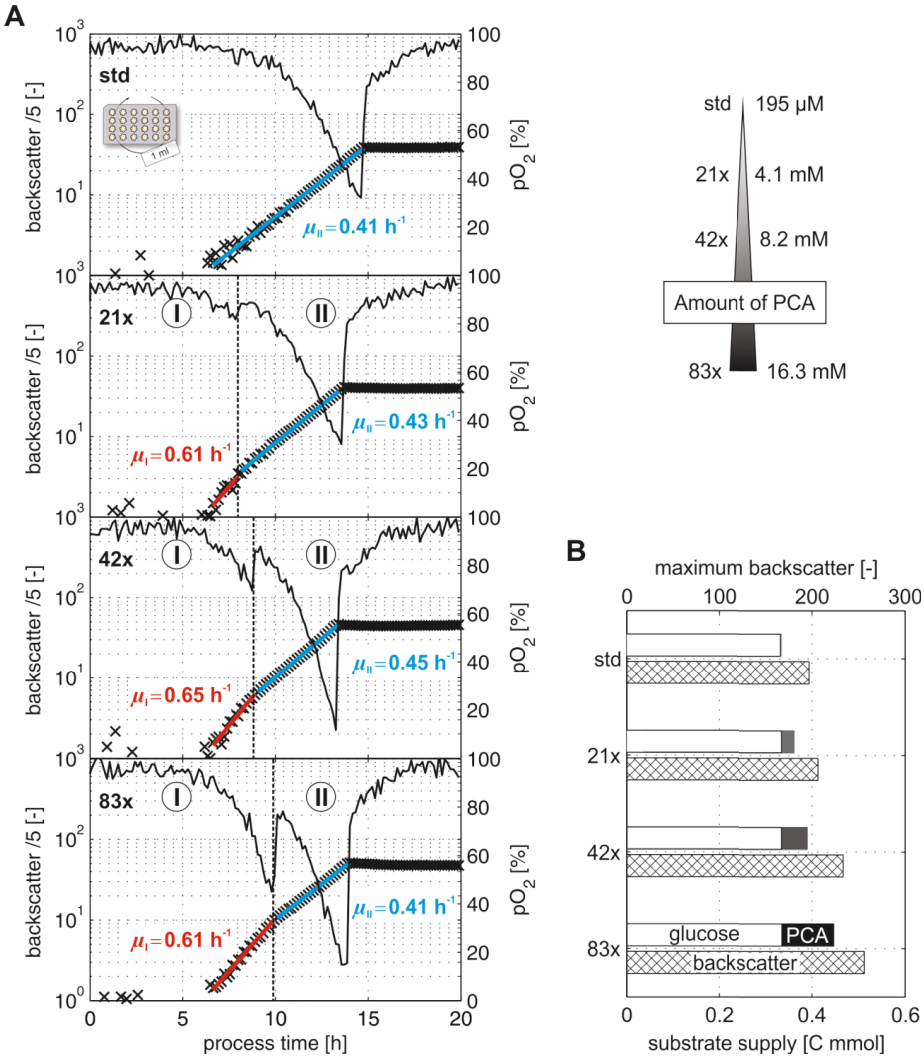

Figure 3.4: Investigations of growth performances of *C. glutamicum* on CGXII medium with altered PCA concentration - modified from Unthan *et al.* 2014 [2]. (A) Cultivations were performed in the BioLector on CGXII medium with standard PCA concentration (195 µM) as well as step-wise increased PCA concentrations up to 16.3 mM (83-fold). The first growth phase is not visible at standard PCA concentration but can be extended to OD ≈ 3 with higher PCA concentrations. (B) Correlation of total carbon supply to maximum backscatter from cultures grown on CGXII medium with varied PCA content.

3.3 Handling and robot–assisted characterization of large strain libraries

3.3.1 Workflow to store and characterize large strain libraries

In the project to construct a chassis organism from *C. glutamicum* wild type, all molecular biology tasks were performed by three project partners on the basis of the initially determined chassis blueprint (cf. chapter 3.1). Strains with deletion of non-essential genes, were received from the project partners on agar plates. Subsequently, all strains needed to be characterized in order to evaluate the relevance of the deleted genes for the biological fitness of *C. glutamicum*. It was crucial to perform this characterization reproducibly and in a short time, in order to give quickly give recommendations for further deletions to the project partners.

Therefore, a workflow was developed to store and characterize large strain libraries (Figure 3.5 A). As a starting point of this routine, biomass from agar plates was suspended in saline solution, from which a first FlowerPlate was inoculated. Here each deletion mutant and reference strain (wild type or DM1933) was cultivated on standard CGXII as well as enriched CGXII medium, in order to adapt the cells to both media variants. Subsequently, glycerol was added to the remaining biomass-saline suspension and the mixture was stored at -80 °C as master cell bank (MCB). The cultivation on both media variants was carried out for two days, until all cultures reached stationary phase. Then the optical density of all wells was measured and all cultures were diluted to OD=26.7 with saline solution. Finally, glycerol was added to reach a final optical density of OD=20 and all suspensions were transferred to multiple sterile MTPs in aliquots, which were subsequently sealed and stored at -80 °C as working cell bank (WCB). For later growth characterization one MTP was thawed, used once as inoculum for one FlowerPlate and discarded after use. This process was later repeated with the remaining WCB plates in order to phenotype all strains in replicates.

During the complete project a total number of 113 strains was received from the project partners. Noteworthy, the majority of these strains were not obtained during the first half of the project, since molecular methods needed to be developed in the beginning (Figure 3.5 B). Once these methods had been established, new strains were constructed rapidly by the project partners and the developed workflow allowed keeping pace during parallel strain characterization. The BioLector data obtained during the phenotyping experiments was analyzed for growth rates and biomass yields, using an excel-routine as described in the following chapter.

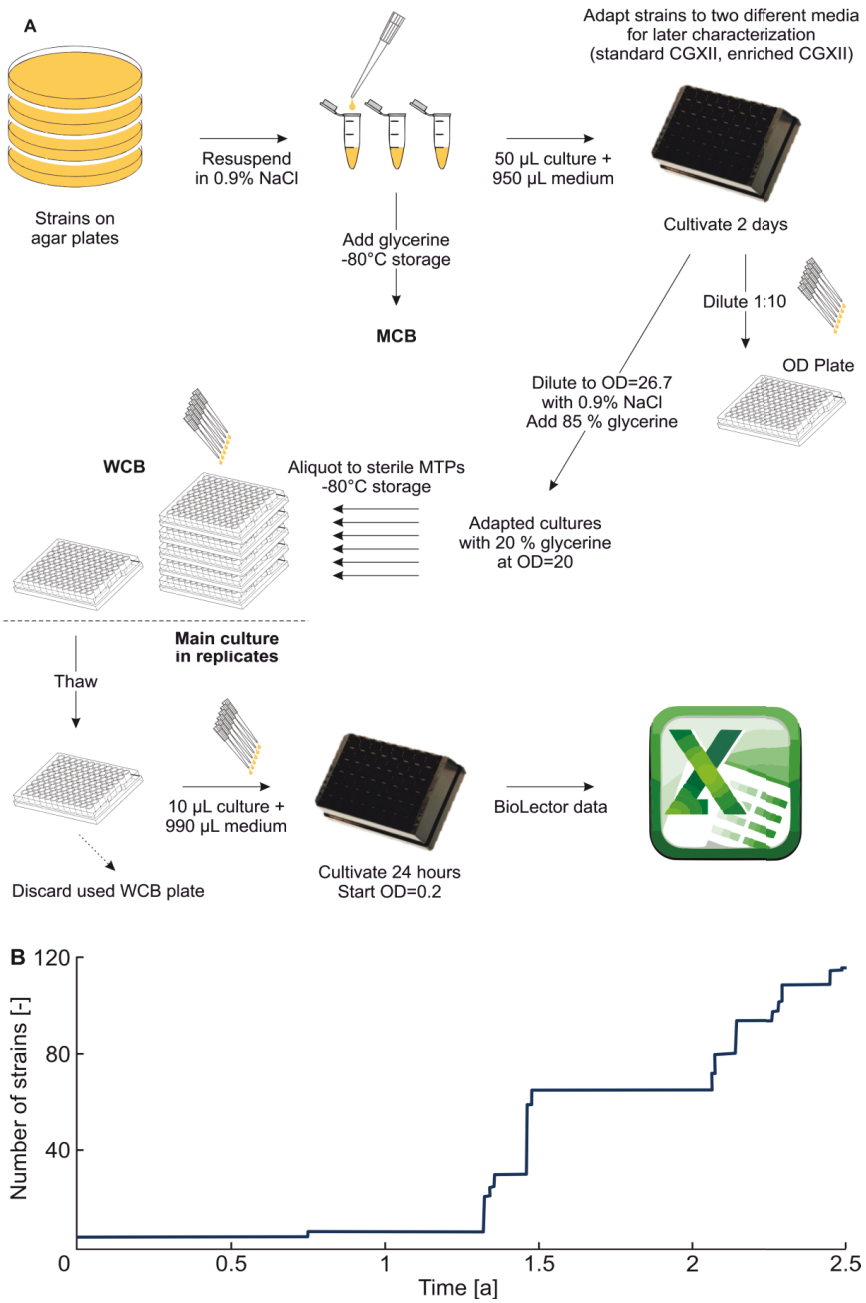

Figure 3.5: Workflow to store and characterize large strain libraries. (A) Strains are obtained on agar plates and stored in a MCB as well as in WCB aliquots after adaption to two different media. (B) Size of the strain library over the course of the genome reduction project.

3.3.2 Standardized data analysis

After standardizing the handling and storage of strain libraries, routines were developed to automatically estimate growth rates and biomass yields from BioLector data. Here a focus was set to strictly define thresholds in order to avoid the subjective selection of data points during the latter estimation of growth parameters throughout different experiments.

The complete data handling was automatized in Excel as described in the following. The raw data of 24 hour BioLector experiments was copied to the Excel routine and each of the 48 cultivations was named with strain and medium used (Figure 3.6 A). Then, each backscatter curve was automatically normalized by subtraction of the mean backscatter value obtained from the period of 0.5 to 2 hours cultivation of the particular well. This was valid since the inoculation density (OD=0.2) was below the limit of detection of the backscatter signal for the first two hours. Each curve was blanked individually, since the 48 wells of a Flowerplate differed to a rather high extent in their optical properties.

In order to estimate specific growth rates of the tested strains, each data set was automatically trimmed to the phase of exponential growth. First, all values below the limit of quantification of the backscatter measurement (LOQ_{BS_gain20}: 10 BS) were deleted from each curve. Secondly, the end of exponential growth was determined from the time when the dissolved oxygen (DO) in each well stopped dropping. Maximum specific growth rates were finally estimated by fitting exponential functions to the remaining set of backscatter values (Figure 3.6 B). Moreover, the maximum biomass value (X_{max}) was determined by averaging the blanked backscatter values of the last two hours cultivation time. Finally, X_{max} was normalized by the mass of substrate applied in the particular well in order to estimate biomass yields, i.e. with the unit BS mg_{GLC}^{-1}.

Finally, all automatically fitted growth curves and their correlation coefficients were plotted together with the raw data in the Excel routine. Thereby, the automated analysis could be controlled quickly to exclude any misinterpretation of the raw data. The developed routine analysis enabled to estimate the growth characteristics of genome-reduced strains at high reproducibility and typically within 15 minutes for 48 cultivations. (cf. Figure 3.12).

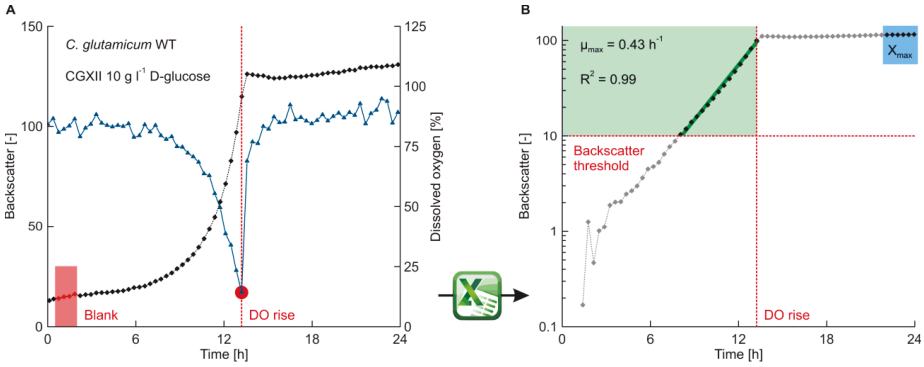

Figure 3.6: Standardized processing of BioLector data in an Excel routine for analysis of large strain libraries. (A) Exemplary raw data of backscatter (gain 20) and dissolved oxygen measurement during a 24 hour cultivation of the *C. glutamicum* wild-type. (B) During automated data analysis, each backscatter curve was first blanked by its initial values (red box). Then a backscatter threshold and the rise in the DO signal were used to trim the data and estimate the maximum specific growth rate from the exponential growth phase (green box). X_{max} was determined from the blanked backscatter values of the last two hours (blue box) and normalized by the applied substrate mass to estimate biomass yields.

3.3.3 Triggered harvesting of cell-free supernatants from BioLector cultivations

For the screening of protein expression hosts on the MPP, it had already been shown that a transfer of cultures to 4 °C at turn to stationary phase, increased the reproducibility of results compared to over-night cultivations [57]. However, for the characterization of genome-reduced strains it was desired to quantify cultivation products, substrates and by-products. The found concentration of these metabolites could have been affected by cell leakage as well as conversion by extracellular enzymes during storage of culture broth at 4 °C for multiple hours. Therefore, in this work the handling of culture samples was extended by steps for a rapid centrifugation in order to remove cells from the samples and freezing at -4 °C to stop any enzymatic activity (Figure 3.7 A).

The newly developed workflow started with the harvest of 500 µl from each BioLector well, provided that the individually defined biomass- or time-dependent trigger for the specific well was reached. A CSV handshake file was generated by the RoboLector Software, which indicated the well number from which culture samples were then pipetted into a 96 deep-well plate (DWP) for subsequent centrifugation. The handshake file was then automatically copied and renamed by a batch script, before the original handshake file was deleted by the liquid handling software. This deletion process served as signal for the RoboLector software to close the BioLector lid and continue the plate incubation after less than 3 minutes. The exact time required for this initial harvest event depended on the number of wells sampled in parallel, which varied between 1 and 48 for each cycle. Therefore, the previously copied handshake file was used as template to fill a second DWP with an equal volume of water and in the same pattern as the sample plate, in order to serve as tare plate for centrifugation. Both plates were then transferred by the gripper arm to the DWP-centrifuge located on the MPP and centrifugation was carried out at 4500 rpm for 5 minutes. The obtained cell-free supernatants were subsequently transferred to a third DWP at -4 °C, the tare DWP was emptied, the copied handshake file deleted and the MPP was ready for the next sampling event.

Each cycle of the developed harvest procedure was finished after 12 to 17.5 minutes (depending on the sample load) and ran fully automated on the MPP without any manual effort or replacement of consumables.

The automated workflow can, for example, be used to compare the product titers of a production strain cultivated in 48 different media compositions or a library of 48 different strains cultivated in the same medium (Figure 3.7 B) Furthermore, it enables insight into the metabolite uptake or production kinetics of an organism, when multiple wells of a plate are inoculated with an identical culture and harvested one after another according to a time-dependent trigger profile (Figure 3.7 C).

A comparable workflow to generate cell-free supernatants on a robotic platform had not been reported before. The most similar strategy using lab automation was reported by Knepper *et al.* for the intermittent measurement of OD, pH and metabolites from cultures in 96-well plates in seven cycles at fixed times during 48 h cultivations [48]. However, their successive sampling from plates incubated without humidity control led to a total volume reduction of 47 % per well over 48 hours. Moreover, enzymatically at-line substrate analytics were performed without biomass separation from cultivation samples, resulting in incorrect measurement values for D-glucose concentrations. In contrast, the BioLector shows lower evaporation (< 10 % per well over 48 hours) and, most importantly, in the MPP workflows the wells are not repeatedly sampled in order to minimize disturbance of the culture, i.e. by altering oxygen transfer due to changing culture volumes [80]. Moreover, the established workflow initiates sampling events in response to individually measured online biomass values and results in cell-free samples that are well suited for subsequent metabolite assays on the MPP as described in the following chapter 3.3.4.

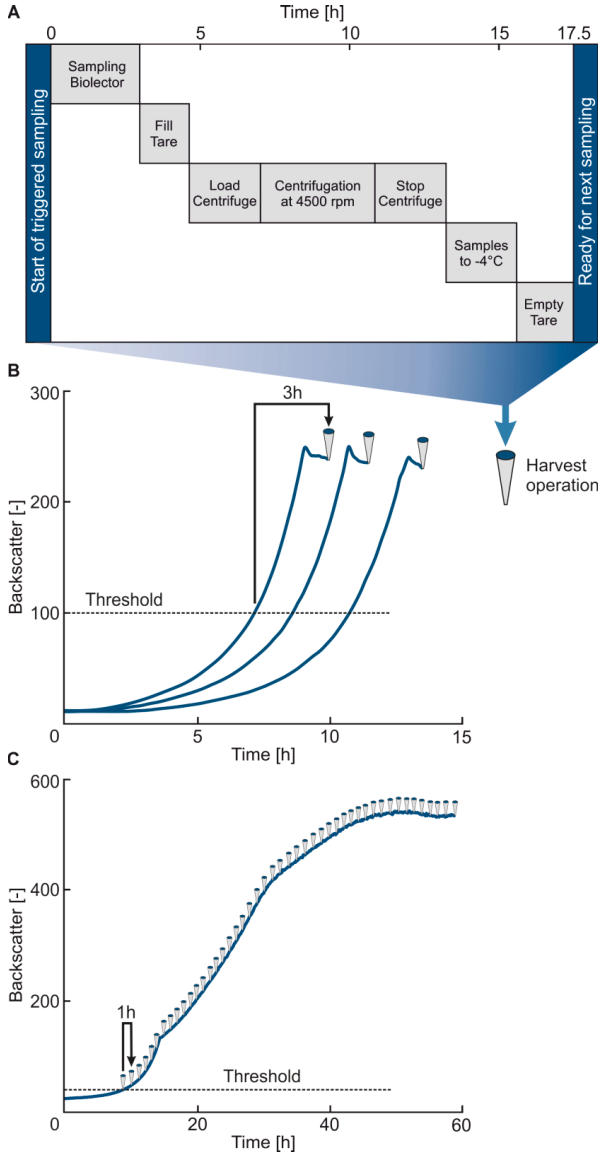

Figure 3.7: Fully automated workflow to harvest cell-free cultivation samples from microtiter plate cultivations on the MPP - modified from Unthan *et al.* 2015 [1]. (A) Steps of the harvest operation to generate a variable number (1 - 48) of cell-free supernatants from BioLector cultivations in parallel in less than 17.5 minutes. (B) Application example to screen producer strains with respect to final product titers by sampling supernatants after turn to stationary phase. (C) Exemplary time-dependent harvest profile of identically inoculated parallel cultivations to assess substrate uptake and metabolite formation kinetics using the automated harvest procedure.

3.3.4 High-throughput metabolite assays in microtiter scale

The beforehand described MPP workflow results in cell-free supernatants from BioLector cultures. Such microtiter scale cultivation devices typically produce high sample loads, which should subsequently be analyzed in a reasonable period of time. In order to enable the quick analyses of clarified samples, photometrical assays for substrate and product metabolites were developed on the MPP in 384-well plate scale.

First, the quantification of the substrate D-glucose was implemented on the MPP using a two-step enzymatic assay (Figure 3.8 D). D-glucose is first phosphorylated via hexokinase (HK) and then oxidized by glucose-6-phosphate dehydrogenase (G6PDH) under formation of NADH. The enzymatic assay was fully automated for routine application and runs without any manual work, except for the preparation of a mastermix (cf. chapter 2.2.11). For each assay 48 cultivation samples were automatically pipetted from a DWP to a 384-well plate in triplicates of two different dilution steps. Standard samples for each run were prepared by the liquid handling from a stock solution of D-glucose and pipetted in 9 replicates per standard on the 384-well plate. The assay was started by addition of the mastermix before the plate was automatically transferred to the photometer integrated on the MPP and monitored at 340 nm for 30 minutes. The dynamic linear range of the method was observed between 0.05 to 0.4 g l^{-1} D-glucose.

For the determination of amino acid concentrations the well-known Ninhydrin-assay was adapted [81]. In short, Ninhydrin reacts with an amino acid to a Schiff base before decarboxylation, dehydration and addition of a second Ninhydrin molecule lead to the formation of the Ruhemanns purple (Figure 3.8 A). However, none of the existing Ninhydrin protocols was suitable for automation, thus, the reaction first needed to be adapted to microtiter scale for application on the MPP. During this transfer to microtiter scale influences of pH, temperature, additives, reagent volumes and reaction times were tested and optimized (data not shown).

In the resulting method, 48 culture supernatants were transferred to a 384-well plate in triplicates, undiluted as well as in one dilution step. Specific standards for the amino acid of interest were prepared by the liquid handling platform from a stock solution in 9 replicates per standard on the same 384-well plate. The

detection reaction was subsequently initiated by the addition of the Ninhydrin solution, which was stopped after 4 minutes incubation by the addition of water (cf. chapter 2.2.11). Finally, the plate was automatically transferred to the photometer integrated on the MPP and the formed Ruhemanns purple was quantified at 570 nm. Noteworthy, the Ruhemanns purple formation results from the reaction of Ninhydrin with any amino acids present in the sample and can consequently not directly be accounted to a single amino acid species.

Moreover, it had been reported that the yield of the Ninhydrin reaction is not identical among different amino acids, since the residual groups can influence conversion rates and equilibria of the reaction intermediates [81]. In order to evaluate the sensitivity and selectivity of the developed microtiter approach, 19 different amino acids were measured with the final Ninhydrin assay protocol, each at a concentration of 10 mM. As a result, the observed signal intensities indeed differed among the tested amino acid species (Figure 3.8 B). In a next step, selected media components and cultivation by-products which are typically found in supernatants of *C. glutamicum* strains were tested. Here, none of the tested compounds resulted in a detectable formation of the Ruhemanns purple in the Ninhydrin assay. Finally, the linear dynamic range of the assay was checked exemplarily for the amino acid L-lysine (Figure 3.8 C). The linear range was found between 1 to 25 mM and thereby directly covers most of the L-lysine titers typically reached by *C. glutamicum* producer strains under lab-scale screening conditions [15, 16, 82]. Therefore, large series of error-prone dilution steps can be skipped, what further improves the speed and accuracy of the microtiter scale assay.

Recently, the Ninhydrin assay had already been successfully applied in an elevated throughput approach to screen 311 bacterial isolates for those growing on 1-aminocyclopropane-1-carboxylate as sole carbon source [83]. However, all pipetting steps as well as culture harvest and clarification were carried out manually and the Ninhydrin reaction was incubated in open 96-well plates in a boiling water bath. In contrast, the Ninhydrin assay developed in this work is operated in 384-well plates and omits heating and sealing steps, which minimizes the assays duration and simplifies its automation. By the usage of DMSO the precipitation of the Ruhemanns purple was reduced which consequently broadened the linear range, as also reported elsewhere [84].

In both developed microtiter assay protocols, all dilutions of standards and samples were executed by the liquid handling platform of the MPP to achieve fast and highly reproducible results. In total, 48 cultivation samples were automatically processed and measured in triplicates of two different dilutions within less than 15 or 45 minutes in case of the Ninhydrin or D-glucose assay, respectively. The throughput of both methods is consequently below one minute per sample measured in replicates and, hence, much faster compared to other quantitative methods based on HPLC or MS technologies. Moreover, the costs per sample for chemicals and consumables are low and analysis of absorption data is highly automatable in contrast to HPLC or MS detector signals, which often require manual peak integration.

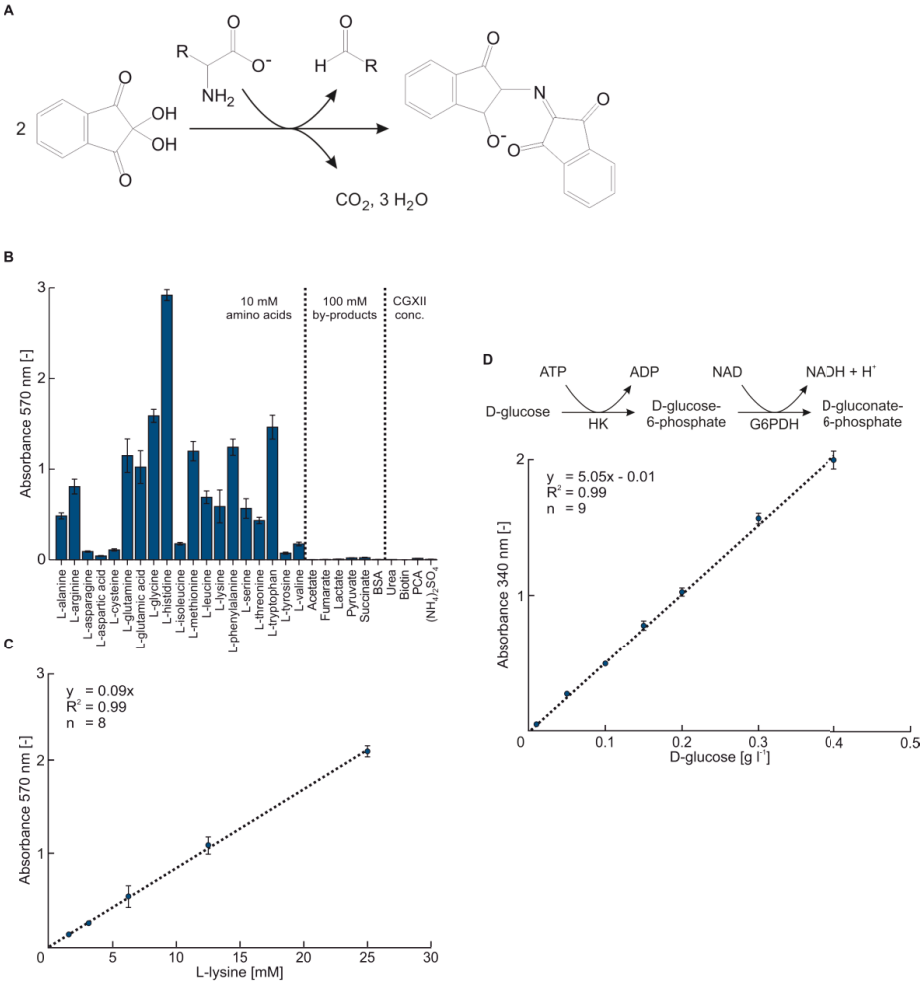

Figure 3.8: Development and validation of metabolite quantification in 384-well plate scale on the MPP - modified from Unthan *et al.* 2015 [1]. (A-C) Photometric quantification of amino acids was realized by the transfer of the well-established Ninhydrin assay to 384-well plates. The assay was tested for its metabolite spectrum, selectivity against typical by-products and media components of *C. glutamicum* cultivations as well as its linear range for L-lysine. (D) Reaction and linear range of the assay developed in 384-well microtiter plate scale to quantify D-glucose in culture supernatants.

3.4 Characterization of prophage-free *C. glutamicum*

3.4.1 Irrelevance of prophage elements for a chassis

The process of genome reduction toward a *C. glutamicum* chassis was undertaken in three major steps, starting with the removal of three *C. glutamicum* prophages (CGP). The first two prophages, namely CGP1 and CGP2, are highly degenerated and rather small with 13.5 kbp and 3.9 kbp, respectively. In contrast, CGP3 can still be induced by stress conditions, includes several expressed genes and accounts with 187.3 kbp for almost 6 % of the wild type genome [85]. In accordance to its large size, CGP3 was excised from *C. glutamicum* alone in the strain ΔCGP3, as well as in combination with CGP1 and CGP2 to derive a fully prophage-free strain, which was called MB001 by the constructing working group of Julia Frunzke at IBG-1.

In order to evaluate these first genome reduction steps, cultivations of ΔCGP3, MB001 and the wild type were carried out in the BioLector on CGXII medium in seven replicates. The obtained growth curves were then analyzed for the maximum specific growth rates and biomass yields utilizing the automated excel routine (cf. chapter 3.3.2). As a result, the growth rate of the wild type was found at μ_{max} = 0.44 ± 0.01 h^{-1} (n=7) and neither ΔCGP3 nor MB001 showed significantly deviating values based on a two-sided t-test with p-value<0.01 (Figure 3.9 A). The biomass yield of the wild type was estimated at $Y_{X/S}$ = 12.4 ± 0.1 BS mg_{GLC}^{-1} and also found unchanged in ΔCGP3 and MB001 (Figure 3.9 B). In summary, the prophage-free strain MB001 met the initially defined criteria of unaltered biological fitness and all prophage elements were consequently classified as irrelevant for growth on CGXII medium.

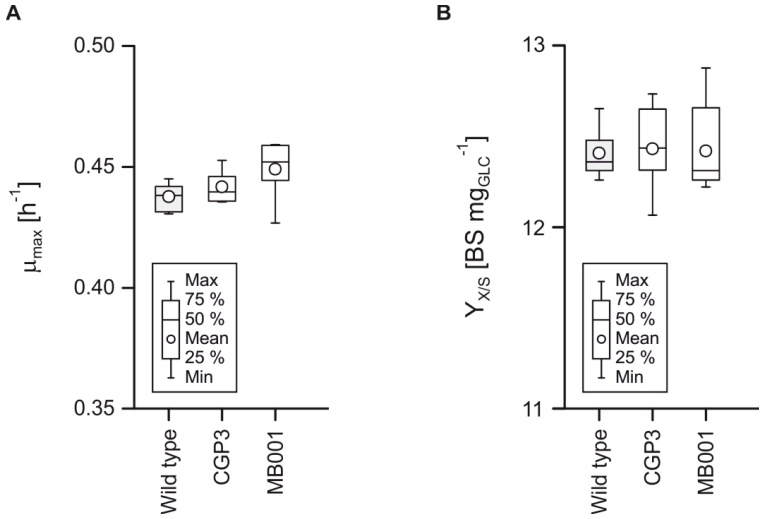

Figure 3.9: Phenotyping of the first generation of genome-reduced *C. glutamicum* strains in the BioLector on CGXII medium with 20 g l^{-1} D-glucose. (A) Maximum growth rate of CGP3 and MB001 compared to the wild type (n=7). (B) Biomass yield of CGP3 and MB001 compared to the wild type (n=7).

3.4.2 Stress response and heterologous protein expression

The prophage-free strain MB001 showed unaltered growth rates and biomass yields compared to the wild type on standard CGXII medium. However, it had been reported that CGP3 can be induced under stress conditions [85]. Consequently, the prophage might include functions to improve the stress tolerance of *C. glutamicum*, what would explain the stable integration of the large prophage fragment (187.3 kbp) in the genome. Otherwise it could also be possible that the induction of CGP3 under stress conditions leads to an increased metabolic burden and its excision in MB001 could ultimately improve the biological fitness of this strain under such conditions.

In order to evaluate the relevance of the prophage genes under stress conditions MB001 was further analyzed and compared to the wild type. Both strains were cultivated in the BioLector in a broad set of different media variants based on CGXII medium. Stress was induced by phosphate limitation, high NaCl concentrations

(osmotic stress) and iron excess. High iron concentrations were expected to increase the formation of reactive oxygen species which ultimately lead to oxidative stress [86]. As a result, MB001 did not display an altered phenotype compared to the wild type under any of the tested conditions (Figure 3.10). Consequently, the prophage elements were also determined as irrelevant for the biological fitness under the tested conditions.

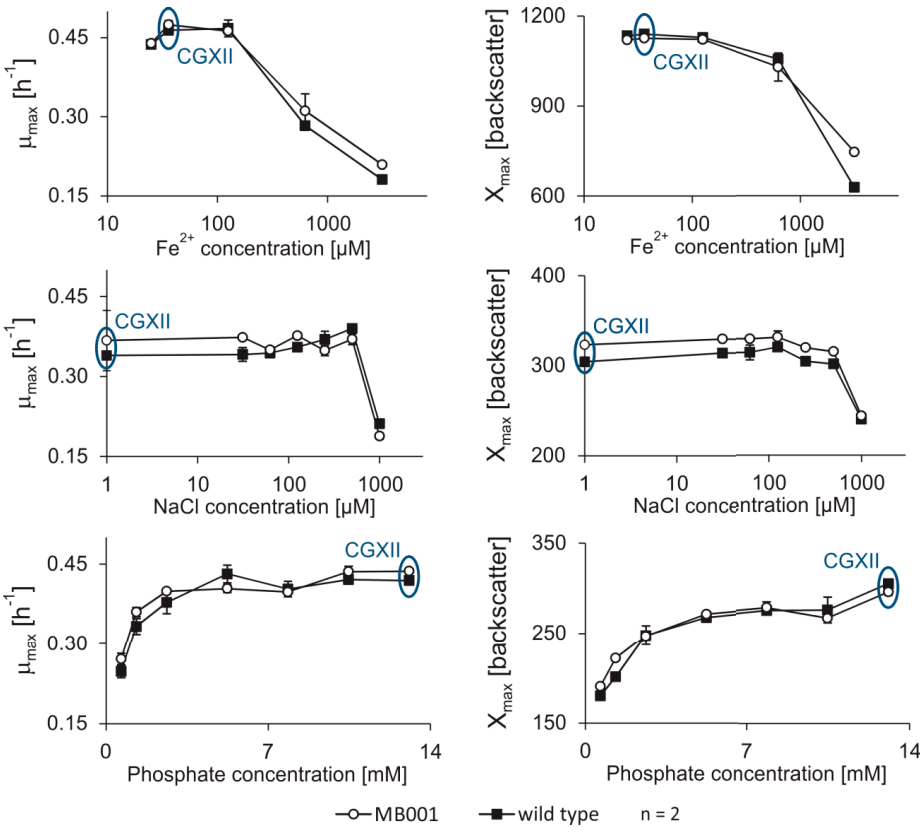

Figure 3.10: *C. glutamicum* wild type and MB001 cultivated in the BioLector under different stress conditions. The maximum specific growth rate and final backscatter values were estimated in each medium variant from two replicates. The particular concentration which resembles the standard CGXII composition is indicated in each diagram.

In further experiments a potential application of the prophage-free strain MB001 was tested. Other reports about the reduction of natural genomes led to altered behaviors of plasmids in the derived genome-reduced cells, especially when mobile elements like prophages had been deleted [87]. Therefore, it was tested if the prophage-free strain MB001 would show an altered expression of a heterologous protein encoded on a plasmid. As model protein eYFP was chosen, since its expression could be monitored online in the BioLector system. The vector used was pEKEX2 with a kanamycine resistance cassette and the tac promotor of eYFP was induced with 1 mM IPTG. The plasmid was transferred to the WT and MB001 and multiple independent clones were picked and cultivated in the BioLector. The biomass formation and eYFP fluorescence was monitored online (Figure 3.11). It was found that all strains grew to a comparable biomass at equal growth rates. Interestingly, MB001 showed an increased production of the plasmid encoded heterologous protein, since the final biomass specific fluorescence of MB001 was 35-40 % higher compared to the wild type (Figure 3.11 B).

A detailed analysis of this finding revealed three genes included in the region of CGP3 that encode a DNA restriction and modification system. These three genes were excised from the wild type and the obtained strain ΔcglMRR was also tested for plasmid encoded eYFP expression. As a result, ΔcglMRR showed an identically increased biomass specific fluorescence compared to MB001 and thereby the effect observed in the prophage-free strain could be narrowed down to these three genes.

In summary, the strain MB001 displayed a genome reduction of 6.2 %, an increased plasmid encoded protein expression and, most importantly, unaltered biological fitness under standard as well as stress conditions. Therefore, it fulfilled the criteria set for a chassis in this study and was consequently used as a starting point in the following genome reduction steps.

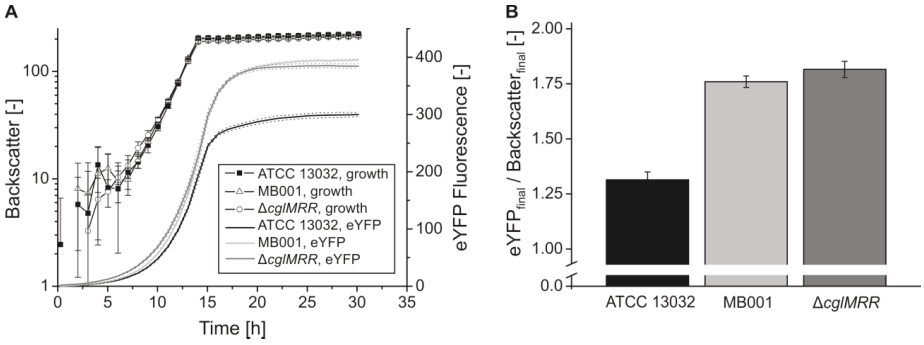

Figure 3.11: Comparison of growth and eYFP expression between *C. glutamicum* wild type (ATCC 13032) and the strains MB001 as well as ΔcglMRR – modified from Baumgart M, Unthan S, *et al.* 2013 [3] (A) Backscatter and eYFP fluorescence in the BioLector on CGXII medium with kanamycine and 1 mM IPTG (n=7). (B) Final biomass specific eYFP fluorescence of all cultures.

3.5 Deletion of non-essential gene clusters from prophage-free *C. glutamicum*

3.5.1 Relevance of non-essential gene clusters for growth of *C. glutamicum*

After the successful construction of the prophage-free strain MB001, two insertion elements were further deleted to increase the genetic stability of subsequent genome-reduced strains. On basis of the derived strain ΔCGP123 ΔISCg12, the next step toward a chassis was undertaken by deletion of gene clusters that resulted as target from the prior genome-wide gene essentiality blueprint (cf. chapter 3.1). In total, the deletion of 41 gene clusters ranging from 3.7 to 49.7 kbp was attempted, of which 36 could be carried out successfully to derive the equivalent number of genome-reduced strains (GRS). This result directly confirmed the prior genome-wide essentiality classification to a wide extent and, concurrently, the status of any unclassifiable gene in those clusters was updated to non-essential. The deletion of the remaining clusters failed repeatedly, probably because they contained yet unknown essential genes.

The next step was to evaluate the relevance of all deleted clusters for the target characteristic of the chassis, which was defined as non-impaired biological fitness on defined glucose medium. As initially defined, biological fitness was assessed by the maximum specific growth rate of each GRS, as a drop in this easily measurable parameter would directly point to an impaired metabolism. Along the construction of a chassis, each genome reduction step was considered acceptable when the outcoming strain did not show a significantly reduced growth rate (cf. Figure 1.2).

The biological fitness of each GRS was determined from 1 ml batch cultivations in multiple replicates ($n \geq 6$) to generate a valid data set for statistical analysis. All cultivations were performed following the prior developed high-throughput phenotyping workflow, in order to evaluate the large GRS library with high reproducibility in a short time (cf. chapters 3.3.1 and 3.3.2). Significantly changed growth rates were determined via t-test (two-sided, p-value<0.01) when comparing each GRS with the *C. glutamicum* wild type (Figure 3.12 A).

For the wild type a maximum growth rate of μ_{max} = 0.43 ± 0.02 h^{-1} (n=27) was estimated and the rates for the 36 GRS ranged between 0.22 ± 0.01 h^{-1} (GRS31) and 0.47 ± 0.06 h^{-1} (GRS33). While, 10 GRS showed significantly slower growth rates for 27 GRS the growth rate and thereby biological fitness was maintained at wild type level. During further analysis, the total biomass yields were estimated by normalizing the maximum backscatter value (gain 20) reached in early stationary growth phase to the amount of D-glucose (GLC) fed to each batch culture (Figure 3.12 B). The biomass yield of the wild type was $Y_{X/S}$ = 19.6 ± 2.1 BS mg_{GLC}^{-1} and found significantly lower for five GRS. Interestingly, all these strains (namely GRS13, GRS15, GRS31, GRS42 and GRS50) also grew significantly slower, what underlines the relevance of one or multiple genes in the respective clusters for biological fitness on CGXII medium.

Next, all GRS were grown on medium enriched with complex additives, which might allow the by-passing of potential limitations in central metabolism created from gene cluster deletions. Batch cultivations were carried out on enriched CGXII, which was obtained by addition of L-threonine, yeast extract and a vitamin mixture (Figure 3.12 C). Here a maximum growth rate of μ_{max} = 0.61 ± 0.04 h^{-1} (n=13) was found for the wild type and the rates for the GRS ranged from 0.44 ± 0.08 h^{-1} (GRS45) to 0.66 ± 0.03 h^{-1} (GRS28). Significantly slower growth rates were observed for four strains, namely GRS41, GRS42, GRS45 and GRS50. Interestingly, three of these strains also grew slower on defined CGXII medium in the previous experiment (cf. Figure 3a). Therefore, at the least one gene in each of the corresponding clusters seems to be of general relevance for *C. glutamicum* and addition of complex substrates cannot recover the biological fitness of the corresponding GRS. However, for GRS13 and GRS25 the biological fitness was recovered to wild type level on enriched CGXII and, conclusively, one or multiple genes in the clusters #13 and #25 are relevant for growth on CGXII medium but irrelevant on enriched CGXII. This observation clearly points to an anabolic function of the respective genes and that their deletion can be complemented by supplementation of complex additives.

For GRS25 an explanation might be the deletion of cg1283 which is (together with cg1835) discussed to encode for a shikimate dehydrogenase (SDH) in the aromatic amino acids biosynthesis [13]. Consequently, amino acids supplemented by the yeast extract in enriched CGXII could compensate the growth defect of GRS25. However, in a recent report the single deletion of cg1835 instead of cg1283 led to a more severe growth defect of *C. glutamicum*, thus the main SDH activity is at the moment assumed to be encoded by cg1835 [88].

One of the genes deleted in GRS13 was *panD* (cg0172) which was set as an unclassifiable gene during the initial essentiality analysis, since findings from knock-out data were in disagreement. However, *panD* encodes for the aspartate-1-decarboxylase that catalyzes the synthesis of ß-alanine as pantothenate precursor [89]. Hence, the decreased biological fitness of GRS13 on CGXII medium could be caused by ß-alanine limitation, which is complemented by the yeast extract on enriched CGXII. Most interestingly, in earlier studies the deletion of *panD* from *C. glutamicum* was reported to result in ß-alanine auxotrophic strains [89]. However, GRS13 showed growth on defined CGXII in all experiments of this work, but at significantly lower rates. In conclusion, *panD* should from now on be considered as non-essential for *C. glutamicum*, but it is most probably relevant for its biological fitness on defined CGXII medium.

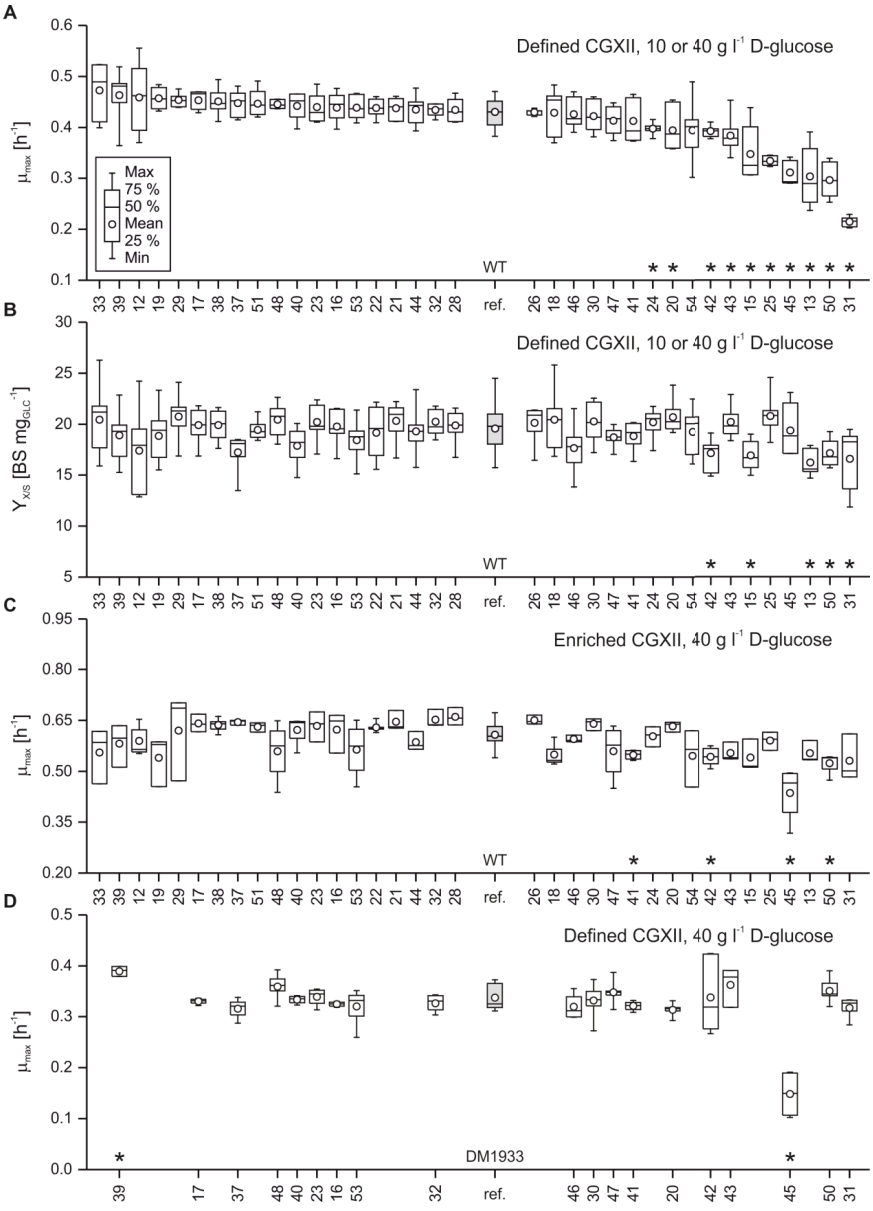

Figure 3.12: Evaluation of non-essential gene clusters deleted one at a time in two strain backgrounds on different medium compositions – modified from Unthan *et al.* 2014 [4]. Significant deviations are marked by an asterisk (two-sided t-test, p-value<0.01). (A) Maximum growth rates of GRS on defined CGXII medium, sorted according to their mean values (n≥6). (B) Biomass yields of all GRS according to the maximum backscatter signal at gain 20 (n≥6). (C) Maximum growth rates of GRS on enriched CGXII medium (n≥3). D) Maximum growth rates of GRLP on CGXII medium compared to DM1933 (n≥3).

In summary, 36 GRS were successfully constructed and 26 strains fulfilled the criteria of unaltered biological fitness on CGXII medium. Consequently, all these clusters exclusively consist of genes that are irrelevant for the target criteria and are therefore valid deletion targets to construct a *C. glutamicum* chassis. However, few deletions resulted in a decreased biological fitness of the corresponding strains and must therefore include at least one relevant gene function. These clusters should therefore be excluded during a chassis construction or could eventually be deleted in a truncated version to retain the relevant genes in the genome.

Nevertheless, those strains showing reduced biological fitness are of high interest, as the observation points to so far not fully understood gene functions in the deleted clusters. In order to narrow such effects down to a single gene, further targeted deletions of single genes and truncated clusters are necessary, which were out of the scope of this work. However, some new conclusions could be drawn from the observed GRS phenotypes in combination with partially existing annotation data of the particular gene clusters.

3.5.2 Growth and product formation of genome-reduced L-lysine producers

In order to test whether the classification of irrelevant genes obtained in the GRS also holds true in another strain background, selected deletions were carried out in the *C. glutamicum* L-lysine model producer DM1933. Moreover, it was of special interest to test if any cluster deletion might alter the L-lysine production capacity of the particular strain. The developed robotic workflows were used to automatically harvest BioLector cultivations at turn to stationary phase and quantify amino acids in microtiter scale (cf. chapter 3.3.3 and 3.3.4).

In total, 19 genome-reduced L-lysine producers (GRLP) were constructed on basis of the prophage-free L-lysine producer DM1933 ΔCGP123. Their biological fitness during growth on CGXII medium was tested in at least three replicates and compared to DM1933, which grew at μ_{max} = 0.34 ± 0.03 h^{-1} (Figure 3.12 D). The tested GRLP showed growth rates ranging from 0.15 ± 0.05 h^{-1} (GRLP45) to 0.39 ± 0.01 h^{-1} (GRLP39). Interestingly, the deletion of the two particular gene clusters #39 and #45 had influenced the biological fitness of the wild type in a comparable way (cf. Figure 3.12 C). While GRS39 showed the second highest growth rate on defined CGXII, the corresponding GRLP39 grew faster than any other GRLP as well as the reference strain DM1933. In contrast, the deletion of cluster #45 in GRS45 and GRLP45 resulted in significantly decreased growth performances under any tested condition. Consequently, statements about gene relevance might not be strictly restricted to a particular strain background.

In further experiments the product formation of 17 GRLP was compared to DM1933 in batch cultures (CGXII medium, 40 g l^{-1} D-glucose, n≥4). L-lysine production is generally coupled to primary metabolism, thus highest product titers are expected after turn to stationary phase in a batch culture [90]. Consequently, the previously developed MPP procedures were used to automatically harvest and freeze cell-free supernatants from all cultures, one hour after turn to stationary phase (cf. Figure 3.7 B). On the next day, the sample-DWP was thawed and total amino acid titers of all cultivations were measured in 384-microtiter scale using the fully automated Ninhydrin assay (Figure 3.13 A). As a first result, the highest amino acid titer was measured in the supernatant of GRLP45 (59.1 ± 1.3 mM) which was 51 % higher compared to the titer for DM1933 (39.2 ± 6.1 mM).

To test whether the MPP screening results considering growth and amino acid production can be transferred to the lab-scale, DM1933 as well as GRLP45 were cultivated in 1 l bioreactors on CGXII medium with 10 g l^{-1} glucose. Both cultivations were sampled every hour and analyzed for total amino acid as well as L-lysine concentrations using the developed Ninhydrin assay as well as an established LC-MS/MS protocol, respectively (Figure 3.13 B). As a first result, the trend of a decreased growth rate of GRLP45 was reproduced in bioreactor scale (μ_{max} = 0.20 h^{-1}). Additionally, the Ninhydrin assay pointed to a higher total amino acid titer of GRLP45 compared to DM1933, which was confirmed as an increased L-lysine titer by the LC-MS/MS measurement.

In conclusion, the developed robotic workflows allowed to quickly assess the production capacity of the GRLP library and exemplary results obtained on the MPP were subsequently confirmed in 1 l bioreactors. GRLP45 does not show improved space-time yields, since the increased L-lysine titer is produced in a longer cultivation due to the decreased growth rate of this strain. Most likely, the deletion of cluster #45 from DM1933 decreased the growth rate, which was also seen in wild type background (GRS45) and thereby led to a prolonged L-lysine production phase and ultimately increased product titers.

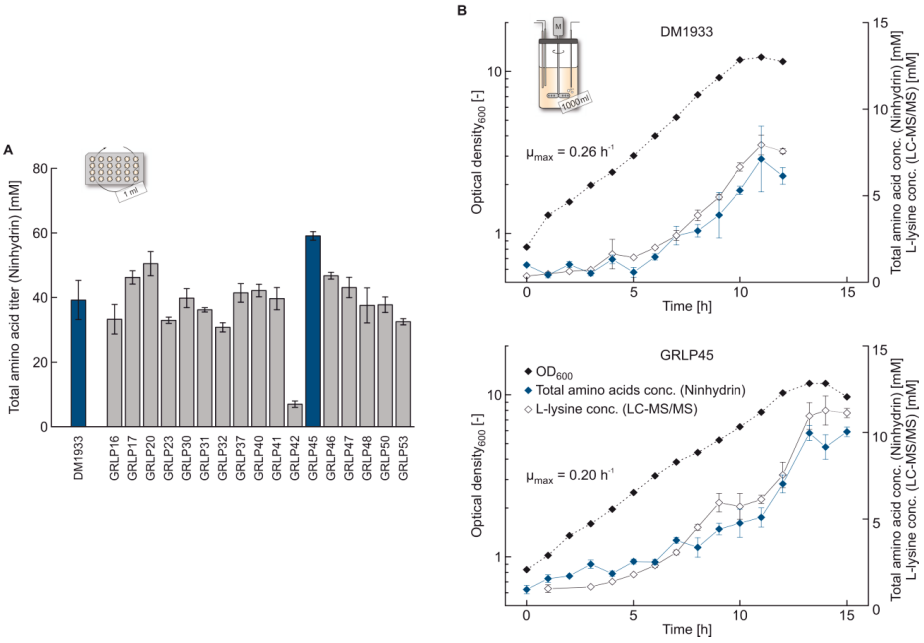

Figure 3.13: Screening of the GRLP library for altered L-lysine production capacity and scale-up of GRLP45 in lab-scale bioreactors - modified from Unthan *et al.* 2015 [1]. (A) Total amino acid concentrations of the GRLP cultivations on CGXII with 40 g l^{-1} D-glucose. Supernatants were analyzed using the developed MPP harvest procedure in combination with the automated Ninhydrin assay (n≥4). (B) Cultivation of GRLP45 and DM1933 in 1 l lab-scale bioreactor experiments. Total amino acids and L-lysine were quantified using the automated Ninhydrin assay (n=3) and an established LC-MS/MS protocol (n=3), respectively.

3.6 Combinatorial deletion of irrelevant gene clusters

3.6.1 Interdependence of irrelevant clusters in *C. glutamicum*

As described in the previous chapter, strains with deletion of single gene clusters were characterized, in order to identify those clusters that are irrelevant for the biological fitness of *C. glutamicum* on CGXII medium. With these results at hand, recommendations could be given to the project partners to guide the combinatorial deletion of those gene clusters to allow the construction of a chassis organism. Noteworthy, it was expected that some combinations would lead to impaired biological fitness of the derived strains, especially when so far unknown but relevant functions were encoded redundantly (i.e. isoenzymes) in the particular clusters. The combinatorial deletions were carried out by the project partners sequentially by homologous recombination, since no technique existed to combine pre-made deletions in *C. glutamicum* as for example possible for *E. coli* using P1 transduction [91, 92]. Throughout each deletion cycle, the first strains with few combinatorial deletions were obtained and quickly analyzed using the established methods (cf. chapters 3.3.1 and 3.3.2) in order to detect combinatorial dead ends and guide the ongoing deletion process.

In the following, a selection of 13 strains with partially overlapping combinatorial deletions is presented and conclusions about the interdependence of some individually irrelevant gene clusters are presented (Figure 3.14 A). The overall genome reduction of the tested strains ranged between 7.69 % (W106) and 12.8 % (W121) as a percentage of the wild type genome (Figure 3.14 B). The biomass yield and maximum specific growth rate of all strains was determined on CGXII medium and compared to the wild type in at least four replicates (Figure 3.14 C and D).

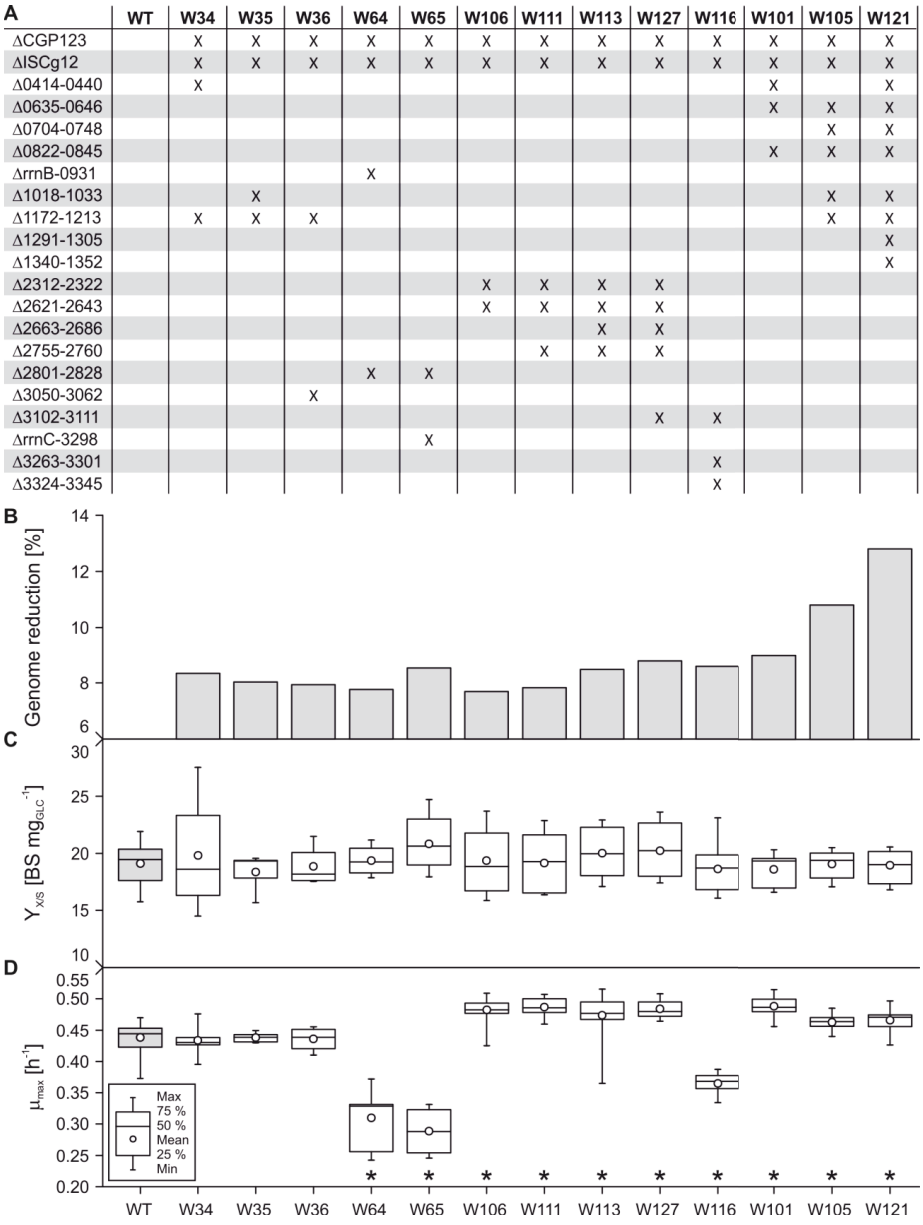

Figure 3.14: Combinatorial deletion and interdependence of selected gene clusters in *C. glutamicum*. (A) Strains with combinatorial deletion of gene clusters that had individually been classified as irrelevant for growth on CGXII medium. (B) Overall genome reduction of the combinatory strains as a percentage of the wild type genome. (C+D) Biomass yield and maximum specific growth rate on CGXII medium in BioLector cultivations (n≥4). Significantly changed values compared to the wild type are marked by an asterisk (two-sided t-test, p-value<0.01).

As a first result, the deletion of cluster Δ1172-1213 together with any of Δ0414-0440, Δ1018-1033 and Δ3050-3062 did not affect the biological fitness of the derived strains W34, W35 and W36, respectively. This exemplary finding already proved the general applicability of the chosen approach to combine deletions of individually irrelevant gene clusters.

In contrast, interdependence was observed for the cluster Δ2801-2828 with ΔrrnB-0931 as well as with ΔrrnC-3298. The corresponding strains W64 and W65 showed compared significantly lower growth rates of μ_{max} = 0.31 ± 0.05 h^{-1} (n=6) and μ_{max} = 0.29 ± 0.03 h^{-1} (n=8), respectively. Consequently, these clusters were excluded from any further combinatorial deletion cycle toward a chassis. The reason for the observed interdependencies in W64 and W65 was further investigated as described in the following chapter 3.6.2.

Another cycle of combinatorial deletions was started along the genome from cluster Δ2312-2322 on and resulted in the strains W106, W111, W113 and W127. During characterization, none of these strains showed an impaired biological fitness but, in fact, the maximum growth rate was even significantly higher as compared to the wild type. Most interestingly, the strain W127 with a total genome reduction of 8.78 % grew with μ_{max} = 0.48 ± 0.01 h^{-1} (n=16) based on the backscatter measurement in the BioLector.

The strain W116 was constructed by deletion of 3 irrelevant clusters of which cluster Δ3102-3111 had already been deleted in W127. The maximum growth rate of W116 was significantly lower with μ_{max} = 0.36 ± 0.02 h^{-1} (n=17), thus, at least two clusters deleted in W116 are interdependent and cannot be deleted simultaneously without affecting the biological fitness of *C. glutamicum*. As a consequence, the two clusters Δ3263-3301 and Δ3324-3345 were excluded from the further step-wise construction of a chassis.

A last cycle of combinatorial deletions was started along the genome from cluster Δ0414-0440 and resulted in the strains W101, W105 and W121. As a result, none those strains was impaired in biological fitness but, in fact, all strains grew significantly faster based on backscatter measurements. As an example, a maximum growth rate of μ_{max} = 0.47 ± 0.02 h^{-1} (n=16) was found for W121, which displayed the largest proportion of genome reduction (12.8 %) of all constructed

strains. Consequently, this strain W121 as well as W127 were chosen for further studies to i.e. test whether the growth rate would also be found increased based on classical biomass signals measured during bioreactor cultivation. The results of this in-depth characterization are summarized in the following chapter 3.7.

3.6.2 Effect of combinatorial deletion in strain W65

As described in the previous chapter, the combinatorial deletion of the clusters Δ2801-2828 and ΔrrnC-3298 led to a significantly impaired biological fitness of the respective strain W65. This was surprising, since both clusters had been classified as irrelevant when deleted solely in the strains GRS41 and GRS51 (Figure 3.12). This phenomenon was tackled with different methods of which an intracellular GC-ToF-MS fingerprint led to a valid explanation of the effect, as described in the following.

The wild type, GRS41 (Δ2801-2828) and W65 (Δ2801-2828 and ΔrrnC-3298) were cultivated in lab-scale bioreactors on CGXII medium with 10 g l^{-1} D-glucose. As a first result, during this cultivation the significantly decreased growth rate of W65, which had so far only been observed during BioLector experiments, was confirmed on basis of optical density and cell number measurements (results not shown). From these bioreactor cultivations, samples were taken during the exponential growth phase at OD = 2 for intracellular GC-ToF-MS fingerprints (cf. chapter 2.2.7). In short, the cells were washed, frozen and later metabolites were extracted with hot MeOH and finally derivatized for GC-ToF-MS analysis. During subsequent data analysis, all peak areas were normalized by the total biovolume (in µl) in the sample and the normalized data of W65 and GRS41 were plotted against the wild type data.

As expected, for GRS41 that did not show an altered phenotype under any testes condition, the GC-ToF-MS fingerprint was highly comparable to the wild type (Figure 3.15 A). In total 53 metabolites could be compared between GRS41 and the wild type (fully separated peaks) and only for 8 metabolites a 2-fold difference was found between the samples. In contrast, the GC-ToF-MS fingerprint for W65 indicated multiple highly altered intracellular metabolite pools (Figure 3.15 B). In total 49 metabolites were analyzed of which 23 were found in the extracts with

two-fold in- or decreased concentration The highest difference was found for L-serine, which was 8.75-fold increase in W65 compared to the wild type. Interestingly, other amino acids pools were also increased more than 2-fold, such as L-alanine, L-glutamine, L-glycine, L-isoleucine, L-lysine, L-proline, L-threonine and L-valine. These amino acids are derived from different branches of glycolysis and the citric acid cycle [6]. Thus, not only a specific amino acid synthesis pathway seems to be affected in mutant strain W65, but the amino acid accumulation is rather unspecific. Consequently, the increased amino acid pools could be explained by a decreased activity of the anabolism that utilized amino acids, namely the translation machinery.

This hypothesis is supported by the genes annotated in the deleted clusters of W65, which in total include three operons for ribosomal RNA (rrn). In the wild type genome, six of those operons exist and hence W65 missed half of the native rrn-operons. The single cluster deletions in the strains GRS51 (ΔrrnC-3298) and GRS41 (Δ2801-2828) include one and two rrn-operons, respectively, and both strains did not show an impaired biological fitness. However, the combinatorial deletion of three rrn-operons in W65 might have limited the ribosome capacity of *C. glutamicum*, which is required for growth rates typically found on CGXII medium. Besides W65 also another strain existed, namely W64, in which three rrn-operons had been deleted simultaneously during combinatorial deletion of two irrelevant gene clusters. Most interestingly, W64 also displayed a significantly decreased growth rate in the range of W65, what further supports the hypothesis of interdependence of ribosomal capacity and maximum growth rate (cf. Figure 3.14).

Thus, a general interdependence of rrn-operon copy number and growth rate seems to exist for *C. glutamicum*. Such a relationship had also been reported for *E. coli* where two of seven rrn-operons could be deleted before growth rates dropped [93]. Moreover, the authors showed that the native surplus in translation capacity is useful for the cell's rapid adaption to changing environments, such as shifts in nutrients or temperature. Consequently, the *C. glutamicum* strains with deletion of few rrn-Operons that maintained identical growth rates in this study (i.e. GRS41 and GRS51), might display longer lag-phases in changing environments. Therefore, those clusters that included rrn operons were excluded as deletion targets for further construction of the *C. glutamicum* chassis.

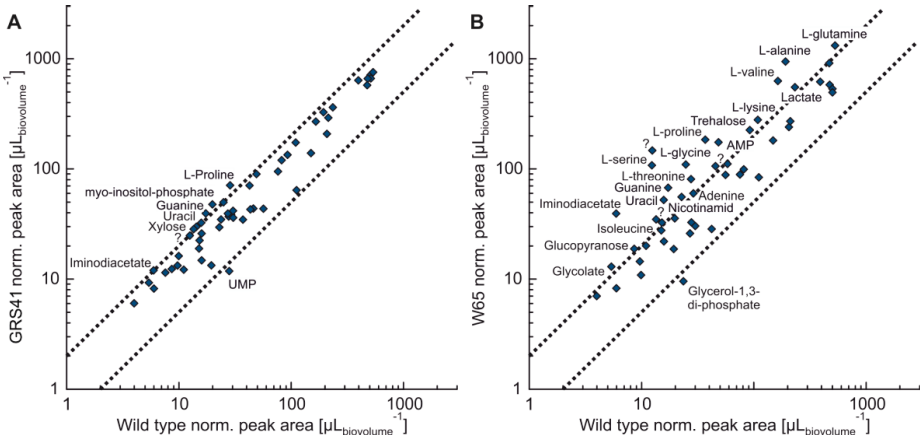

Figure 3.15: Intracellular GC-ToF-MS fingerprint of GRS41 (A) and W65 (B) compared to the *C. glutamicum* wild type. Strains were grown in 1 l bioreactors on defined CGXII medium and sampling was performed during exponential growth phase. The resulting peak areas for all detectable metabolites were normalized by the total biovolume in each sample. Dashed lines represent levels of 2-fold increased or decreased values compared to the wild type. Metabolites which could not be identified using the JuPOD database are labeled with a question mark.

3.7 In-depth characterization of pre-chassis W121 and W127

3.7.1 Biological fitness under stress conditions and on other C-sources

The previous tests of strains with combinatorial deletions resulted in the two functional pre-chassis W121 and W127 which display the highest degree of genome reduction reached in the cooperation project so far. Both strains showed, compared to the wild type, unaltered biomass yields and significantly increased growth rates on defined CGXII medium in the BioLector (cf. Figure 3.14). During following experiments both pre-chassis were studied under varying conditions to further check to what extent the strains remained the properties of the originating wild type.

First, the response of W121 and W127 against nitrogen and phosphate limitation as well as osmotic stress was tested in a series of BioLector experiments. For each condition the maximum specific growth rate and final biomass concentration according to backscatter as well as CDW were estimated as shown in the supplement (Figure S-3 - Figure S-5). In short, both pre-chassis did not show any altered response to the applied stress conditions compared to the *C glutamicum* wild type.

Next, both strains and the wild type were grown on carbon sources other than D-glucose, including hexoses, disaccharides, sugar alcohols as well as organic acids. During medium preparation the C-sources were added to reach the same total amount of carbon compared to the standard D-glucose concentration of 10 g l^{-1}. All cultivations were performed at least in triplicates and analyzed for maximum specific growth rates and final CDW (Figure 3.16).

Interestingly, the strain W127 grew significantly faster on D-glucose, acetate, citrate and D-maltose compared to the wild type and all other μ_{max} as well as all X_{max} values were found unchanged. (Figure 3.16 A+B). In contrast, the strain W121 did not maintain the biological fitness at wild-type level on multiple C-sources (Figure 3.16 C+D). As observed before the maximum growth rate on D-glucose was significantly higher, however, the final biomass was significantly lower when CDW was applied as biomass signal instead of backscatter (cf. Figure 3.14). The latter result is most likely caused by altered cell morphology of W121, which is further

investigated in the following chapter 3.7.3. W121 grew significantly slower on acetate and had lost the ability to grow on citrate, succinate and D-malate. Besides D-glucose, the final CDW of W121 was also significantly lower compared to the wild type on succinate as well as D-malate.

In summary, the pre-chassis W121 showed several drawbacks compared to the wild type considering utilization of different C-sources. However, the decreased biological fitness under the tested conditions was not surprising, as the target criteria during the previous screening approaches was unaltered growth on D-glucose. Consequently, genes relevant for i.e. utilization of acetate, succinate or D-malate could have been deleted from W121 within the genome reduction cycles. In contrast, the biological fitness of W127 on the tested C-sources exceeds expectations one might have for a chassis designed for unaltered growth on D-glucose. In W127 all values estimated for μ_{max} as well as final CDW were at least maintained at wild type level and even significantly higher in some instances. These results could point to a decreased metabolic burden of W127, which should be confirmed in following studies and might be a beneficial feature for its future application.

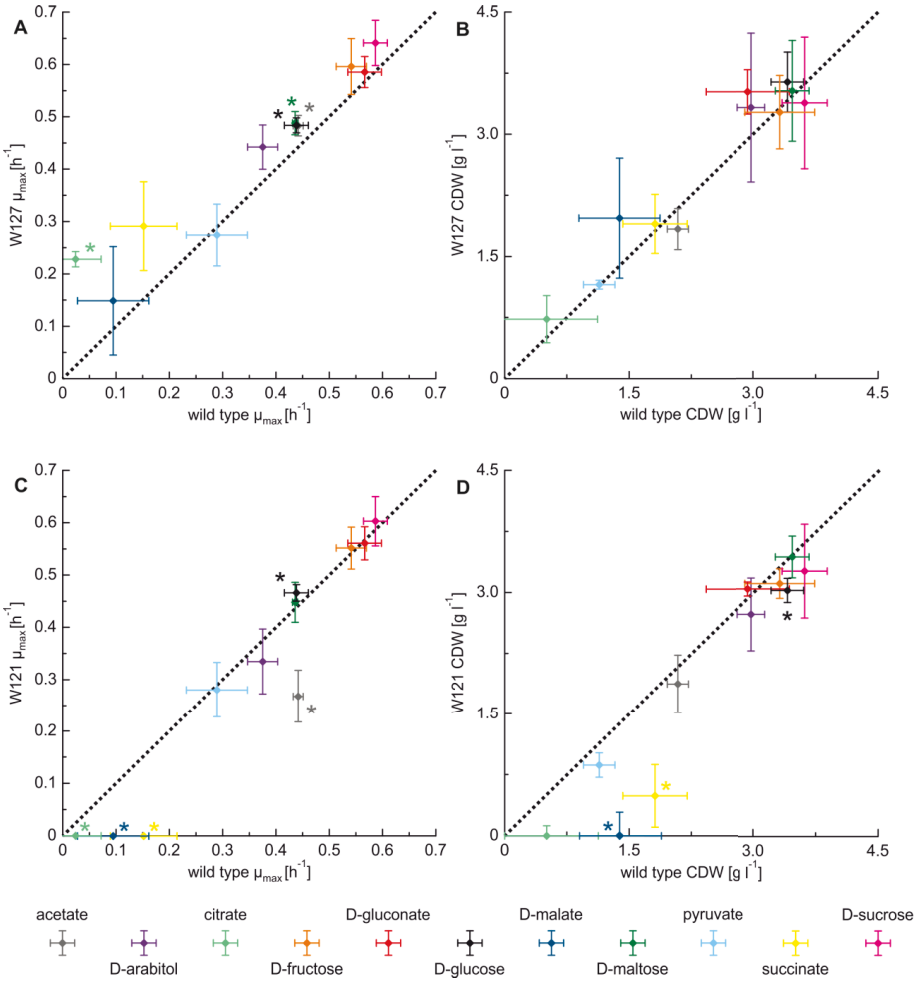

Figure 3.16: Biological fitness of pre-chassis W127 (A+B) and W121(C+D) in comparison to the wild type. Cultivations were performed on CGXII media variants in which D-glucose was replaced by the listed C-sources (n≥3). Significantly changed μ_{max} or CDW values compared to the wild type were marked by an asterisk in the color of the respective C-source (two-sided t-test, p-value<0.01).

3.7.2 Growth in lab-scale bioreactors

After intensive characterization of W121 and W127 in the BioLector system, both pre-chassis were cultivated in lab-scale bioreactors in order to evaluate their growth properties under controlled conditions. Of particular interest was the analysis of the classical biomass values, i.e. OD and CDW, because W121 had displayed contrary trends when assessing Xmax based on CDW or backscatter in the previous BioLector runs. W121, W127 and the wild type were cultivated at least in triplicates and the cultivation data can be found in the supplement (Figure S-6 - Figure S-8).

Parameters derived from the bioreactor cultivations are summarized in Table 3.17 and maximum growth rates are compared to the estimates from previous BioLector runs. As a first result, the mean growth rate estimates obtained by the five different biomass signals used in this study show systematic differences for all tested strain, however, the rates are not significantly different. For example the μ_{max} of the wild type was calculated as 0.41 ± 0.03 h^{-1} or 0.46 ± 0.02 h^{-1} when using the CDW or cell number data, respectively. These differences in mean growth rates estimates might be caused by dynamic changes in cell size and composition over the course of the exponential growth phase (cf. Figure 3.19 C). Interestingly, the significantly higher maximum growth rates of W121 and W127 observed in the BioLector, were not observed when using other biomass signals from bioreactor cultivations.

This observation can be commented with the phrase “you get what you screen for”, which describes the tendency of screenings to result in biological entities that follow the applied selection pressure but not do not display any other closely related characteristic [94]. As the GRS were initially screened according to growth rate based on backscatter measurements, this parameter was found increased in the following pre-chassis W121 and W127, but μ was not found increased in any other biomass signal. Thus, clusters were most likely deleted in both strains that altered the cell structure and led to changed optical attributes during backscatter measurement.

Table 3.17: Overview of results obtained from lab-scale bioreactor cultivations of *C. glutamicum* wild type and the pre-chassis W121 and W127 on defined CGXII medium with 10 g l^{-1} D-glucose. For comparison the maximum growth rates from previous BioLector experiments are also displayed (cf. Figure 3.14)

Parameter	WT (n≥4)	W121 (n≥3)	W127 (n≥3)
μ_{max} [h^{-1}] according to:			
OD	0.43 ± 0.02	0.43 ± 0.02	0.42 ± 0.01
CDW	0.41 ± 0.03	0.36 ± 0.04	0.38 ± 0.02
Cell concentration	0.46 ± 0.02	0.54 ± 0.03	0.48 ± 0.01
Biovolume	0.43 ± 0.01	0.46 ± 0.01	0.44 ± 0.01
Backscatter (Biolector)	*0.44 ± 0.02*	*0.47 ± 0.02*	*0.48 ± 0.01*
$Y_{x/s}$ [g g^{-1}]	0.60 ± 0.04	0.49 ± 0.05	0.56 ± 0.01
Base used [mL]	3.48 ± 0.61	3.20 ± 0.49	3.36 ± 0.55
Acid used [mL]	0.69 ± 0.31	0.65 ± 0.30	1.01 ± 0.59

Considering all values obtained in the bioreactor, the pre-chassis W127 did not show any alterations exceeding standard deviation compared to the wild type. However, one difference observed was the color of culture supernatants during stationary phase. While supernatants of the wild type and other strains were bright yellowish, W127 developed a dark brownish supernatant. The brown color was not clearly visible at turn to stationary phase, but increased in intensity during further aeration in the bioreactor (supplement, Figure S-9). The effect was addressed using untargeted GC-ToF-MS, thin layer chromatography and extraction with organic solvents. However, the substance could not be isolated nor identified. Nevertheless, it can be stated that the brownish substance or substance mixture is hydrophilic, exclusively present in the supernatant and its color formation seems to depend on oxidation.

Between W121 and the wild type few significant differences were observed in the bioreactor (Table 3.17). The maximum growth rate based on cell concentration measurement was found at 0.46 ± 0.02 h^{-1} for the wild type but at significantly higher values of 0.54 ± 0.03 h^{-1} for W121. Moreover, in all bioreactor experiments with W121 and increased foaming took place and a thick film of cells attached to

the inner reactor wall was observed after the end of exponential growth. The removal of cells from the liquid phase during foaming might also have contributed to the significantly lower biomass yield of W121 ($Y_{X/S}$=0.49 ± 0.05 g g^{-1}) compared to the wild type ($Y_{X/S}$=0.60 ± 0.04 g g^{-1}). The aspects of foaming and morphology that are of particular relevance for W121 were addresses in additional experiments as reported in chapter 3.7.3.

Finally, GC-ToF-MS fingerprinting was carried out by analyzing bioreactor samples of both pre-chassis and the wild type from the exponential and stationary growth phase. In short, both fingerprints of W127 showed only few alterations in intracellular metabolite pools, what further supported the similarity of this pre-chassis to the wild type. In contrast, for W121 multiple metabolites were present in higher intracellular pools during exponential growth, as for example true for the amino acids L-proline, L-glutamine, L-valine and L-arginine, the sugar phosphates fructose-6-phosphate and glucose-6-phosphate as well as the organic acids pyruvate, α-ketoglutarate and malate. Since those metabolites are derived from different branches of the central metabolism and large genomic regions were deleted from W121, the reason for the increased pools cannot be clearly identified.

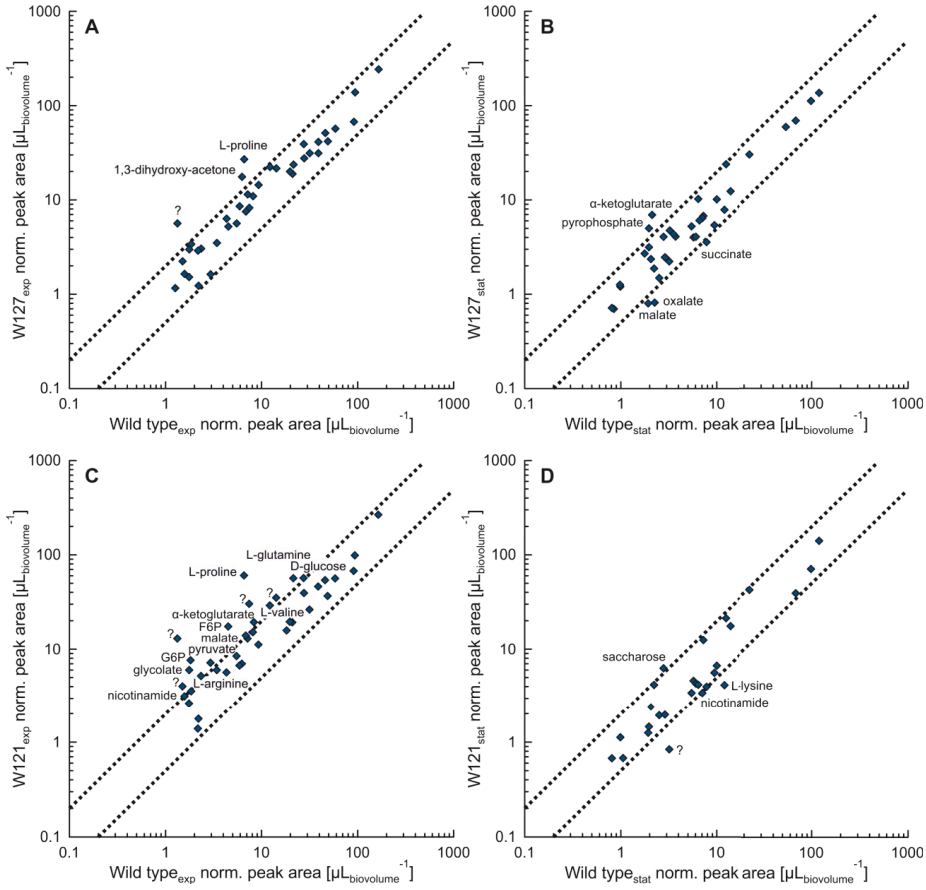

Figure 3.18: Intracellular GC-ToF-MS fingerprints of strains W127 (A+B) and W121 (C+D) during exponential and stationary growth phase on defined CGXII medium in bioreactors. Peak areas detected for all metabolites were normalized by the total biovolume applied during methanol extraction and dashed lines represent levels of 2-fold increased or decreased values compared to the wild type. Question marks label metabolites that could not be identified using the JuPOD database.

3.7.3 Morphology of W121

As mentioned in the previous chapter, W121 displayed some unexpected attributes during bioreactor cultivations, such as strongly increased foaming, lower biomass yield as well as an increased growth rate calculated from cell number measurements. To further investigate these findings another series of bioreactor experiments on defined CGXII medium were carried out for the wild type as well as W121, W105 and W101. The latter two strains include different sub-sets of the deletions combined in W121 (Figure 3.19 B) and might therefore allow to identify the deletions that causes the altered phenotype of W121. Noteworthy, all bioreactor cultivations were initially supplemented with a fixed amount of 300 ppmv antifoam reagent (AF204), which had been determined as sufficient for the general *C. glutamicum* cultivations during initial experiments.

As a first result, W121 showed again a highly increased foaming up to 5 cm above the liquid phase, while for the wild type no foam formation was observed. Moreover, W121 biomass was removed from the liquid phase during foaming and found attached to the inner reactor wall after turn to stationary phase (Figure 3.19 A). Interestingly, the strain W101 showed the same foaming and biomass removal as W121, while the strain W105 behaved comparable to the wild type. Thus, all clusters deleted in W105 could be excluded as reason for the phenotype of W121. Moreover, by taking the genotype of W101 into account, the deletion of the cluster Δ0414-0440 was deduced as most promising candidate to cause the phenotype of increased foaming (Figure 3.19 B). In the next step, the strain with the sole deletion of this region, namely GRS16, was also cultivated in a bioreactor and the phenotype of increased foaming was fully reproduced with this strain.

Moreover, during all bioreactor cultivations the mean cell volumes were monitored using a coulter counter (Figure 3.19 C). Here, all strains showed after inoculation an increase in median cell volume before cell division set in and the cell volume continuously dropped along the course of cultivation, as typically observed for *C. glutamicum* [1]. The strain W101 reached a maximum median cell volume of 5.8 fl which was in the range typically encountered during wild type cultivation. In contrast, the strains with increased foaming W121, W105 as well as GRS16 reached double as high maximum median cell volumes (9.8 to 11.9 fl).

Nevertheless, at the end of exponential growth phase all cultures showed similar cell volumes. The observation of an increased maximum cell volume of W121 in early exponential growth phase moreover explains the elevated maximum growth rate of this strain that was only observed in cell number measurements (cf. Table 3.17). Cells of W121 initially grow to double cell volumes compared to the wild type, followed by an increased segmentation frequency.

During further characterization of W121 and GRS16 in a microfluidic chip, some cells of both strains grew in long chains which were impaired in their separation into individual cells and, moreover, the cells stuck together to large cell aggregates what is normally not observed for *C. glutamicum* (results not shown). The formation of such cell aggregates might directly explain the attachment of the biomass to the foam and the inner wall of the stirred and aerated bioreactors.

In summary, the increased median cell volume and highly increased foaming of the pre-chassis W121 could quickly be narrowed down to be caused by the deletion of the cluster Δ0414-0440. Multiple genes in this cluster were annotated to play a role in cell wall formation in other organisms, such as anchoring of polyglutamate capsule to peptidoglycan (*CapD*) during synthesis of cell surface polysaccharides (*wzy, wzx* and *wzz*) and murein synthesis (*murA* and *murB*) [95–97]. As an example, in *Listeria monocytogenes* the sole *murA* deletion led to long cell chains, comparable to the results obtained in this study in the microfluidic chip [98]. Most interestingly, the complete cluster Δ0414-0440 misses in the *C. glutamicum* strain R which can be differentiated from ATCC 13032 by cell wall staining [99]. However, it so far the altered phenotype von W121 could not be deduced to single genes in the cluster Δ0414-0440 and could result from combinatorial deletion of multiple genes. Nevertheless, the results show how libraries of genome reduced strains can be used to quickly connect an altered phenotype to a comparable small genomic region.

A

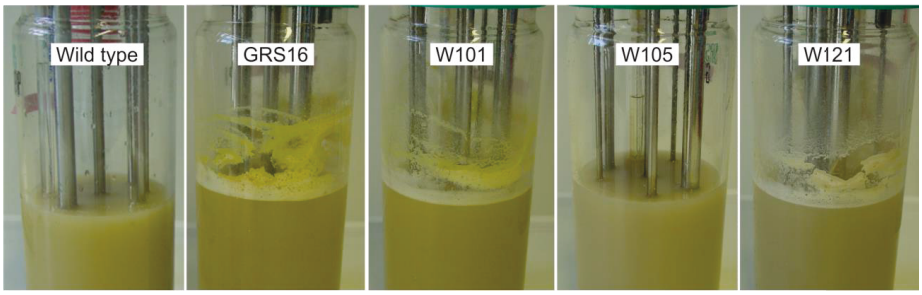

B

	WT	GRS16	W101	W105	W121
ΔCGP123		X	X	X	X
ΔISCg12		X	X	X	X
Δ0414-0440		**X**	**X**		**X**
Δ0635-0646			X	X	X
Δ0704-0748				X	X
Δ0822-0845			X	X	X
Δ1018-1033				X	X
Δ1172-1213				X	X
Δ1291-1305					X
Δ1340-1352					X

C

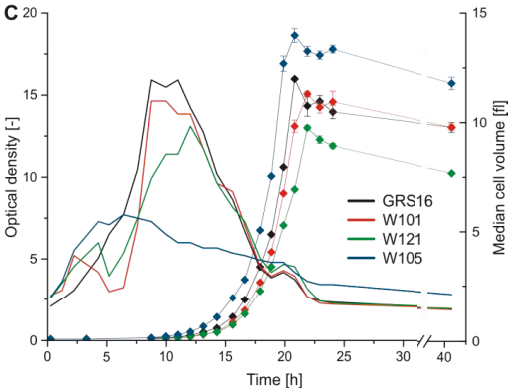

Figure 3.19: Effect of gene cluster deletions on the morphology of W121. Lab-scale bioreactor experiments were conducted on defined CGXII medium. (A) Pictures of bioreactor broth after turn to stationary growth phase. (B) Genotypes of strains GRS16, W101, W105 and W121. (C) Time courses of median cell volumes during the cultivations, each inoculated at low cell densities ($OD_{initial} \approx 0.005$).

4. Summary

Aim of this work was the establishment of methods to characterize a large strain library, of which some methods were supported by laboratory automation on a mini pilot plant (MPP). These workflows were then applied during the step-wise reduction of the natural *C. glutamicum* genome toward a chassis for synthetic biology. Each strain obtained in the project was tested for biological fitness, which was defined by the biomass yield and maximal specific growth rate on the well-known defined CGXII medium with D-glucose as primary carbon source. Both of these parameters were then compared between each partially genome-reduced strain to the *C. glutamicum* wild type ATCC 13032. Any genome reduction leading to no significant decrease in both parameters was considered as successful and recommended for the further successive genome reduction.

In first reference experiments, bioreactor cultivations were combined with microfluidic chips and analyzed using methods from transcriptomics and metabolomics. Here, protocatechuic acid was identified as hidden co-substrate in CGXII medium, which elevates growth rates by about 50 %. However, the effect is only visible in highly diluted cultures [2, 73].

Initially, methods were developed to handle and characterize large strain libraries. A workflow was developed to generate WCBs and MCBs from strains derived by project partners, to enable a subsequent strain characterization in short times and high reproducibility. Data analysis was standardized to comparably estimate maximal growth rates from BioLector cultivations throughout the project. Moreover, robotic workflows were established to harvest cell-free cultivation supernatants from BioLector cultivations in response to individually defined triggers [1]. These workflows were finally completed by metabolite assays for amino acids and D-glucose that were automated in 384-well plate scale. All methods were subsequently applied to characterize libraries of genome-reduced *C. glutamicum* strains.

In a first step toward a chassis, project partners deleted three prophage elements from the *C. glutamicum* wild type, which together contributed for 6.7 % of the genome. The respective strain MB001 was thoroughly characterized using the established methods and fulfilled the criterion of unaltered biological fitness. Most interestingly, the removal of prophage elements in MB001 was found to improve heterologous protein expression in this host and the effect could be narrowed down to the deletion of three genes of a restriction-modification system [3].

As a next step, non-essential gene clusters were deleted from the previously established prophage-free strain, after additional removal of other mobile genetic elements. In total, the deletion of 41 clusters with sizes between 3.7 and 49.7 kbp was attempted, of which 36 could be carried out successfully to derive the respective number of genome-reduced strains (GRS). The deletion of the remaining 5 clusters could repeatedly not been achieved, most probably because they contain at least one yet unknown essential gene. All GRS were characterized using the beforehand developed methods and, in summary, 26 clusters could be classified as irrelevant for the biological fitness of *C. glutamicum* on CGXII medium [4]. At this point, the combinatorial deletion of all 26 irrelevant clusters offered the potential to reduce the *C. glutamicum* genome by about 22 %.

In further experiments, all GRS were tested on an enriched medium variant. This led to some assumptions about some yet unknown gene functions in those clusters that were proven to be relevant for the biological fitness on defined CGXII medium. Moreover, some clusters were also deleted from the L-lysine model producer DM1933 and the obtained genome reduced L-lysine producers (GRLP) were tested for biological fitness as well as production attributes using the developed MPP workflows. As a result, GRLP45 was identified to produce a 51 % higher L-lysine titer while growing proportionally slower compared to DM1933. The results obtained on the MPP could subsequently be confirmed using conventional lab-scale bioreactors [1].

Further steps toward a *C. glutamicum* chassis were subsequently taken by combinatorial deletion of clusters that had previously been identified as irrelevant. As expected, some clusters showed interdependencies among each other during combinatorial deletion, what pointed to yet not fully understood analogous functions of genes of the respective clusters. One example was the strain W65 that showed an impaired growth rate after deletion of two irrelevant gene clusters. During in-depth characterization, intracellular fingerprints pointed toward a limitation in the translation machinery of W65. Indeed, both deleted clusters contained operons for ribosomal RNA and, thus, the results might indicate the general interplay of ribosome capacity and maximum growth rates in *C. glutamicum*.

Fortunately, other combinatorial deletions were carried out successfully and resulted in the pre-chassis W127 and W121 with a total genome reduction of 8.8 % and 12.8 %, respectively. Both pre-chassis showed, compared to the wild type, unaltered final backscatter values and, in fact, grew at significantly higher maximal growth rates but only in the BioLector. In further studies, both strains showed tolerance against osmotic stress as well as nitrogen and phosphate limitation at wild-type level. Nevertheless, W121 displayed impaired biological fitness on some C-sources other than D-glucose, what was understandable since growth on this hexose was the sole criterion during the targeted strain development. However, W127 maintained growth phenotype on all C-sources at wild-type level and grew even faster on few of the alternative substrates. This result might point to a reduced metabolic burden of W127 after removal of irrelevant genetic elements.

Finally, the pre-chassis W127 and W121 were transferred to lab-scale bioreactors. Here, the faster growth rates obtained based on the backscatter signal could not be observed in any other biomass signal. Thus, some clusters that alter the cells optical attributes might have been chosen as deletion targets during the initial screening for backscatter growth rates. This finding ultimately follows the principle "you get what you screen for" encountered in most screening approaches, which in this case means that a screening for growth rates based on the backscatter signal does not necessarily result in strains growing faster considering any other biomass signal [94]. However, also in the bioreactor W127 displayed unaltered growth behavior and intracellular GC-ToF fingerprints without major changes.

In contrast, the transfer of W121 to stirred and aerated bioreactors was rather unsuccessful, as these cultivations developed foam to an unusual extend, resulting in biomass being transported out of the liquid phase. This unexpected behavior was subsequently assessed by bioreactor cultivations of different precursors of W121 and could thereby be rapidly narrowed down to the deletion of the cluster Δ0414-0440.

In summary, W127 was identified as a promising pre-chassis for future synthetic biology approaches. Moreover, the library comprising 116 partially genome-reduced *C. glutamicum* strains was characterized thoroughly in this joined cooperation project and enabled some discoveries on the genetic organization of *C. glutamicum* and is therefore a valid basis for future research.

5. Conclusion and Outlook

The identification of protocatecuic acid as hidden co-substrate in CGXII medium is for batch cultures only relevant at low cell densities, since PCA is consumed before the cells reach significant biomass densities. However, when metabolic flux studies with labelled substrates are carried out in fed-batch or continuous mode the steady co-consumption of PCA must be taken into account.

The developed workflows to handle and characterize strains might serve as blueprint for following projects. This holds especially true for the quantitative assessment of growth phenotypes or automated sampling of cell-free supernatants with subsequent metabolite quantification in 384-well scale. In contrast, the strain handling should be reconsidered when it is applied for other organisms or when heading for different target criteria. In any case, it is of outmost importance to clearly define target criteria and experimental strategies in the beginning of such iterative strain development projects. Today, robotic applications are still far away from routine application and further work could therefore aim for a more consistent strategy to transfer bioprocesses back and forth between microtiter plates and large bioreactors.

The development of chassis organisms will remain an important field in synthetic biology. The targeted strategy followed in this work is at first sight comparably slow, but has already led to degrees of genome reduction which were not obtained in other projects without affecting the organisms biological fitness. Clearly, the remaining irrelevant gene clusters should also be deleted from the promising pre-chassis W127, since this strain did not show any growth defect and grew in fact better compared to the wild type on few C-sources. The derived chassis is expected to display a total genome reduction of up to 22 % while displaying unimpaired biological fitness and, potentially, a reduced metabolic burden.

Ultimately, the use of a genome reduced *C. glutamicum* host for production of food additives is questionable as the large genome rearrangements intrinsically result in a new strain that might lose its GRAS status. Despite of that, for academic purposes genome reduction offers the potential to better understand a cells genetic arrangement and offers in the end the opportunity to construct artificial biological systems.

6. References

1. Unthan S, Radek A, Wiechert W, Oldiges M, Noack S (2015) Bioprocess automation on a Mini Pilot Plant enables fast quantitative microbial phenotyping. Microb Cell Fact 14:32. doi: 10.1186/s12934-015-0216-6

2. Unthan S, Grünberger A, van Ooyen J, Gätgens J, Heinrich J, Paczia N, Wiechert W, Kohlheyer D, Noack S (2014) Beyond growth rate 0.6: What drives Corynebacterium glutamicum to higher growth rates in defined medium. Biotechnol Bioeng 111:359–71. doi: 10.1002/bit.25103

3. Baumgart M, Unthan S, Rückert C, Sivalingam J, Grünberger A, Kalinowski J, Bott M, Noack S, Frunzke J (2013) Construction of a prophage-free variant of Corynebacterium glutamicum ATCC 13032 for use as a platform strain for basic research and industrial biotechnology. Appl Environ Microbiol 79:6006–15. doi: 10.1128/AEM.01634-13

4. Unthan S, Baumgart M, Radek A, Herbst M, Siebert D, Brühl N, Bartsch A, Bott M, Wiechert W, Marin K, Hans S, Krämer R, Seibold G, Frunzke J, Kalinowski J, Rückert C, Wendisch VF, Noack S (2014) Chassis organism from Corynebacterium glutamicum - a top-down approach to identify and delete irrelevant gene clusters. Biotechnol J 1–12. doi: 10.1002/biot.201400041

5. Udaka S (2008) The discovery of Corynebacterium glutamicum and birth of amino acid fermentation industry in japan. Corynebacteria: genomics Mol. Biol. Caister Academic, Norfolk, pp 1–6

6. Becker J, Wittmann C (2012) Bio-based production of chemicals, materials and fuels -Corynebacterium glutamicum as versatile cell factory. Curr Opin Biotechnol 23:631–40. doi: 10.1016/j.copbio.2011.11.012

7. Wieschalka S, Blombach B, Bott M, Eikmanns BJ (2013) Bio-based production of organic acids with Corynebacterium glutamicum. Microb Biotechnol 6:87–102. doi: 10.1111/1751-7915.12013

8. Becker J, Wittmann C (2012) Systems and synthetic metabolic engineering for amino acid production - the heartbeat of industrial strain development. Curr Opin Biotechnol 23:718–26. doi: 10.1016/j.copbio.2011.12.025

9. Wittmann C (2010) Analysis and Engineering of Metabolic Pathway Fluxes in Corynebacterium glutamicum. Biosystems Engineering, Springer Berlin Heidelberg 21–49. doi: 10.1007/10

10. Wendisch VF, de Graaf a. a., Sahm H, Eikmanns BJ (2000) Quantitative Determination of Metabolic Fluxes during Coutilization of Two Carbon Sources: Comparative Analyses with Corynebacterium glutamicum during Growth on Acetate and/or Glucose. J Bacteriol 182:3088–3096. doi: 10.1128/JB.182.11.3088-3096.2000

11. Gerstmeir R, Wendisch VF, Schnicke S, Ruan H, Farwick M, Reinscheid D, Eikmanns BJ (2003) Acetate metabolism and its regulation in Corynebacterium glutamicum. J Biotechnol 104:99–122. doi: 10.1016/S0168-1656(03)00167-6

12. Peters-Wendisch PG, Schiel B, Wendisch VF, Katsoulidis E, Mockel B, Sahm H, Eikmanns BJ (2001) Pyruvate Carboxylase is a Major Bottleneck for Glutamate and Lysine Production by Corynebacterium glutamicum. J Mol Microbiol Biotechnol 3:295–300.

13. Kalinowski J, Bathe B, Bartels D, Bischoff N, Bott M, Burkovski A, Dusch N, Eggeling L, Eikmanns BJ, Gaigalat L, Goesmann A, Hartmann M, Huthmach K, Krämer R, Linke B, McHardy AC, Meyer F, Mocker B, Pfefferle W, Pühler A, rey DA, Rükert D, Rupp O, Sahm H, Wendisch VF, Wiegrabe I, Tauch A (2003) The complete Corynebacterium glutamicum ATCC 13032 genome sequence and its impact on the production of l-aspartate-derived amino acids and vitamins. J Biotechnol 104:5–25. doi: 10.1016/S0168-1656(03)00154-8

14. Ikeda M, Nakagawa S (2003) The Corynebacterium glutamicum genome: features and impacts on biotechnological processes. Appl Microbiol Biotechnol 62:99–109. doi: 10.1007/s00253-003-1328-1

15. Buchholz J, Schwentner A, Brunnenkan B, Gabris C, Grimm S, Gerstmeier R, Takors R, Eikmanns BJ, Blombach B (2013) Platform engineering of Corynebacterium glutamicum with reduced pyruvate dehydrogenase complex activity for improved production of L-lysine, L-valine, and 2-ketoisovalerate. Appl Environ Microbiol 79:5566–75. doi: 10.1128/AEM.01741-13

16. Van Ooyen J, Noack S, Bott M, Reth A, Eggeling L (2012) Improved L-lysine production with Corynebacterium glutamicum and systemic insight into citrate synthase flux and activity. Biotechnol Bioeng 109:2070–81. doi: 10.1002/bit.24486

17. Blombach B, Schreiner ME, Holátko J, Bartek T, Oldiges M, Eikmanns BJ (2007) L-valine production with pyruvate dehydrogenase complex-deficient Corynebacterium glutamicum. Appl Environ Microbiol 73:2079–84. doi: 10.1128/AEM.02826-06

18. Radek A, Krumbach K, Gätgens J, Wiechert W, Bott M, Noack S, Marienhagen J (2014) Engineering of Corynebacterium glutamicum for minimized carbon loss during utilization of d-xylose containing substrates. J Biotechnol 192:156–160. doi: 10.1016/j.jbiotec.2014.09.026

19. Witthoff S, Schmitz K, Niedenführ S, Nöh K, Noack S, Bott M, Marienhagen J (2015) Metabolic Engineering of Corynebacterium glutamicum for the Metabolization of Methanol. Appl Environ Microbiol AEM.03110–14–. doi: 10.1128/AEM.03110-14

20. Wiechert W, Noack S (2011) Mechanistic pathway modeling for industrial biotechnology: challenging but worthwhile. Curr Opin Biotechnol 22:604–10. doi: 10.1016/j.copbio.2011.01.001

21. Chopra P, Kamma A (2006) Engineering Life through Synthetic Biology. In silico biology 6:401–410.

22. Cohen C (1996) The early history of chemical engineering: a reassessment. Br J Hist Sci 29:171–194.

23. Paddon CJ, Westfall PJ, Pitera DJ, Benjamin K, Fisher K, McPhee D, Leavell MD, Tai A, Main A, Eng D, Plichuk DR, Teoh KH, Reed DW, Treynor T, Lenihan J, Jiang H, Fleck M, Bajad S, Dang G, Dengrove D, Diola D, Dorin G, Ellens KW, Fickes S, Galazzo J, Gaucher SP, Geistlinger T, Henry R, Hepp M, Horning T, Iqbal T, Kizer L, Lieu B, Melis D, Moss N, Regentin R, Secrest S, Tsuruta H, Vazquez R, Westblade LF, Xu L, Yu M, Zhang Y, Zhao L, Lievense J, Covello PS, Keasling JD, Reiling KK, Renninger NS, Newman JD (2013) High-level semi-synthetic production of the potent antimalarial artemisinin. Nature 496:528–32. doi: 10.1038/nature12051

24. Shipp SS, Gupta N, Lal B, Scott JA, Weber CJ, Finnin MS, Blake M, Newsome S, Thomas S (2012) Emerging Global Trends in Advanced Manufacturing. (No. IDA-P-4603). Institute for defense analyses analyses alexandria VA.

25. Gibson DG, Glass JI, Lartigue C, Noskov VN, Chuang RY, Algire MA, Benders GA, Montague MG, Ma L, Moodle MM, Merryman C, Vashee S, Krishnakumar R, Assad-Garcia N, Andrews-Pfannkoch C, Denisova EA, Young L, Qi ZQ, Segall-Shapiro TH, Calvey CH, Parmar PP, Hutchison CA; Smith HA, Venter JC (2010) Creation of a bacterial cell controlled by a chemically synthesized genome. Science 329:52–6. doi: 10.1126/science.1190719

26. Takano E, Bovenberg R a L, Breitling R (2012) A turning point for natural product discovery--ESF-EMBO research conference: synthetic biology of antibiotic production. Mol Microbiol 83:884–93. doi: 10.1111/j.1365-2958.2012.07984.x

27. Zhang L-Y, Chang S-H, Wang J (2010) How to make a minimal genome for synthetic minimal cell. Protein Cell 1:427–34. doi: 10.1007/s13238-010-0064-4

28. Leprince A, van Passel MWJ, dos Santos VAPM (2012) Streamlining genomes: toward the generation of simplified and stabilized microbial systems. Curr Opin Biotechnol 23:651–8. doi: 10.1016/j.copbio.2012.05.001

29. De Lorenzo V (2011) Beware of metaphors: chasses and orthogonality in synthetic biology. Bioeng Bugs 2:3–7. doi: 10.4161/bbug.2.1.13388

30. Esvelt KM, Wang HH (2013) Genome-scale engineering for systems and synthetic biology. Mol Syst Biol 9:641. doi: 10.1038/msb.2012.66

31. Gao H, Zhuo Y, Ashforth E, Zhang L (2010) Engineering of a genome-reduced host: practical application of synthetic biology in the overproduction of desired secondary metabolites. Protein Cell 1:621–6. doi: 10.1007/s13238-010-0073-3

32. Razin S, Hayflick L (2010) Highlights of mycoplasma research-an historical perspective. Biologicals 38:183–90. doi: 10.1016/j.biologicals.2009.11.008

33. Suzuki N, Okayama S, Nonaka H, Tsuge Y, Inui M, Yukawa H (2005) Large-Scale Engineering of the Corynebacterium glutamicum Genome. Appl Environ Microbiol 71:3369-3372 doi: 10.1128/AEM.71.6.3369

34. Tsuge Y, Suzuki N, Inui M, Yukawa H (2007) Random segment deletion based on IS31831 and Cre/loxP excision system in Corynebacterium glutamicum. Appl Microbiol Biotechnol 74:1333–41. doi: 10.1007/s00253-006-0788-5

35. Kjeldsen KR, Nielsen J (2009) In silico genome-scale reconstruction and validation of the Corynebacterium glutamicum metabolic network. Biotechnol Bioeng 102:583–97. doi: 10.1002/bit.22067

36. Puskeiler R, Kaufmann K, Weuster-Botz D (2005) Development, parallelization, and automation of a gas-inducing milliliter-scale bioreactor for high-throughput bioprocess design (HTBD). Biotechnol Bioeng 89:512–23. doi: 10.1002/bit.20352

37. Kensy F, Zang E, Faulhammer C, Tan RK, Büchs J (2009) Validation of a high-throughput fermentation system based on online monitoring of biomass and fluorescence in continuously shaken microtiter plates. Microb Cell Fact 8:31. doi: 10.1186/1475-2859-8-31

38. Schäpper D, Alam MNHZ, Szita N, Lantz AE, Gernacy V (2009) Application of microbioreactors in fermentation process development: a review. Anal Bioanal Chem 395:679–95. doi: 10.1007/s00216-009-2955-x

39. Kondragunta B, Drew JL, Brorson K a, Moreira AR, Rao G (2010) Advances in clone selection using high-throughput bioreactors. Biotechnol Prog 26:1095–103. doi: 10.1002/btpr.392

40. Barrett TA, Wu A, Zhang H, Levy MS, Lye GJ (2010) Microwell engineering characterization for mammalian cell culture process development. Biotechnol Bioeng 105:260–75. doi: 10.1002/bit.22531

41. Kumada Y, Takase Y, Sasaki E, Kishimoto M (2011) High-throughput, high-level production of PS-tag-fused single-chain Fvs by microplate-based culture. J Biosci Bioeng 111:569–73. doi: 10.1016/j.jbiosc.2011.01.008

42. Funke M, Buchenauer A, Mokwa W, Kluge S, Hein L, Müller C, Kensy F, Büchs J (2010) Bioprocess control in microscale: scalable fermentations in disposable and user-friendly microfluidic systems. Microb Cell Fact 9:86. doi: 10.1186/1475-2859-9-86

43. Panula-Perälä J, Siurkus J, Vasala A, Wilmanowski R, Casteleijn MG, Neubauer P (2008) Enzyme controlled glucose auto-delivery for high cell density cultivations in microplates and shake flasks. Microb Cell Fact 7:31. doi: 10.1186/1475-2859-7-31

44. Long Q, Liu X, Yang Y, Li L, Harvey L, McNeil B, Bai Z (2014) The development and application of high throughput cultivation technology in bioprocess development. J Biotechnol 192 Pt B:323–38. doi: 10.1016/j.jbiotec.2014.03.028

45. Huber R, Ritter D, Hering T, Hilmer AK, Kensy F, Müller C, Wang L, Büchs J (2009) Robo-Lector - a novel platform for automated high-throughput cultivations in microtiter plates with high information content. Microb Cell Fact 8:42. doi: 10.1186/1475-2859-8-42

46. Hemmerich J, Adelantado N, Barrigón JM, Ponte X, Hörmann A, Ferrer P, Kensy F, Valero F (2014) Comprehensive clone screening and evaluation of fed-batch strategies in a microbioreactor and lab scale stirred tank bioreactor system: application on Pichia pastoris producing Rhizopus oryzae lipase. Microb Cell Fact 13:36. doi: 10.1186/1475-2859-13-36

47. Rohe P, Venkanna D, Kleine B, Freudl R, Oldiges M (2012) An automated workflow for enhancing microbial bioprocess optimization on a novel microbioreactor platform. Microb Cell Fact 11:144. doi: 10.1186/1475-2859-11-144

48. Knepper A, Heiser M, Glauche F, Neubauer P (2014) Robotic Platform for Parallelized Cultivation and Monitoring of Microbial Growth Parameters in Microwell Plates. J Lab Autom. doi: 10.1177/2211068214547231

49. Sonnleitner B (1997) Bioprocess automation and bioprocess design. J Biotechnol 52:175–179. doi: 10.1016/S0168-1656(96)01642-2

50. Lorenz MG. (2004) Liquid-handling robotic workstations for functional genomics. J Assoc Lab Autom 9:262–267. doi: 10.1016/j.jala.2004.03.010

51. Nealon AJ, Willson KE, Pickering SCR, Clayton TM, O'Kennedy RD, Titchener-Hooker NJ, Lye GJ (2005) Use of operating windows in the assessment of integrated robotic systems for the measurement of bioprocess kinetics. Biotechnol Prog 21:283–91. doi: 10.1021/bp049868+

52. Nettekoven M, Thomas A (2002) Accelerating Drug Discovery by Integrative Implementation of Laboratory Automation in the Work Flow. Curr Med Chem 9:2179–2190. doi: 10.2174/0929867023368764

53. Smith A (2002) Screening for drug discovery: the leading question. Nature 418:453–9. doi: 10.1038/418453a

54. Scheel M, Lütke-Eversloh T (2013) New options to engineer biofuel microbes: development and application of a high-throughput screening system. Metab Eng 17:51–8. doi: 10.1016/j.ymben.2013.03.002

55. Parekh S, Vinci VA, Strobel RJ (2000) Improvement of microbial strains and fermentation processes. Appl Microbiol Biotechnol 54:287–301. doi: 10.1007/s002530000403

56. Koryakina I, Neville J, Nonaka K, Van Lanen SG, Williams GJ (2011) A high-throughput screen for directed evolution of the natural product sulfotransferase LipB. J Biomol Screen 16:845–51. doi: 10.1177/1087057111413273

57. Rohe P, Venkanna D, Kleine B, Freudl R, Oldiges M (2012) An automated workflow for enhancing microbial bioprocess optimization on a novel microbioreactor platform. Microb Cell Fact 11:144. doi: 10.1186/1475-2859-11-144

58. Zimmermann HF, Raebiger T (2006) Evaluation of the applicability of backscattered light measurements to the determination of microbial cell densities in microtiter plates. Anal Bioanal Chem 386:2245–7. doi: 10.1007/s00216-006-0837-z

59. Samorski M, Müller-Newen G, Büchs J (2005) Quasi-continuous combined scattered light and fluorescence measurements: a novel measurement technique for shaken microtiter plates. Biotechnol Bioeng 92:61–8. doi: 10.1002/bit.20573

60. John GT, Klimant I, Wittmann C, Heinzle E (2003) Integrated optical sensing of dissolved oxygen in microtiter plates: a novel tool for microbial cultivation. Biotechnol Bioeng 81:829–36. doi: 10.1002/bit.10534

61. Funke M, Diederichs S, Kensy F, Müller C, Büchs J (2009) The baffled microtiter plate: increased oxygen transfer and improved online monitoring in small scale fermentations. Biotechnol Bioeng 103:1118–28. doi: 10.1002/bit.22341

62. Hermann R, Lehmann M, Büchs J (2002) Characterization of gas-liquid mass transfer phenomena in microtiter plates. Biotechnol Bioeng 81:178–86. doi: 10.1002/bit.10456

63. Niebisch A, Bott M (2001) Molecular analysis of the cytochrome bc 1 - aa 3 branch of the Corynebacterium glutamicum respiratory chain containing an unusual diheme cytochrome c 1. Arch Microbiol 175:282–294. doi: 10.1007/s002030100262

64. Keilhauer C, Eggeling L, Sahm H (1993) Isoleucine Synthesis in Corynebacterium glutamicum : Molecular Analysis of the ilvB-ilvN-ilvC Operon. 175:5595–5603.

65. Grünberger A, Paczia N, Probst C, Schendzielorz G, Eggeling L, Noack S, Wiechert W, Kohlheyer D (2012) A disposable picolitre bioreactor for cultivation and investigation of industrially relevant bacteria on the single cell level. Lab Chip 12:2060–8. doi: 10.1039/c2lc40156h

66. Gruenberger A, Probst C, Heyer A, Wiechert W, Frunzke J, Kohlheyer (2013) Microfluidic picoliter bioreactor for microbial single-cell analysis: fabrication, system setup, and operation. J Vis Exp 50560. doi: 10.3791/50560

67. Paczia N, Nilgen A, Lehmann T, Gätgens J, Wiechert W, Noack S (2012) Extensive exometabolome analysis reveals extended overflow metabolism in various microorganisms. Microb Cell Fact 11:122. doi: 10.1186/1475-2859-11-122

68. Wu L, Mashego MR, van Dam JC, Proell AM, Vinke JL, Ras C, Van Winden QA, Van Gulik WM, Heijnen JJ (2005) Quantitative analysis of the microbial metabolome by isotope dilution mass spectrometry using uniformly 13C-labeled cell extracts as internal standards. Anal Biochem 336:164–71. doi: 10.1016/j.ab.2004.09.001

69. Paczia N (2012) Metabolomanalyse von Mikroorganismen : Methodenetablierung und Konzepte zur Automatisierung. Bielefeld University

70. Möker N, Brocker M, Schaffer S, Kramer R, Morbach S, Bott M (2004) Deletion of the genes encoding the MtrA-MtrB two-component system of Corynebacterium glutamicum has a strong influence on cell morphology, antibiotics susceptibility and expression of genes involved in osmoprotection. Mol Microbiol 54:420–38. doi: 10.1111/j.1365-2958.2004.04249.x

71. Pfeifer-Sancar K, Mentz A, Rückert C, Kalinowski J (2013) Comprehensive analysis of the Corynebacterium glutamicum transcriptome using an improved RNAseq technique. BMC Genomics 14:888. doi: 10.1186/1471-2164-14-888

72. Frunzke J, Bramkamp M, Schweitzer J-E, Bott M (2008) Population Heterogeneity in Corynebacterium glutamicum ATCC 13032 caused by prophage CGP3. J Bacteriol 190:5111–9. doi: 10.1128/JB.00310-08

73. Grünberger A, van Ooyen J, Paczia N, Rohe P, Schendzielorz G, Eggeling L, Wiechert W, Kohlheyer D, Noack S (2013) Beyond growth rate 0.6: Corynebacterium glutamicum cultivated in highly diluted environments. Biotechnol Bioeng 110:220–8. doi: 10.1002/bit.24616

74. Liebl W, Klamer R, Schleifer K (1989) Applied Microbiology Biotechnology Requirement of chelating compounds for the growth of Corynebacterium ylutamicum in synthetic media. 205–210.

75. Von der Osten CH, Gioannetti C, Sinskey AJ (1989) Design of a defined medium for growth of Cornybacterium glutamicum in which citrate facilities iron uptake. Biotechnology letters 11(1):11-16

76. Haussmann U, Poetsch A (2012) Global proteome survey of protocatechuate- and glucose-grown Corynebacterium glutamicum reveals multiple physiological differences. J Proteomics 75:2649–59. doi: 10.1016/j.jprot.2012.03.005

77. Merkens H, Beckers G, Wirtz A, Burkovski A (2005) Vanillate metabolism in Corynebacterium glutamicum. Curr Microbiol 51:59–65. doi: 10.1007/s00284-005-4531-8

78. Shen X-H, Zhou N-Y, Liu S-J (2012) Degradation and assimilation of aromatic compounds by Corynebacterium glutamicum: another potential for applications for this bacterium? Appl Microbiol Biotechnol 95:77–89. doi: 10.1007/s00253-012-4139-4

79. Brinkrolf K, Brune I, Tauch A (2006) Transcriptional regulation of catabolic pathways for aromatic compounds in Corynebacterium glutamicum. Genet Mol Res 5:773–789.

80. Käß F, Prasad A, Tillack J, Moch M, Giese H, Büchs J, Wiechert W, Oldiges M (2014) Rapid assessment of oxygen transfer impact for Corynebacterium glutamicum. Bioprocess Biosyst Eng. doi: 10.1007/s00449-014-1234-1

81. Friedman M (2004) Applications of the ninhydrin reaction for analysis of amino acids, peptides, and proteins to agricultural and biomedical sciences. J Agric Food Chem 52:385–406. doi: 10.1021/jf030490p

82. Kind S, Becker J, Wittmann C (2013) Increased lysine production by flux coupling of the tricarboxylic acid cycle and the lysine biosynthetic pathway--metabolic engineering of the availability of succinyl-CoA in Corynebacterium glutamicum. Metab Eng 15:184–95. doi: 10.1016/j.ymben.2012.07.005

83. Li Z, Chang S, Lin L, Li Y, An Q (2011) A colorimetric assay of 1-aminocyclopropane-1-carboxylate (ACC) based on ninhydrin reaction for rapid screening of bacteria containing ACC deaminase. Lett Appl Microbiol 53:178–85. doi: 10.1111/j.1472-765X.2011.03088.x

84. Friedman M (1971) Solvent effects in the absorption spectra of the Ninhydrin chromophore. Microchem J 16:204–209. doi: 10.1016/0026-265X(71)90110-X

85. Frunzke J, Bramkamp M, Schweitzer J-E, Bott M (2008) Population Heterogeneity in Corynebacterium glutamicum ATCC 13032 caused by prophage CGP3. J Bacteriol 190:5111–9. doi: 10.1128/JB.00310-08

86. Pierre JL, Fontecave M (1999) Iron and activated oxygen species in biology: The basic chemistry. Biometals 12:195–199. doi: 10.1023/A:1009252919854

87. Pósfai G, Plunkett G, Fehér T, Frisch D, Keil GM, Umenhoffer K, Kolisnychenko V, Stahl B, Sharma SS, de Arruda M, Burland V, Harcum SW, Blattner FR (2006) Emergent properties of reduced-genome Escherichia coli. Science 312:1044–6. doi: 10.1126/science.1126439

88. Choorapoikayil S, Schoepe J, Buchinger S, Schomburg D (2012) Analysis of in vivo function of predicted isoenzymes:a metabolomic approach. OMICS 16:668–80. doi: 10.1089/omi.2012.0055

89. Dusch N, Puhler A, Kalinowski J (1999) Expression of the Corynebacterium glutamicum panD Gene Encoding L-Aspartate-alpha -Decarboxylase Leads to Pantothenate Overproduction in Escherichia coli. Appl Envir Microbiol 65:1530–1539.

90. Eggeling L, Bott M (2005) Handbook of Corynebacterium glutamicum. CRC press.

91. Tran KT, Maeda T, Wood TK (2014) Metabolic engineering of Escherichia coli to enhance hydrogen production from glycerol. Appl Microbiol Biotechnol 98:4757–70. doi: 10.1007/s00253-014-5600-3

92. Thomason LC, Costantino N, Court DL (2007) E. coli genome manipulation by P1 transduction. Curr Protoc Mol Biol Chapter 1:Unit 1.17. doi: 10.1002/0471142727.mb0117s79

93. Condon C, Liveris D, Squires C, Schwartz I, Squires CL (1995) rRNA operon multiplicity in Escherichia coli and the physiological implications of rrn inactivation. J Bacteriol 177:4152–4156.

94. Schmidt-Dannert C, Arnold FH (1999) Directed evolution of industrial enzymes. Trends Biotechnol 17:135–6.

95. Candela T, Fouet A (2005) Bacillus anthracis CapD, belonging to the gamma-glutamyltranspeptidase family, is required for the covalent anchoring of capsule to peptidoglycan. Mol Microbiol 57:717–26. doi: 10.1111/j.1365-2958.2005.04718.x

96. Haussmann U, Qi S-W, Wolters D, Rögner M, Liu SJ, Poetsch A (2009) Physiological adaptation of Corynebacterium glutamicum to benzoate as alternative carbon source - a membrane proteome-centric view. Proteomics 9:3635–51. doi: 10.1002/pmic.200900025

97. Machata S, Hain T, Rohde M, Chakraborty T (2005) Simultaneous Deficiency of both MurA and p60 Proteins Generates a Rough Phenotype in Listeria monocytogenes Simultaneous Deficiency of both MurA and p60 Proteins Generates a Rough Phenotype in Listeria monocytogenes. doi: 10.1128/JB.187.24.8385

98. Carroll SA, Hain T, Technow U, Darji A, Pashalidis P, Joseph SW, Chakraborty T (2003) Identification and Characterization of a Peptidoglycan Hydrolase, MurA, of Listeria monocytogenes, a Muramidase Needed for Cell Separation. J Bacteriol 185:6801–6808. doi: 10.1128/JB.185.23.6801-6808.2003

99. Yukawa H, Omumasaba AC, Nonaka H, Kos P, Okai N, Suzuki N, Suda M, Tsuge Y, Watanabe J, Ikeda Y, Vertes AA, Inui M (2007) Comparative analysis of the Corynebacterium glutamicum group and complete genome sequence of strain R. Microbiology 153:1042–58. doi: 10.1099/mic.0.2006/003657-0

7. Supplement

Table S-1: Strains used in this study. All deletions from the genome were carried out in-frame and gene annotations refer to cg numbers. Strains were obtained from project partners in the working groups of A) Frunzke (Jülich, Germany), B) Kalinowski (Bielefeld, Germany), C) Wendisch (Bielefeld, Germany), D) Krämer (Cologne, Germany) and E) EVONIK Industries (Germany).

Name	Characteristic	Source/Reference
***C. glutamicum* wild type ATCC 13032**		B, [5]
ΔcglMRR	Deletion of restriction-modification system in CGP3 (Δ1996-1998)	A, [3]
ΔCGP3	Deletion of prophage CGP3 (Δ1890-2071)	A, [3]
MB001	Deletion of prophages CGP1,2 and 3 (Δ1890-2071, Δ1746-1752 and Δ1890-2071)	A, [3]
W11	Δ0414-0440	B
W12	Δ1172-1213	B
GRS12	ΔCGP123 ΔISCg12 Δ0116-0147	D, [4]
GRS13	ΔCGP123 ΔISCg12 Δ0158-0183	D, [4]
GRS15	ΔCGP123 ΔISCg12 Δ0311-0333	C, [4]
GRS16	ΔCGP123 ΔISCg12 Δ0414-0440	B, [4]
GRS17	ΔCGP123 ΔISCg12 Δ0635-0646	B, [4]
GRS18	ΔCGP123 ΔISCg12 Δ0704-0748	D, [4]
GRS19	ΔCGP123 ΔISCg12 Δ0822-0845	D, [4]
GRS20	ΔCGP123 ΔISCg12 Δ0900-0909	B, [4]
GRS21	ΔCGP123 ΔISCg12 ΔrrnB-0931	B, [4]
GRS22	ΔCGP123 ΔISCg12 Δ1018-1033	B, [4]
GRS23	ΔCGP123 ΔISCg12 Δ1172-1213	B, [4]
GRS24	ΔCGP123 ΔISCg12 Δ1219-1247	B, [4]
GRS25	ΔCGP123 ΔISCg12 Δ1281-1289	B, [4]
GRS26	ΔCGP123 ΔISCg12 Δ1291-1305	B, [4]
GRS28	ΔCGP123 ΔISCg12 Δ1340-1353	B, [4]
GRS29	ΔCGP123 ΔISCg12 Δ1370-1385	B, [4]
GRS30	ΔCGP123 ΔISCg12 Δ1540-1549	B, [4]
GRS31	ΔCGP123 ΔISCg12 Δ1843-1853	B, [4]
GRS32	ΔCGP123 ΔISCg12 Δ2136-2139	B, [4]
GRS33	ΔCGP123 ΔISCg12 Δ2312-2322	D, [4]
GRS37	ΔCGP123 ΔISCg12 Δ2621-2643	B, [4]
GRS38	ΔCGP123 ΔISCg12 Δ2663-2686	B, [4]
GRS39	ΔCGP123 ΔISCg12 Δ2701-2716	C, [4]
GRS40	ΔCGP123 ΔISCg12 Δ2755-2760	B, [4]
GRS41	ΔCGP123 ΔISCg12 Δ2801-2828	B, [4]
GRS42	ΔCGP123 ΔISCg12 Δ2880-2904	B, [4]
GRS43	ΔCGP123 ΔISCg12 Δ2925-2943	C, [4]
GRS44	ΔCGP123 ΔISCg12 Δ2965-2973	C, [4]
GRS45	ΔCGP123 ΔISCg12 Δ2990-3006	A, [4]

GRS46	ΔCGP123 ΔISCg12 Δ3050-3062	B, [4]
GRS47	ΔCGP123 ΔISCg12 Δ3072-3091	A, [4]
GRS48	ΔCGP123 ΔISCg12 Δ3102-3111	A, [4]
GRS50	ΔCGP123 ΔISCg12 Δ3208-3236	A, [4]
GRS51	ΔCGP123 ΔISCg12 ΔrrnC-3298	B, [4]
GRS52	ΔCGP123 ΔISCg12 Δ3263-3301	D, [4]
GRS53	ΔCGP123 ΔISCg12 Δ3324-3345	A, [4]
GRS54	ΔCGP123 ΔISCg12 Δ3365-3413	D, [4]
W34	ΔCGP123 ΔISCg12 Δ1172-1213 Δ0414-0440	B, [4]
W35	ΔCGP123 ΔISCg12 Δ1172-1213 Δ1018-1033	B, [4]
W36	ΔCGP123 ΔISCg12 Δ1172-1213 Δ3050-3062	B, [4]
W64	ΔCGP123 ΔISCg12 Δ2801-2828 ΔrrnB-0931	B, [4]
W65	ΔCGP123 ΔISCg12 Δ2801-2828 ΔrrnC-3298	B, [4]
W85	ΔCGP123 ΔISCg12 Δ2990-2999	A
W86	ΔCGP123 ΔISCg12 Δ3000-3006	A
W55	ΔCGP123 ΔISCg12 ΔIScg5a ΔIScg5b	B
W56	ΔCGP123 ΔISCg12 ΔIScg5a ΔIScg5b ΔISCg5c-ISCg19a	B
W52	ΔCGP123 ΔISCg12 ΔrrnB	B
rrnBC	ΔCGP123 ΔISCg12 ΔrrnB ΔrrnC	B
rrnBF	ΔCGP123 ΔISCg12 ΔrrnB ΔrrnF	B
rrnCF	ΔCGP123 ΔISCg12 ΔrrnC ΔrrnF	B
rrnBCF	ΔCGP123 ΔISCg12 ΔrrnB ΔrrnC ΔrrnF	B
rrnABCEF #29	ΔCGP123 ΔISCg12 ΔrrnA ΔrrnB ΔrrnC ΔrrnE ΔrrnF (Colony #29)	B
rrnABCEF #83	ΔCGP123 ΔISCg12 ΔrrnA ΔrrnB ΔrrnC ΔrrnE ΔrrnF (Colony #83)	B
W100	ΔCGP123 ΔISCg12 Δ0414-0440 Δ0635-0646	B
W101	ΔCGP123 ΔISCg12 Δ0414-0440 Δ0635-0646 Δ0822-0845	B
W102	ΔCGP123 ΔISCg12 Δ0635-0646 Δ1018-1033 Δ1172-1213	B
W103	ΔCGP123 ΔISCg12 Δ0635-0644 Δ0822-0845 Δ1018-1033 Δ1172-1213	B
W104	ΔCGP123 ΔISCg12 Δ0414-0440 Δ0635-0646 Δ0822-0845 Δ1018-1033 Δ1172-1213	B
W105	ΔCGP123 ΔISCg12 Δ0635-0646 Δ0704-0748 Δ0822-0845 Δ1018-1033 Δ1172-1213	B
W106	ΔCGP123 ΔISCg12 Δ2312-2322 Δ2621-2643	D
W107	ΔCGP123 ΔISCg12 Δ2312-2322 Δ2663-2686	D
W108	ΔCGP123 ΔISCg12 Δ2312-2322 Δ2755-2760	D
W109	ΔCGP123 ΔISCg12 Δ2312-2322 Δ3050-3062	D
W110	ΔCGP123 ΔISCg12 Δ2312-2322 Δ2621-2643 Δ2663-2686	D
W111	ΔCGP123 ΔISCg12 Δ2312-2322 Δ2621-2643 Δ2755-2760	D
W112	ΔCGP123 ΔISCg12 Δ2312-2322 Δ2663-2686 Δ2755-2760	D
W113	ΔCGP123 ΔISCg12 Δ2312-2322 Δ2621-2643 Δ2663-2686 Δ2755-2760	D
W114	ΔCGP123 ΔISCg12 Δ3072-3091 Δ3102-3111	A
W115	ΔCGP123 ΔISCg12 Δ3072-3091 Δ3102-3111 Δ3263-3301	A
W116	ΔCGP123 ΔISCg12 Δ3072-3091 Δ3102-3111 Δ3263-3301 Δ3324-3345	A

W118	ΔCGP123 ΔISCg12 ΔIScg5a ΔIScg5b ΔISCg5c ΔISCg13a ΔISCg13b	B
W119	ΔCGP123 ΔISCg12 Δ0414-0440 Δ0635-0646 Δ0704-0748 Δ0822-0845 Δ1018-1033 Δ1172-1213	B
W120	ΔCGP123 ΔISCg12 Δ0414-0440 Δ0635-0646 Δ0704-0748 Δ0822-0845 Δ1018-1033 Δ1172-1213 Δ1291-1305	B
W121	ΔCGP123 ΔISCg12 Δ0414-0440 Δ0635-0646 Δ0704-0748 Δ0822-0845 Δ1018-1033 Δ1172-1213 Δ1291-1305 Δ1340-1352	B
W122	ΔCGP123 ΔISCg12 Δ2312-2322 Δ2621-2643 Δ2663-2686 Δ2755-2760 Δ3050-3062	D
W124	ΔCGP123 ΔISCg12 Δ2312-2322 Δ2621-2643 Δ2663-2686 Δ2755-2760 Δ3324-3345	D
W125	ΔCGP123 ΔISCg12 Δ2312-2322 Δ2621-2643 Δ2663-2686 Δ2755-2760 Δ3365-3413	D
W127	ΔCGP123 ΔISCg12 Δ2312-2322 Δ2621-2643 Δ2663-2686 Δ2755-2760 Δ3102-3111	D
W129	ΔCGP123 ΔISCg12 Δ2312-2322 Δ2621-2643 Δ2663-2686 Δ2755-2760 Δ3050-3062 Δ3102-3111	D
W130	ΔCGP123 ΔISCg12 Δ2312-2322 Δ2621-2643 Δ2663-2686 Δ2755-2760 Δ3102-3111 Δ3324-3345	D
W131	ΔCGP123 ΔISCg12 Δ2312-2322 Δ2621-2643 Δ2663-2686 Δ2755-2760 Δ3102-3111 Δ3365-3413	D
W134	ΔCGP123 ΔISCg12 Δ0414-0440 Δ0635-0646 Δ0704-0748 Δ0822-0845 Δ1018-1033 Δ1172-1213 Δ1291-1305 Δ1340-1352 Δ1370-1385	B
***C. glutamicum* DM1933 model L-Lysine producer**		E, [17]
D14	ΔCGP1	B
D15	ΔCGP2	B
D16	ΔCGP3	B
D17	ΔCGP123	B
GRLP16	ΔCGP123 Δ0414-0440	B, [4]
GRLP17	ΔCGP123 Δ0635-0646	B, [4]
GRLP20	ΔCGP123 Δ0900-0909	B, [4]
GRLP23	ΔCGP123 Δ1172-1213	B, [4]
GRLP30	ΔCGP123 Δ1540-1549	B, [4]
GRLP31	ΔCGP123 Δ1843-1853	B, [4]
GRLP32	ΔCGP123 Δ2136-2139	B, [4]
GRLP37	ΔCGP123 Δ2621-2643	B, [4]
GRLP39	ΔCGP123 Δ2701-2716	C, [4]
GRLP41	ΔCGP123 Δ2801-2828	B, [4]
GRLP42	ΔCGP123 Δ2880-2904	B, [4]
GRLP43	ΔCGP123 Δ2925-2943	C, [4]
GRLP45	ΔCGP123 Δ2990-3006	A, [4]
GRLP46	ΔCGP123 Δ3050-3062	B, [4]
GRLP47	ΔCGP123 Δ3072-3091	A, [4]
GRLP48	ΔCGP123 Δ3102-3111	A, [4]
GRLP49	ΔCGP123 Δ2755-2760	B, [4]
GRLP50	ΔCGP123 Δ3208-3236	A, [4]
GRLP53	ΔCGP123 Δ3324-3345	A, [4]

D87	ΔCGP123 Δ3001	D
D132	ΔCGP123 Δ0704-0748 Δ0635-0645	D
D133	ΔCGP123 Δ0704-0748 Δ0822-0845	D
D117	ΔCGP123 Δ2990-3006 Δ3050-3062	A

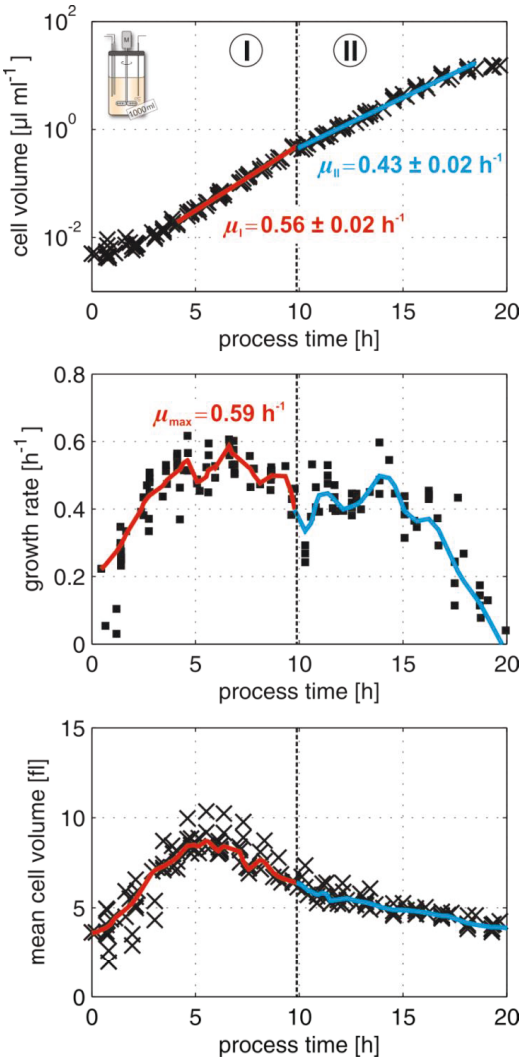

Figure S-1: Time dependent changes in the overall cell volume, the specific growth rate (based on cell volume measurements) and the mean single cell volume of *C. glutamicum* during batch cultivation in 1 l bioreactors on CGXII glucose medium - modified from Unthan *et al.* 2014 [2].

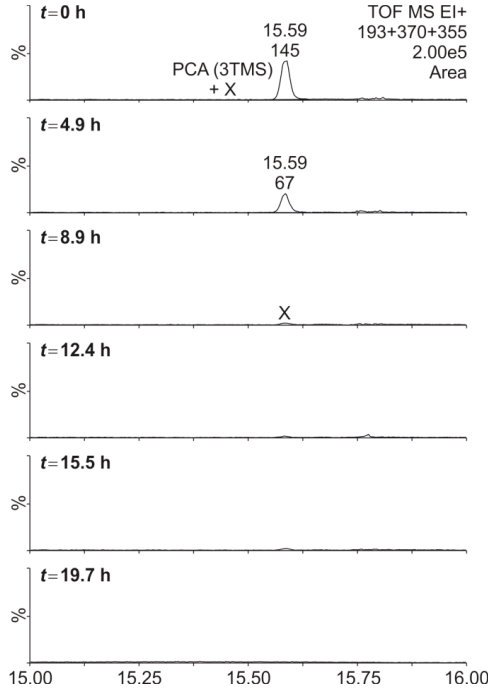

Figure S-2: Selected chromatograms from untargeted metabolome screening of culture supernatant samples from batch cultivations of *C. glutamicum* on CGXII glucose medium. The iron-chelator PCA decreased during the first growth phase and was already absent at the switch to the second phase - modified from Unthan *et al.* 2014 [2].

Table S-2: Significantly up- or down-regulated genes between the first and second growth phase of *C. glutamicum* wild type during 1 l bioreactor batch cultivations on CGXII medium with 10 g l^{-1} glucose - modified from Unthan *et al.* 2014 [2].

Gene	Annotation	M-value	p-value
cg0201	*iolB*, enzyme involved in inositol metabolism	1.04	0.00
cg1765	predicted transcriptional regulator	1.06	0.00
cg1761	*nifS2*, cysteine desulfhydrase / selenocysteine lyase	1.07	0.00
cg3321	ABC-type transport system, involved in lipoprotein release, ATPase component	1.09	0.00
cg2560	*aceA*, isocitrate lyase	1.12	0.03
cg0337	*whcA*, negative role in SigH-mediated (oxidative) stress response	1.13	0.03
cg1090	*ggtB*, probable gamma-glutamyltranspeptidase precursor PR	1.14	0.08
cg1762	*sufC*, iron-regulated ABC transporter ATPase subunit	1.16	0.00
cg1764	*sufB*, component of an uncharacterized iron-regulated ABC-type transporter	1.20	0.00
cg3048	*pta*, phosphate acetyltransferase	1.21	0.02
cg3011	*groEL*, chaperonin groel	1.31	0.00
cg0834	bacterial extracellular solute-binding protein, fa	1.32	0.00
cg0197	*iolC*, myo-Inositol catabolism, carbohydrate kinase	1.35	0.01
cg0346	*fadE*, glutaryl-CoA dehydrogenase	1.46	0.00
cg2137	*gluB*, glutamate secreted binding protein	1.47	0.05
cg1091	hypothetical protein cg1091	1.53	0.00
cg1411	ABC-type sugar (aldose) transport system, ATPase component	1.56	0.00
cg2628	*pcaI*, 3-oxoadipate enol-lactone hydrolase/4-carboxymuconolactonedecarboxylase	1.60	0.00
cg0444	*ramB*, transcriptional regulator, involved in acetate metabolism	1.66	0.04
cg3195	flavin-containing monooxygenase (FMO)	1.69	0.05
cg2181	ABC-type peptide transport system, secreted component	1.72	0.05
cg2184	ATPase component of peptide ABC-type transport system, contains duplicated ATPase domains	1.75	0.03
cg0953	Na+/proline, Na+/panthothenate symporter or related permease	1.86	0.03
cg2610	ABC-type dipeptide/oligopeptide/nickel transport system, secreted component	1.86	0.00
cg3216	*gntP*, gluconate permease	1.93	0.01
cg2629	*pcaB1*, 3-carboxy-cis,cis-muconate cycloisomerase	1.93	0.00
cg0344	*fabG1*, 3-oxoacyl-(acyl-carrier protein) reductase	1.93	0.00
cg2623	*scoA*, probable FESUCCINYL-CoA:3-ketoacid-coenzyme A transferase subunit	1.96	0.01
cg3022	acetyl-CoA acetyltransferase	1.96	0.00
cg1226	*pobB*, 4-hydroxybenzoate 3-monooxygenase	2.24	0.00
cg2630	*pcaG*, protocatechuate dioxygenase alpha subunit	2.88	0.00
cg3107	*adhA*, Zn-dependent alcohol dehydrogenase	3.01	0.02
cg2631	*pcaH*, protocatechuate dioxygenase beta subunit	3.12	0.00
cg2636	*catA1*, catechol 1,2-dioxygenase	4.46	0.01
cg3213	putative secreted protein	-1.01	0.01
cg1484	putative secreted protein	-1.03	0.00
cg0317	*arsR2*, arsenate/arsenite regulatory protein	-1.04	0.00

cg1256	*dapD*, tetrahydrodipicolinate succinylase	-1.05	0.01
cg0933	DNA or RNA helicase of superfamily II	-1.09	0.01
cg1218	ADP-ribose pyrophosphatase	-1.13	0.03
cg1279	putative secreted protein	-1.13	0.04
cg2880	HIT family hydrolase	-1.18	0.00
cg1514	secreted protein	-1.22	0.00
cg1343	*narH*, probable respiratory nitrate reductase oxidoreduct	-1.23	0.00
cg1551	*uspA1*, universal stress protein UspA and related nucleotide-binding proteins	-1.30	0.01
cg1341	*narI*, respiratory nitrate reductase 2 gamma chain	-1.46	0.00
cg2211	hypothetical protein cg2211	-1.53	0.00
cg3082	bacterial regulatory proteins, ArsR family	-1.60	0.00
cg1342	*narJ*, nitrate reductase delta chain	-1.64	0.00
cg0078	hypothetical protein cg0078	-2.27	0.01
cg3286	putative secreted protein	-3.44	0.02

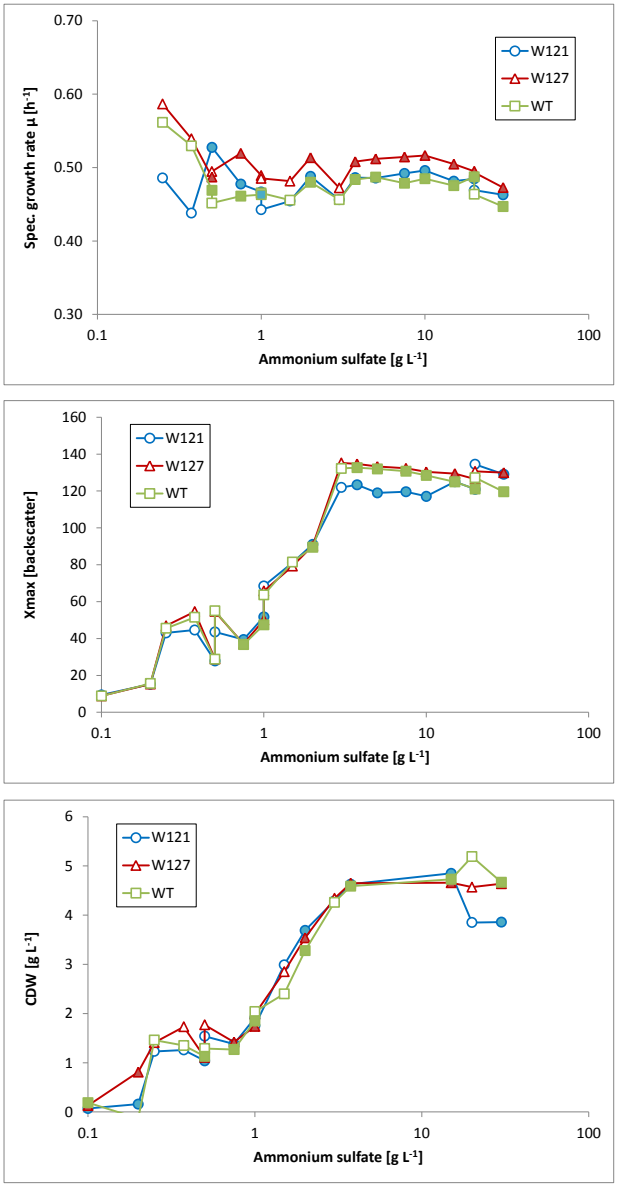

Figure S-3: Response of the *C. glutamicum* wild type and pre-chassis W121 and W127 to nitrogen limitation during BioLector experiments on defined CGXII medium without urea. Symbols with different brightness represent values obtained in independent experiments.

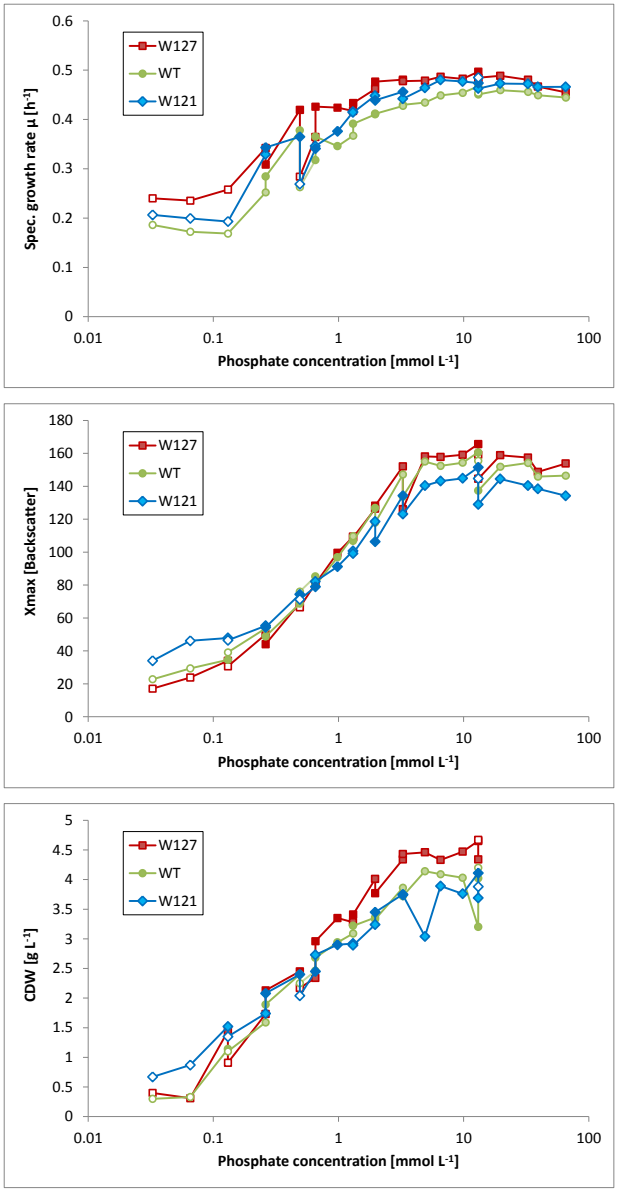

Figure S-4: Response of the *C. glutamicum* wild type and pre-chassis W121 and W127 to phosphate limitation during BioLector experiments on defined CGXII medium. Symbols with different brightness represent values obtained in independent experiments.

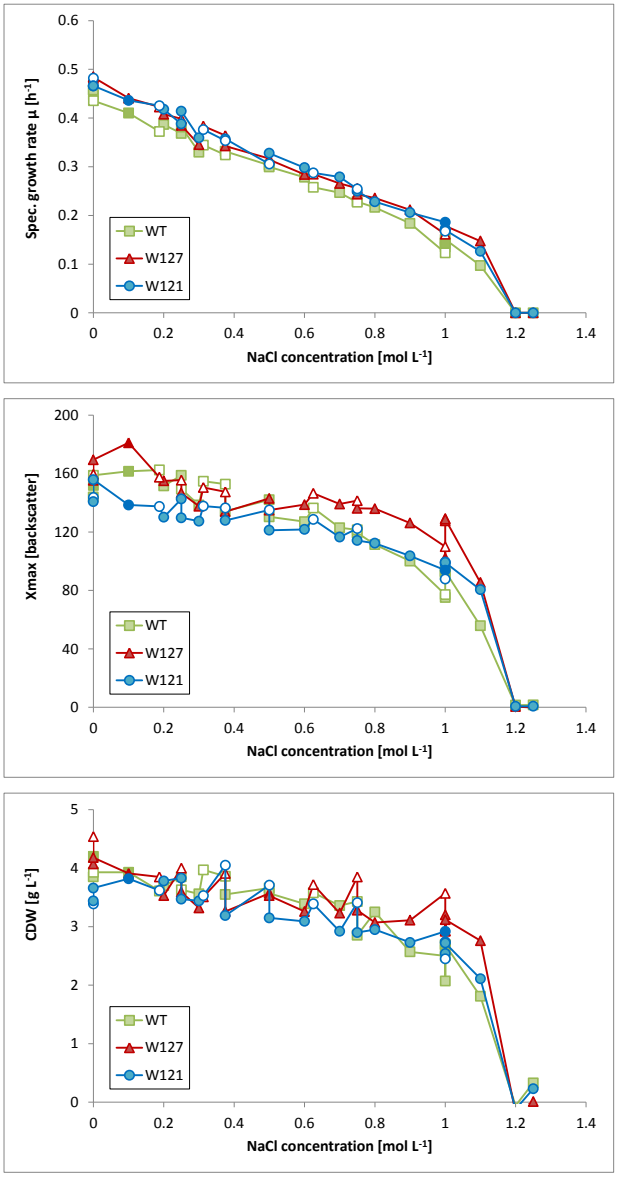

Figure S-5: Response of the *C. glutamicum* wild type and pre-chassis W121 and W127 to osmotic stress during BioLector experiments on defined CGXII medium supplemented with NaCl. Symbols with different brightness represent values obtained in independent experiments.

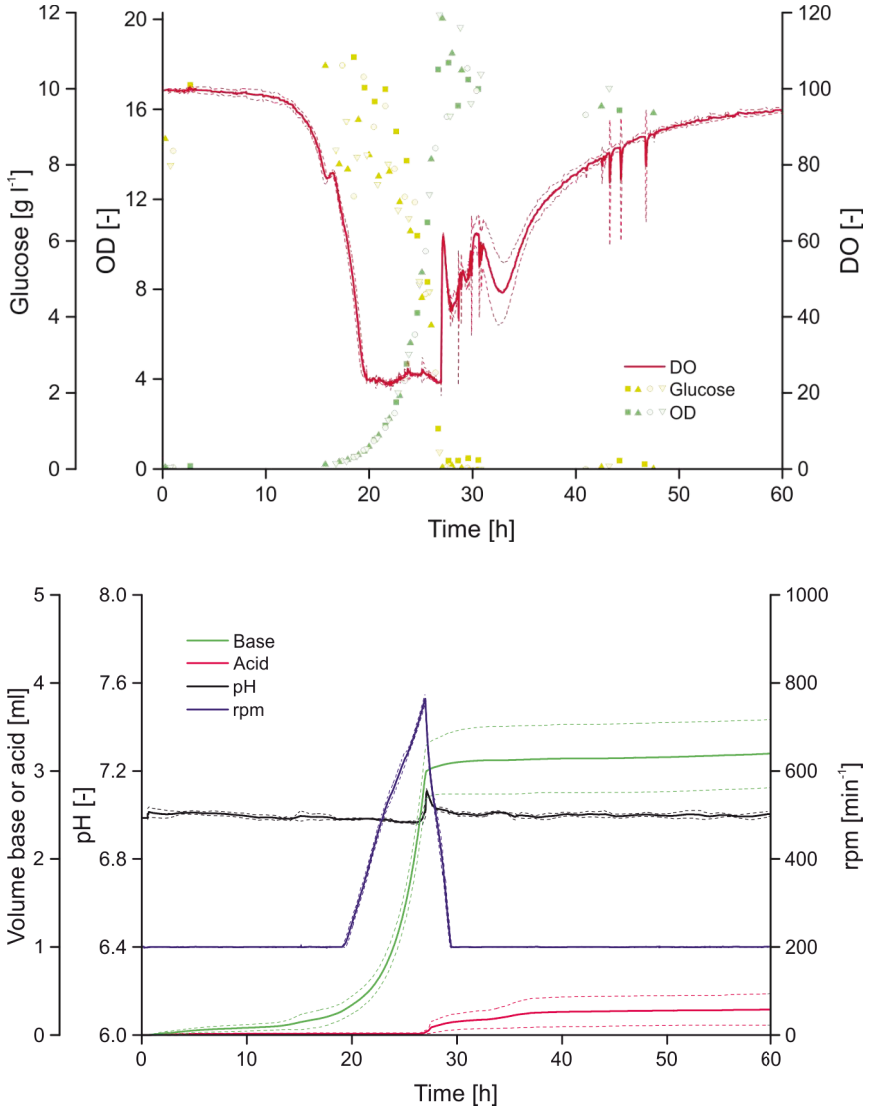

Figure S-6: Cultivation of *C. glutamicum* wild type in lab-scale bioreactors (1 l) on CGXII medium with 10 g L^{-1} glucose regulated at 30 °C, 30 % DO and pH 7. All graphs of online measured values are mean of four replicates with standard deviation drawn in dashed lines. Offline values derived from samples are displayed in different symbols for each run.

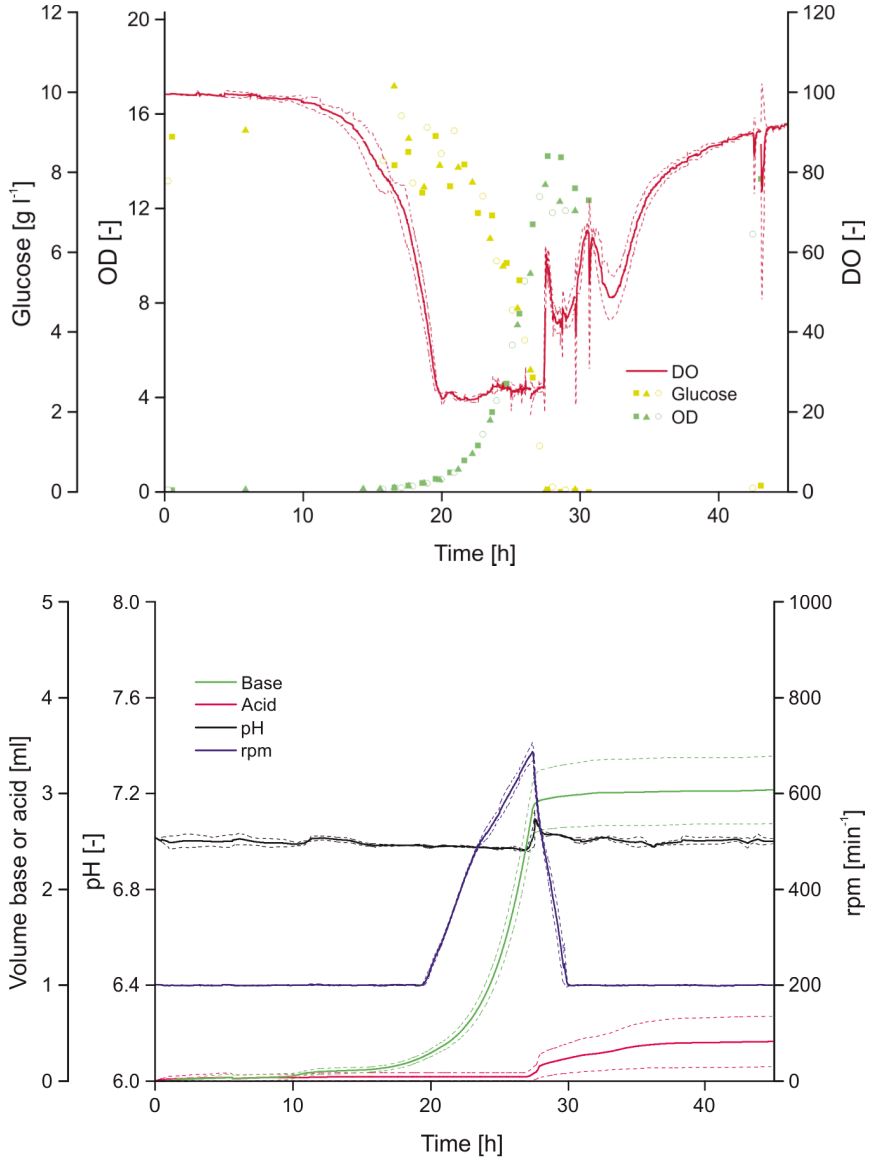

Figure S-7: Cultivation of pre-chassis W121 in lab-scale bioreactors (1 l) on CGXII medium with 10 g L^{-1} glucose regulated at 30 °C, 30 % DO and pH 7. All graphs of online measured values are mean of three replicates with standard deviation drawn in dashed lines. Offline values derived from samples are displayed in different symbols for each run.

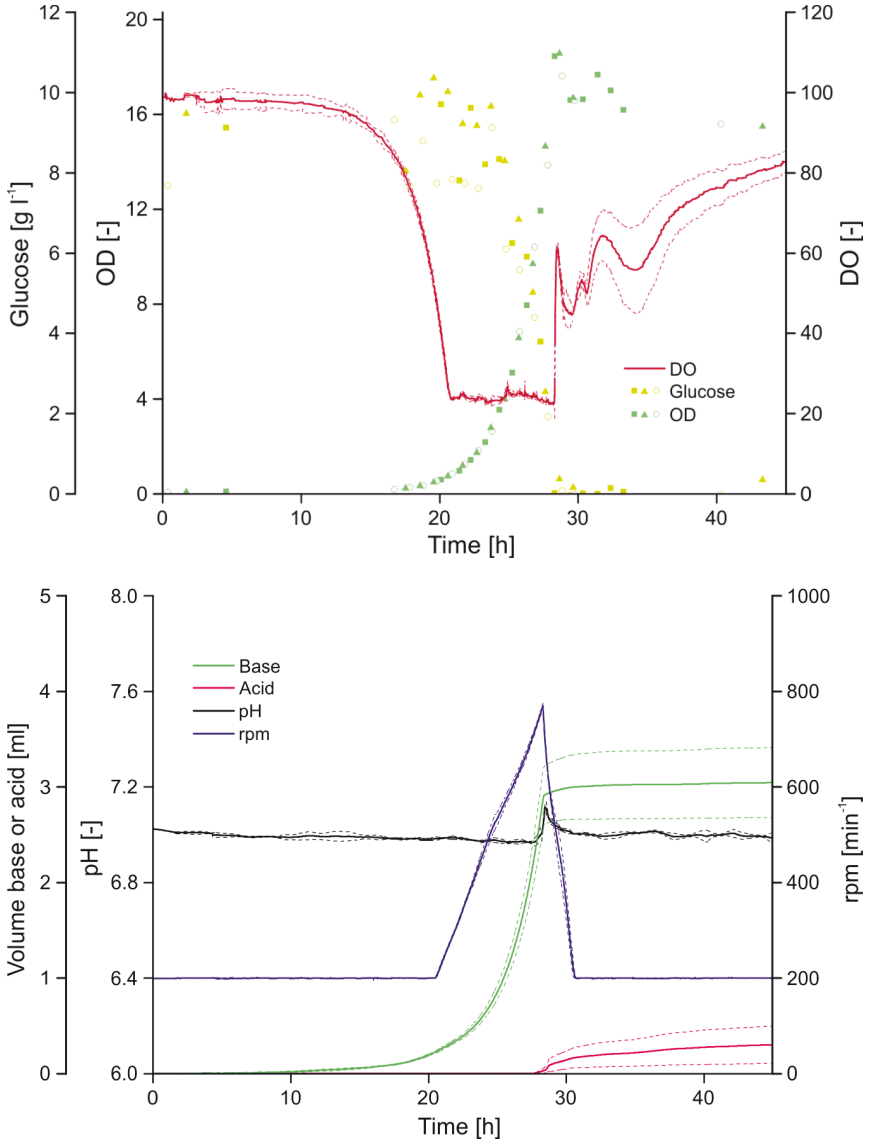

Figure S-8: Cultivation of pre-chassis W127 in lab-scale bioreactors (1 l) on CGXII medium with 10 g L^{-1} glucose regulated at 30 °C, 30 % DO and pH 7. All graphs of online measured values are mean of three replicates with standard deviation drawn in dashed lines. Offline values derived from samples are displayed in different symbols for each run.

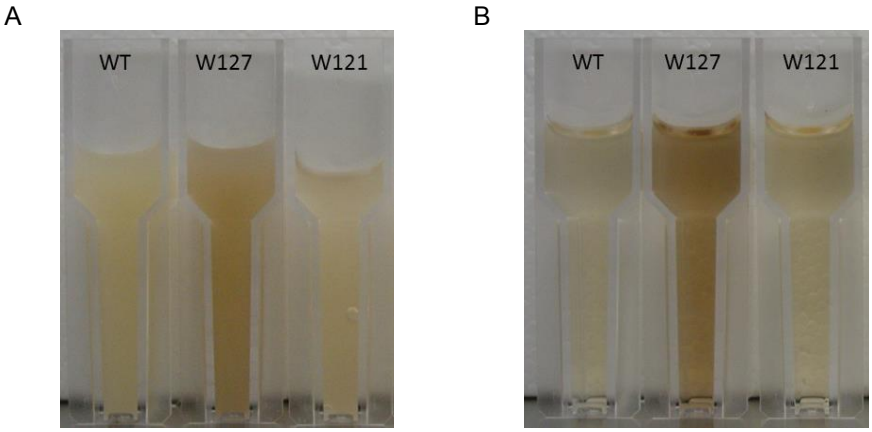

Figure S-9: Culture broth (A) and filtrated supernatant (B) from bioreactor cultivations of *C. glutamicum* wild type, W121 and W127 on defined CGXII medium. After 30 h of exponential growth the reactors were stirred and aerated for further 132 h before the pictures were taken.

Band / Volume 118
Magnetic, structural, and electronic properties of $NiFe_2O_4$ ultrathin films
M. Hoppe (2016), vii, 118 pp
ISBN: 978-3-95806-122-4

Band / Volume 119
First-principle investigation of displacive response in complex solids
D. A. Klüppelberg (2016), xi, 179 pp
ISBN: 978-395806-123-1

Band / Volume 120
Beam Cooling at COSY and HESR - Theory and Simulation -
Part 1 Theory
H. Stockhorst, T. Katayama and R. Maier (2016), v, 192 pp
ISBN: 978-3-95806-127-9

Band / Volume 121
Scanning tunneling microscopy of single-molecule magnets and hybrid-molecular magnets: Two approaches to molecular spintronics
V. Heß (2016), x, 127 pp
ISBN: 978-3-95806-128-6

Band / Volume 122
Bulk and surface sensitive energy-filtered photoemission microscopy using synchrotron radiation for the study of resistive switching memories
M. C. Patt (2016), viii, 247 pp
ISBN: 978-3-95806-130-9

Band / Volume 123
Group IV Epitaxy for Advanced Nano- and Optoelectronic Applications
S. Wirths (2016), vi, 116, XXX pp
ISBN: 978-3-95806-132-3

Band / Volume 124
Strained Silicon-Germanium/Silicon Heterostructure Tunnel FETs for Low Power Applications
S. Blaeser (2016), iv, 91, xvii pp
ISBN: 978-3-95806-135-4

Band / Volume 125
Nanocavity Arrays for Extracellular Recording and Stimulation of Electroactive Cell Systems
A. Czeschik (2016), x, 162 pp
ISBN: 978-3-95806-144-6

Band / Volume 126
Band Structure Engineering in 3D Topological Insulators Investigated by Angle-Resolved Photoemission Spectroscopy
M. Eschbach (2016), VIII, 153 pp
ISBN: 978-3-95806-149-1

Band / Volume 127
Dynamics in colloid and protein systems: Hydrodynamically structured particles, and dispersions with competing attractive and repulsive interactions
J. Riest (2016), ix, 226 pp
ISBN: 978-3-95806-153-8

Band / Volume 128
Self-purifying $La_{2/3}Sr_{1/3}MnO_3$ epitaxial films: Observation of surface precipitation of Mn_3O_4 particles for excess Mn ratios
A. Steffen (2016), 154 pp
ISBN: 978-3-95806-162-0

Band / Volume 129
Strain and electric field mediated manipulation of magnetism in $La_{(1-x)}Sr_xMnO_3/BaTiO_3$ heterostructures
M. Schmitz (2016), VI, 141 pp
ISBN: 978-3-95806-164-4

Band / Volume 130
High-Throughput Live-Cell Imaging for Investigations of Cellular Heterogeneity in *Corynebacterium glutamicum*
S. Helfrich (2016), xvi, 217 pp
ISBN: 978-3-95806-167-5

Band / Volume 131
Laser-Induced Ultrafast Electron- and Spin-Dynamics in the Electronic Band Structure of Co(001)
M. A. Plötzing (2016), ii, 109, XXXIV pp
ISBN: 978-3-95806-168-2

Band / Volume 132
Robot-Assisted Phenotyping of Genome-Reduced *Corynebacterium glutamicum* Strain Libraries to Draft a Chassis Organism
S. Unthan (2016), 122 pp
ISBN: 978-3-95806-169-9

Schlüsseltechnologien /
Key Technologies
Band / Volume 132
ISBN 978-3-95806-169-9